A Novel Fully 3D Modeling of Two-Phase Fluid Flow in Fractured-Vuggy Carbonate Formations Using the Transient Brinkman Equation Coupled with the Second-order Gradient Rock Mechanics Equation Including Porosity Evolution

By

Mustafa M. Alhubail

Submitted to the graduate degree program in Chemical & Petroleum Engineering and the Graduate Faculty of the University of Kansas in partial fulfillment of the requirements for the degree of Doctor of Philosophy.

_____

Chair: Dr. Barati, Reza

_____

Member 2: Dr. Misra, Anil

_____

Member 3: Dr. Rasoulzadeh, Mojdeh

_____

Member 4: Dr. Goldstein, Robert

_____

Member 5: Dr. Saiedian, Hossein

_____

Member 6: Dr. Vossoughi, Shapour

_____

Member 7: Dr. Ostermann, Russell

Date Defended: 05/12/2020

The dissertation committee for Mustafa M. Alhubail certifies that this is the approved version of the following dissertation:

A Novel Fully 3D Modeling of Two-Phase Fluid Flow in Fractured-Vuggy Carbonate Formations Using the Transient Brinkman Equation Coupled with the Second-order Gradient Rock Mechanics Equation Including Porosity Evolution

_____

Chair: Dr. Reza Barati

Date Approved: 05/12/2020

Abstract

Describing the fluid flow behavior in heterogeneous carbonate formations is a challenging task due to the existence of natural fractures and vugs. The fractures and vugs are not porous regions; hence, the fluid flow in those regions cannot be described by Darcy's law. The Brinkman's equation describes the co-existing flow in the porous and free-flow regions without the need of using complex boundary conditions on the interface between the two flow regions. A comprehensive model, which considers rock deformation with second-order stress-strain gradient, the transient form of the Brinkman's equation and the evolution of porosity, has been developed to capture and study the two-phase fluid flow behavior and vug deformation in fractured-vuggy carbonate formations considering the co-existing flows in the porous matrix and in the free-flow regions. The model is designed using advanced numerical techniques so that both the microscale and macroscale heterogeneities can be captured. The model is also designed to handle two-phase flow. The developed model was used to study how the vugs' shape and volume change with time due to production and how those changes affect the cumulative production. The effect of elasticity was also examined to capture the changes of the vugs' shape during production and when the production is halted. The finite element mesh was also interrogated to check the effects of the mesh size on the model's accuracy, convergence and stability. Capillary pressure tests were conducted for the two-phase model to examine the capillary pressure effect on injectivity. The developed model can be extended to other disciplines that deal with conjugate flow problems, and it can also be improved to account for rock dissolution to study the impact of that on the fluid flow behavior.

Dedication

To my family.

Acknowledgements

I would like to express my sincere gratitude and appreciation to my adviser and committee chair, Dr. Reza Barati, for his motivation, guidance, encouragement and continuous support throughout my PhD study. I am truly grateful, Dr. Barati, for all the discussions that are related to this research and beyond. I would like, also, to extend my gratitude and appreciation to Dr. Anil Misra for his valuable comments, assistance and advice in this study and beyond. I extend my thanks and appreciation to Dr. Mojdeh Rasoulzadeh for her advice, valuable suggestions and support. Special thanks to Dr. Robert Goldstein for his valuable remarks and insightful advice. I extend my appreciation to the committee members, Dr. Shapour Vossoughi, Dr. Russell Ostermann and Dr. Hossein Saiedian, for their valuable advice and encouragement. I also acknowledge Idaho National Laboratory for providing the framework Multiphysics Object-Oriented Simulation Environment (MOOSE) and technical support and Coreform for providing the software package Coreform Trelis and technical support. Finally, I acknowledge SACM for the financial support.

Table of Contents

1 Chapter I: Introduction

1.1 Importance of Carbonate Formations

Carbonate rocks are of great interest for several reasons. First, carbonate rocks are estimated to hold more than 60% and 40% of the world's oil and gas reserves, respectively (Akbar et al., 2000; Schlumberger, 2007). In the U.S., carbonate reservoirs are estimated to hold more than 100 billion barrels of light recoverable oil (i.e., oil API gravity is greater than 20^{o} API) (Nuckols, 1992). However, developing carbonate reservoirs for commercial production is a challenging task due to their unique and complex characteristics (Burchette, 2012; Chilingar, Bissell, & Wolf, 1967; Gomes, Narayanan, Parra, Saputelli, & Bansal, 2018; Nuckols, 1992; Rieke, Mannon, & Chilingar, 1972). Consequently, carbonate reservoirs have an average recovery factor that is less than 35% when the conventional recovery methods are utilized, and enhanced recovery methods (e.g., CO_2 injection) improve the recovery factor by an additional 8% to 15% (Chilingarian, Mazzullo, & Rieke, 1996; Nuckols, 1992; Sheng, 2013; Wardlaw, 1996). Therefore, any improvement in recovery factor would result in a tremendous amount of additional recoverable hydrocarbons.

Another reason that makes the carbonate rock formations an important subject of study is the increased activity of geological sequestration of carbon dioxide in such formations (Holloway, 1997; Kovacs, Poulussen, & de Dios, 2015; Wildgust, Gilboy, & Tontiwachwuthikul, 2013). Geological sequestration of CO_2 is the last part of carbon dioxide capture and storage (CCS) process. This process involves: 1) capturing CO_2 from large industrial sites, 2) compressing and transporting CO_2 to the injection sites, and 3) injecting CO_2 into formations with strong storage capacity (Metz, Davidson, de Coninck, Loos, & Meyer, 2005). CCS is a valuable technique in reducing the carbon emissions, and it is estimated that effective CCS would contribute to 20%

reduction of the global carbon emissions by 2050 (Ketzer, Iglesias, & Einloft, 2012). However, it is important to note that CCS by itself is not adequate to address the climate change issue as the cost of capturing CO_2 and transporting it to injection sites is a complicated process, and it is not economically sustainable according to the US Department of Energy (Kilisek, 2015; U.S. DOE, 2016). Therefore, CCUS (Carbon Capture Utilization and Storage) is the way forward to address the climate change issue as it is economically viable to reach the needed global emission cuts (U.S. DOE, 2016). One form of utilizing CO_2 is CO_2-EOR. Underground injection of CO_2 has been practiced in the petroleum industry for more than 40 years as an enhanced oil recovery (EOR) method (Gozalpour, Ren, & Tohidi, 2005; Siqueira, Iglesias, & Ketzer, 2017). It was found that injecting CO_2 enhances oil recovery, and the reservoirs securely retain a high percentage of the injected CO_2 (Wildgust et al., 2013). In fact, the oil and gas reservoirs are favorable CO_2 storage sites as they have geological traps that have retained the oil and gas for millions of years (Gozalpour et al., 2005). Depleted reservoirs, especially the depleted gas reservoirs, are considered to be one of the best storage site candidates for CO_2 geological sequestration (Tambach, Koenen, Wasch, & van Bergen, 2015). However, reservoirs have to be accurately characterized for the CO_2 sequestration process before the injection takes place to ensure: 1) the integrity and the storage safety so that the deposited CO_2 does not enter the atmosphere, and 2) the storage capacity as the CO_2 reacts with the fluids in the carbonate formations, and such a reaction lowers the pH and causes mineral dissolution; thus, altering the porosity and the permeability of the formation (Bacci, Korre, & Durucan, 2011; Gaus, 2010; Kovacs et al., 2015; Thordsen, Gans, Thomas, Kharaka, & Cole, 2013). Figure 1 shows how the CO_2 injection altered the porosity and permeability of a carbonate rock sample after just 2 hours (Luquot & Gouze, 2009; Siqueira et al., 2017).

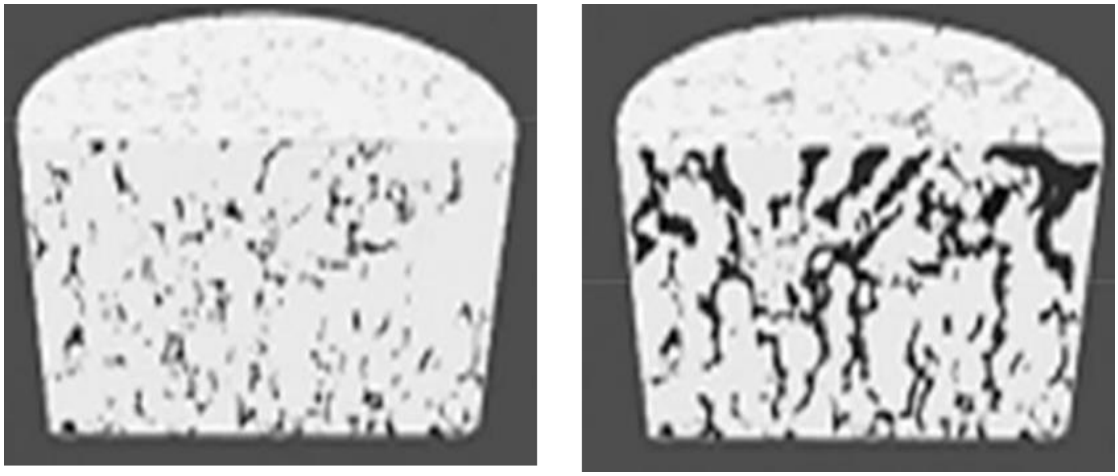

Figure 1: CO_2 injection in a carbonate core sample before (left) and after (right) at 10 MPa (Luquot & Gouze, 2009)

Carbonate rock characterization is also essential before conducting the secondary recovery treatments (i.e., waterflooding), and it is a vital factor in estimating the reserves, predicting the expected ultimate recovery (EUR) and also in building advanced reservoir simulators to properly predict the reservoirs performance (Burchette, 2012; Dominguez, Fernando, & Chilingarian, 1992; Lian, Ma, Ji, Duan, & Tan, 2017; Lie, Aarnes, Kippe, & Rustad, 2007; Rieke, Chilingarian, & Mazzullo, 1996).

Characterizing and developing the carbonate formations is also important as they hold tremendous amount of groundwater. A substantial number of aquifers are developed in karst regions, and the deep karst carbonate rocks are also a great source for thermal water resources (Goldscheider, Mádl-Szőnyi, Erőss, & Schill, 2010). The aquifers are estimated to supply drinking water for 2 billion people worldwide, and they also play a role in the food security as they provide water for agricultural irrigation (Morris et al., 2003).

1.2 Challenges in Characterization of Carbonate Rocks

Characterizing and developing carbonate rocks is a difficult task because the formation properties vary within the reservoir (i.e., heterogeneity) which is due to the depositional environment as well as the diagenetic history that have occurred after the deposition of the carbonate sediments (Chilingarian et al., 1996). There are multiple factors that influence the diagenesis of carbonate sediments; they are: 1) geographic factors (e.g., climate, rainfall and water chemistry), 2) grain size and rate of accumulation, 3) sediments purity (e.g., amount of clay and organic matter) and 4) physicochemical conditions (e.g., pH and CO_2 content) among other factors (Chilingar et al., 1967). Heterogeneity in the carbonate rocks exists in the pores, grains and textures; hence, the wide range of porosity and permeability in them (Nuckols, 1992; Sheng, 2013). The carbonate diagenesis causes the heterogeneities, and it also complicates the structures and the wettability conditions (i.e., mixed-wet and oil-wet) of the carbonate formations (Wardlaw, 1996). Consequently, the development of carbonate rocks becomes even more complicated. The drilling process is also a challenging procedure in carbonate rocks as a significant volume of the drilling mud might be lost to the vugs and the natural fractures; therefore, the probability of loss of drilling mud circulation increases and hence the risks of kicks increases, accordingly (Sheng, 2013). Characterizing carbonate rock samples in the lab is also a challenging task as: 1) transporting the samples could be difficult due to the brittleness nature of the carbonate rocks and 2) the core samples may not capture the vugs' size accurately.

The unique challenges that have a significant impact on the development of carbonate rocks include: 1) the complex pore-size distribution (e.g., from micro-porosity to vugs) and tortuous pore networks, 2) the non-linear relationship between the porosity and permeability, 3) the physicochemical conditions of the carbonate reservoirs which influence the wettability, and 4) the

dual- and sometimes triple porosity/permeability flow behavior due to connected vugs and fractures (Alotaibi, Azmy, & Nasr-El-Din, 2010; Burchette, 2012; Guo, Nie, & Jia, 2012). Carbonate rocks exhibit the triple-porosity system, which consists of matrix, fracture and vugular porosity subsystems as can be seen in Figure 2 (Dominguez et al., 1992; Kovacs et al., 2015; Lucia, 1983; Rieke et al., 1972). The matrix porosity, which is known as the intergranular porosity, is the preserved porosity after lithification. The fracture porosity, which is also known as the fracture-matrix porosity, is generated after rock deposition due to stress, and since the carbonate rocks are brittle, it is estimated that approximately 80% of the carbonate reservoirs are naturally fractured reservoirs (Sheng, 2013; Total, 2017). The vugs, which are cavities or voids in the rocks, form the vugular porosity subsystem, which is also known as the vugular-solution porosity, and it is also called the karst porosity. The vugular-solution porosity is typically generated during diagenesis due to dissolution of calcite, and it is considered to be the most complex porosity subsystem (Rieke et al., 1996).

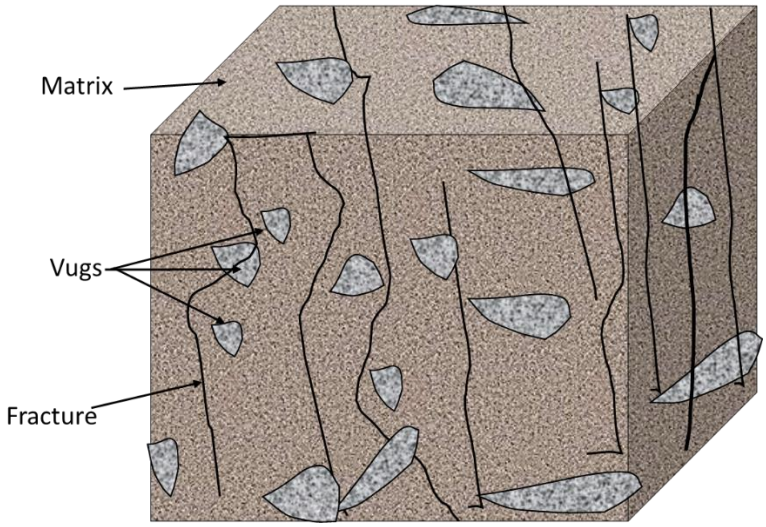

Figure 2: Display of matrix, fractures and vugs

The permeability is also impacted by the existence of vugs especially the connected vugs, which are considered to be the main heterogeneity contributor in the vuggy carbonate reservoirs (Vik, Sylta, & Skauge, 2012). Thus, heterogeneity, which exists at all scales and significantly affects the sweep efficiency, the wettability and the triple porosity system complicates the fluid flow characteristics in carbonate rocks. Hence, describing carbonate rocks and predicting their performance is an exceptional challenge (Sheng, 2013). What adds to the complexity even more is the difficulty of capturing the presence of fractures and vugs in the core samples (Chilingarian, Mazzullo, & Rieke, 1992). The heterogeneity (e.g., fractures and vugs) is difficult to capture at the core scale; however, this becomes a serious issue at the simulation scale due to grid upscaling measures, which are unavoidable in the current conventional simulators as can be seen in Figure 3 (Lie et al., 2007). Therefore, large portions of the reservoirs are homogenized; thus, the effects of the existing fractures and vugs, which play fundamental roles in achieving commercial flow rates from carbonate reservoirs, are disregarded (Burchette, 2012; Chilingarian et al., 1992). Consequently, the results from such simulators may be inaccurate and misleading as will be shown in the literature review section (Dominguez et al., 1992).

It is also important to mention that the mechanical properties of carbonate rocks are typically investigated by laboratory tests on small samples, which needs to be scaled up to reservoir scales (Kovacs et al., 2015).

1.3 Upscaling

Nowadays, the geological reservoir models, which are used to characterize the reservoirs' geometry and rock parameters (e.g., faults, fractures, vugs, porosity and permeability), are capable of accurately capturing both the large-scale and the fine-scale properties of the reservoirs using advanced techniques and several millions of grid cells (Aarnes, Kippe, & Lie, 2005). On the other

hand, the capability of the existing conventional reservoir simulators is several orders of magnitude less than the geological models; this is mostly due to the limited computational power as multiple simulations must be performed to conduct necessary history matching and optimization processes. The typical way of tackling this issue is upscaling of the details so that the simulators can be conveniently utilized, and the results can be achieved in a timely manner (Aarnes et al., 2005; Lie et al., 2007). However, since upscaling does not accurately represent the actual reservoir behavior (i.e., heterogeneity) as can be seen in Figure 3, then the results from the simulators may be misleading. Accurate representation of the reservoir heterogeneity is a major issue in the existing simulators due to upscaling practices (Burchette, 2012). Thus, there are emerging techniques such as the mixed multi-scale finite element method that are designed specially to resolve the issue of upscaling in the reservoir simulators (Aarnes et al., 2005).

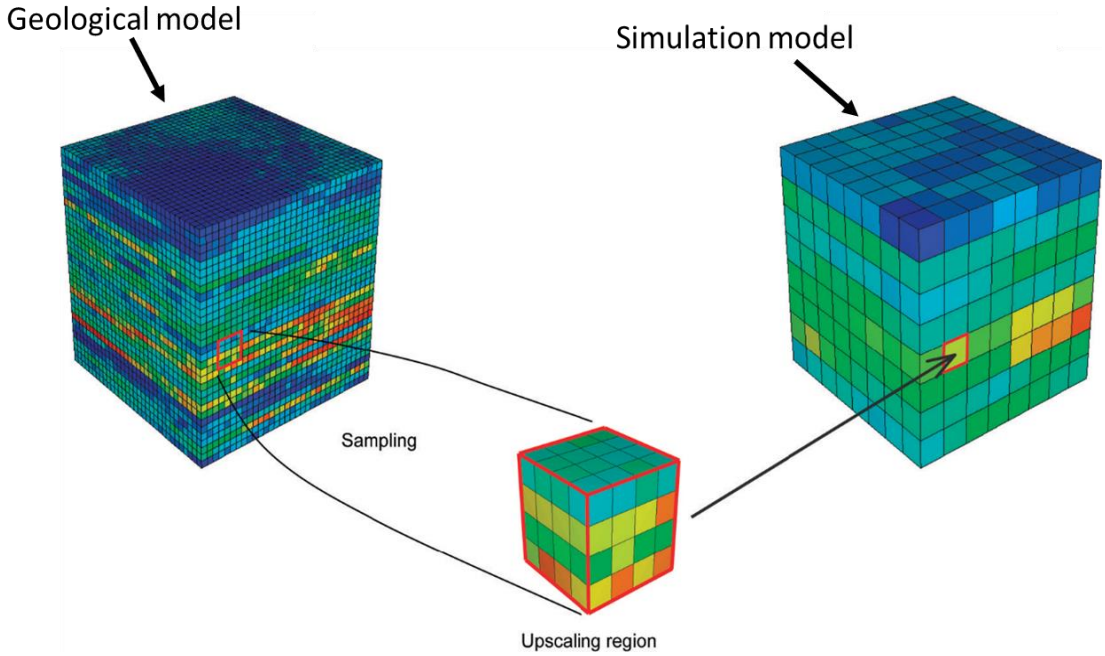

Figure 3: Upscaling process (modified after (SPE, 2019), courtesy of SPE)

1.4 Simulating the Fluid Flow

The first step towards an accurate simulation of fluid flow in the reservoirs is a proper representation of the reservoirs, which can be achieved by building sophisticated high-resolution geological models. The main issue that imposes the use of upscaling measures is the simulation of fluid flow in pours media. The high-resolution geological models are capable of capturing the heterogeneities in the reservoirs with several millions of grid cells; however, those models cannot be used to simulate the fluid flow behavior due to computational power limitations (Aarnes et al., 2005; Dehghani, Edwards, & Harris, 1997). The issue of upscaling is not only the construction of coarser grid cells and averaging the reservoir properties, which lead to misleading results, but also the negligence of some of the forces that drive the fluid flow in the fine-scale details, which could influence the overall flow behavior (Lie et al., 2007; L. Zhang, Bryant, Jennings, Arbogast, & Paruchuri, 2004).

The simulation of fluid flow through different porous media (e.g., dual-porosity systems) has been practiced since the 1960s. However, due to the limited knowledge of the importance of vugs and also the limited computational power back then, most of the studies were focused toward fractured and naturally fractured reservoirs, without considering the influence of cavities or vugs on the flow behavior (Arbogast, 1997; Barenblatt, Zheltov, & Kochina, 1960; Kazemi & Merrill, 1979; Pruess, 1985; Saidi, 1983; Sarkar, Toksoz, & Burns, 2002; Warren & Root, 1963).

The vugs significantly impact the reserves estimation, the rate of oil recovery and also influence the overall production performance as was found by conducting history matching studies (Dehghani et al., 1997; Gulbransen, Hauge, & Lie, 2010; Kossack & Gurpinar, 2001). In the fractured-vuggy reservoirs (i.e., triple porosity system), the vugs and matrix are typically

considered as fluid storage spaces whereas the fractures are the main driver of the fluid to the wellbore (Y. Wu et al., 2006).

Modeling the fluid flow in the multi-scale heterogeneous systems requires dealing with two types of fluid flow behaviors; 1) flow in the porous regions (i.e., matrix) and 2) flow in the free-flow regions (i.e., vugs and fractures) as can be seen in Figure 4 (Mikelic, 1997; Popov et al., 2009).

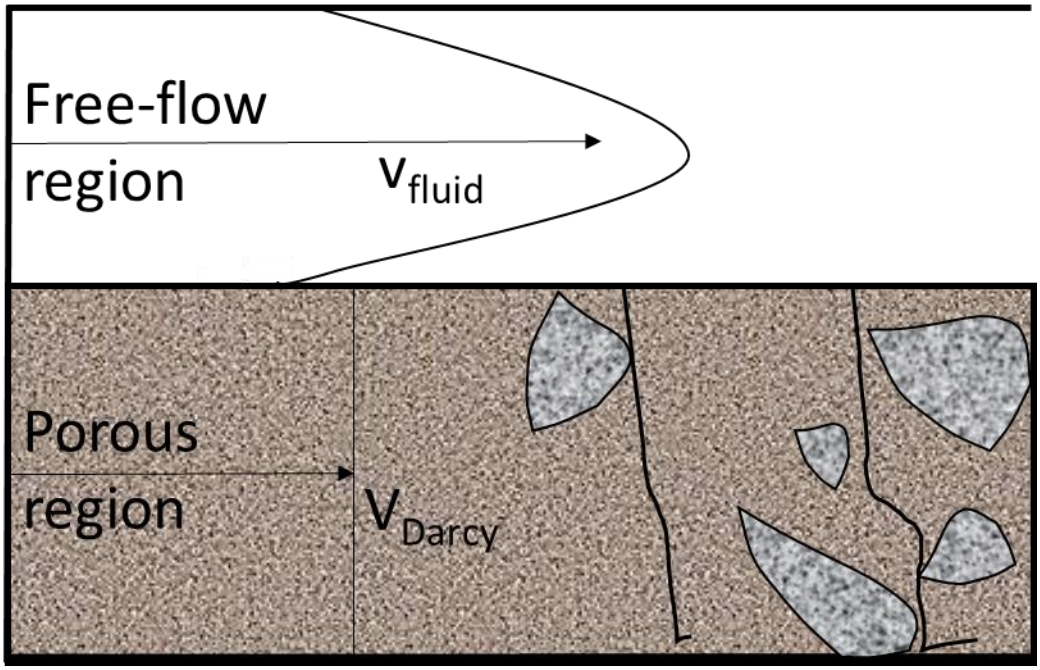

Figure 4: Fluid flow behaviors in carbonate rocks

1.5 Geomechanics

The geomechanical properties of the reservoir rocks are of great importance in the petroleum industry as they play a major role in the reservoir management and stability (e.g., predicting stresses around the wellbore) especially in carbonate rocks where a triple porosity system exists (F. Zhang, An, Yan, & Wang, 2017). The interaction between the fluid flow and the

structural deformation in the porous media is described by the theory of poroelasticity. The term poroelasticity was first introduced in the petroleum industry in 1966 by Geertsma who was affiliated with the Royal Dutch Shell company (Geertsma, 1966). However, most of the pioneering work on soil mechanics was conducted experimentally in the 1920s by Karl von Terzaghi where he also showed the importance of the effective stress in soils (Terzaghi, 1943). The Terzaghi's effective stress in soils is achieved by subtracting the pore pressure from the applied stress as shown in Eq. 1.

$$\sigma' = \sigma - P_p \qquad Eq.\ 1$$

where σ' is the effective stress, σ is the applied stress and P_p is the pore pressure

In the 1940s, Maurice Biot formulated the theory of poroelasticity in his famous paper entitled "General theory of three-dimensional consolidation" where he derived the governing equations for deformation of porous rocks filled with fluids (Biot, 1941). Biot extended his work to account for deformation in viscoelastic anisotropic porous rocks (Biot, 1955, 1956). Biot also modified the definition of the effective stress in the porous rocks by including the poroelastic constant, which is also known as the Biot's poroelastic term (Biot, 1941, 1962). The basic ideas behind the poroelasticity theory is the coupling of: 1) solid-to-fluid and 2) fluid-to-solid interactions. The coupling of the solid-to-fluid is considered when variation in the applied stress changes the fluid pressure whereas the fluid-to-solid interaction coupling occurs when a change in the fluid pressure changes the porous material volume (Biot, 1941; Rice & Cleary, 1976; Terzaghi, 1943; Wang, 2000). In this project, the geomechanical effects will be considered to account for the possibility of rock deformation (e.g., changes in the vugs' shape and volume) by considering the theory of poroelasticity.

1.6 Objective

The aim of this project is to design a fully coupled multiscale 3D model that is capable of simulating the fluid flow in fractured-vuggy carbonate rocks considering the co-existing flows in the porous matrix and in the free-flow regions while accounting for the geomechanical effects and the evolution of porosity and permeability using the mixed finite element method with weak formulation. The developed model is unique as: 1) the model handles the flow in both the porous matrix and vugs/fractures using the Brinkman equation and ensuring flow continuity without the need of complex boundary conditions, 2) the second stress-strain gradient in the rock mechanical equation is implemented in the model, which makes it more responsive to the geomechanical effects by accounting for nonlocality, 3) the model considers the porosity and permeability evolution and 4) the model is capable of handling two-phase flow.

2 Chapter II: Literature Review

2.1 Modeling of Fluid Flow

Describing the fluid flow behavior in heterogeneous carbonate rocks is a challenging task due to the existence of two flow regions; porous region (i.e., matrix) and free-flow region (i.e., fractures and vugs). The fluid flow in the porous region is described by Darcy's law; however, the fluid flow in the free-flow regions cannot be described by Darcy's law, and the Navier-Stokes equations should be used (Rasoulzadeh & Panfilov, 2018). In the literature, there are three ways to model the fluid flow behaviors (i.e., flow in the porous regions and the free-flow regions) that are encountered in the multiscale heterogeneous fractured-vuggy carbonate rocks; they are: 1) the extended Darcy models, 2) the Darcy-Stokes model and 3) the Stokes-Brinkman model.

2.1.1 Extended Darcy Models

The extended Darcy models are classified into two types, and both types are designed based on the continuum approach. The concept of the continuum approach is basically the modeling of both the porous regions and the free-flow regions as porous media. The first type is based on the concept of modeling the free-flow regions (i.e., vugs and fractures) as porous media but high permeability values are assigned in those regions. This approach is based on the triple porosity/permeability concept which was introduced in 1986 (Abdassah & Ershaghi, 1986). The triple porosity/permeability concept is utilized to capture the different porosity subsystems of fracture, vugular and the matrix in the simulation models (Bai, Elsworth, & Roegiers, 1993). This approach has become the standard option to model the fluid flow behavior in such heterogeneous systems in the commercial simulators (Khvatova et al., 2012; Kossack & Gurpinar, 2001; Vasquez-Cruz & Castrejon-Aivar, 2005; Y. Wu et al., 2006).

In fact, this approach is also the main approach that is being used today in the commercial simulators to model the fluid flow in the hydraulically fractured unconventional reservoirs by simply utilizing the triple porosity concept in the models, which are superposition models with three grid systems at one location where two grids serve as storage and the third serves as a conduit for the media. Figure 5 represents a schematic of how the formations are presented in reality (Yan, Alfi, Wang, & Killough, 2013; Yan, Wang, & Killough, 2016).

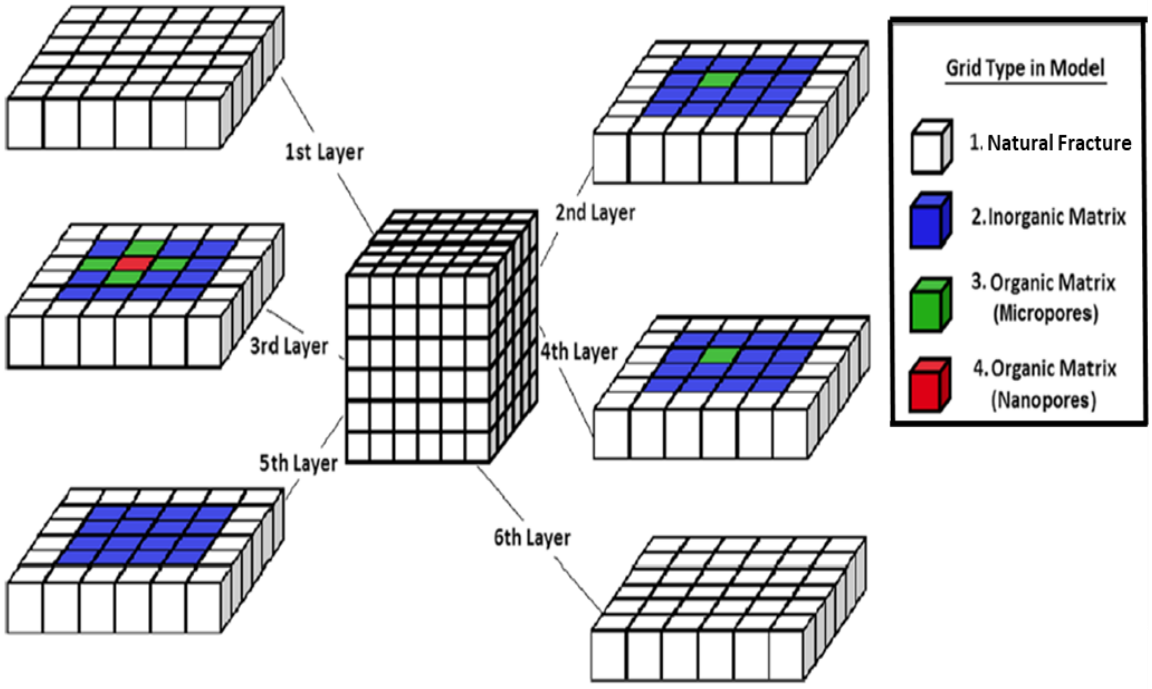

Figure 5: Schematic of triple porosity/permeability grid system (modified after (Yan et al., 2016))

The second type of the extended Darcy models is the concept of using one "effective" value for porosity and permeability. Instead of using multiple values for porosity and permeability as in the dual-triple porosity/permeability schemes, an effective and representative value, for each the

porosity and the permeability, is used in the entire simulation model. The effective value is expected to represent all the heterogeneities that are captured in the geological model (Oda, 1986; Sitharam, Sridevi, & Shimizu, 2001; Y.-S. Wu, 2000). The main challenge with these models is the difficulty of estimating the "effective value" for the formation as the core samples are small and not representative of the entire formation. Also, the well logging methods cannot be relied on to estimate the effective value as their radius of investigation is limited to a specific range. Inputting incorrect effective value in the models would lead to unreliable outcomes (He, Killough, Fadlelmula, & Fraim, 2015; Yao, Huang, Li, Wang, & Lv, 2010).

In 1967, Beavers and Joseph conducted experiments studying the fluid flow behavior in porous regions and free-flow regions, and they concluded that the fluid flows faster in the free-flow regions than in the matrix (Beavers & Joseph, 1967). Consequently, Darcy's law does not govern the fluid flow in the free-flow regions; hence, it does not accurately capture the flow behavior in vugs and fractures. Thus, it is more appropriate to use two models (i.e., one for porous regions and one for free-flow regions) to accurately capture the flow behavior in fractured-vuggy carbonate rocks, and for that reason, the extended Darcy models are inadequate models for such systems.

That said, the extended Darcy models are considered to be the most convenient models to simulate the fluid flow in the multi-scale heterogeneous formations as they already exist in the advanced commercial simulators, and they do not require intensive computational power. However, finding the representative values either for the dual-triple porosity/permeability method or the single-effective value method is a challenging task, and inputting wrong representative values on the simulators results in misleading outcomes (Burchette, 2012; Hidajat, Mohanty, Flaum, & Hirasaki, 2004; Yao et al., 2010).

2.1.2 Darcy-Stokes Model

The concept of the Darcy-Stokes model is simply to use Darcy's law to model the flow in the porous regions, and the flow in the free-flow regions (i.e., vugs and fractures) is modeled by the Stokes equation as can be seen in Figure 6 (Darcy, 1856; Hubbert, 1957; Stokes, 1851). However, the challenge is locating where one flow region stops and the other starts while ensuring the continuity of mass (Arbogast & Lehr, 2006).

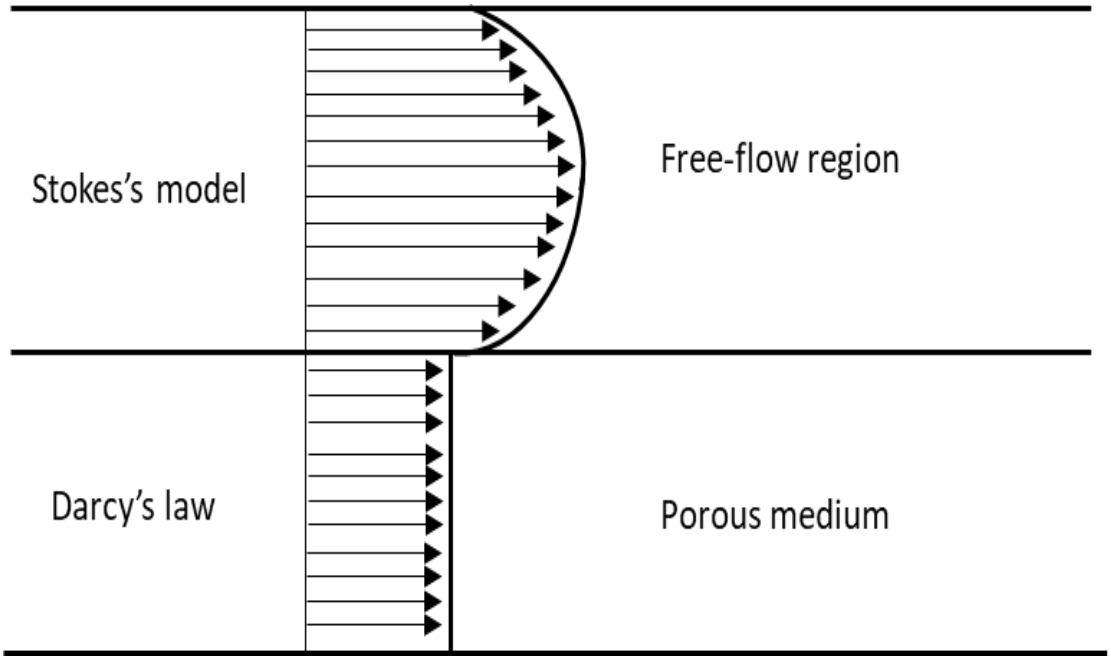

Figure 6: Porous flow region and free-flow region modified after (Salinger, Aris, & Derby, 1994)

In 1994, Salinger et al. developed a model for the coal stockpile ignition problem where the coal stockpile was considered as a porous media and the air surrounding the pile was the open region (Salinger et al., 1994). Salinger et al. used Darcy's law to model the flow of Oxygen inside the pile, and the steady-state Navier-Stokes equations for incompressible fluid were used to model the flow in the free-flow domain. They also modeled the flow in the porous media using the

Brinkman's formulation and compared the results. While both formulations (i.e., Darcy and Brinkman) gave similar results, Salinger et al. concluded 1) Brinkman's formulation is much simpler to use than Darcy's formulation as extra care is required in Darcy's formulation due to the slip and jump conditions in the porous and free-flow domains, 2) Brinkman's formulation required finer mesh to achieve smooth velocity profile while Darcy's formulation yielded smooth solutions with the coarse mesh; hence, the Brinkman's formulation could be computationally demanding, and 3) Darcy's formulation is sufficient to capture the large-scale properties with coarse meshes (Salinger et al., 1994). The Salinger et al. model was a simple one without much heterogeneity in the system; hence, Darcy's formulation was not as complex as it would be for fractured-vuggy carbonate systems; such systems would complicate the formulation of the Darcy-Stokes model resulting in the necessity for using finer mesh to get smooth solutions.

In 1996, Gartling et al. developed a general model to study the flow behavior for the conjugate flow problems that involve viscous fluid flow and fluid flow in porous medium using the finite element method (FEM) (Gartling, Hickox, & Givler, 1996). Gartling et al. used the Navier-Stokes equations to model the viscous fluid flow and Darcy's law to model the fluid flow in the porous media. Gartling et al. concluded 1) the coupling of Darcy's law and the Navier-Stokes equations cause discontinuity in the velocity components, and boundary conditions (e.g., Beavers and Joseph boundary condition) are required to ensure continuity, 2) Darcy's law is incapable of capturing the flow behavior that occurs near the porous and free-flow region interface, and 3) they recommended the use of Brinkman's equation instead of Darcy's law as it is capable of capturing the flow behavior near the interfaces (Gartling et al., 1996). They cited the work of Martys et al. as a proof of the capability of the Brinkman's equation to model the flow near the interfaces (Martys, Bentz, & Garboczi, 1994). It is clear from the work of Gartling et al. that

formulating the Darcy-Stoke model is challenging due to the jump conditions, and its accuracy in capturing the fluid flow behavior is questionable due to the issue of the flow near the interfaces as can be seen in Figure 7.

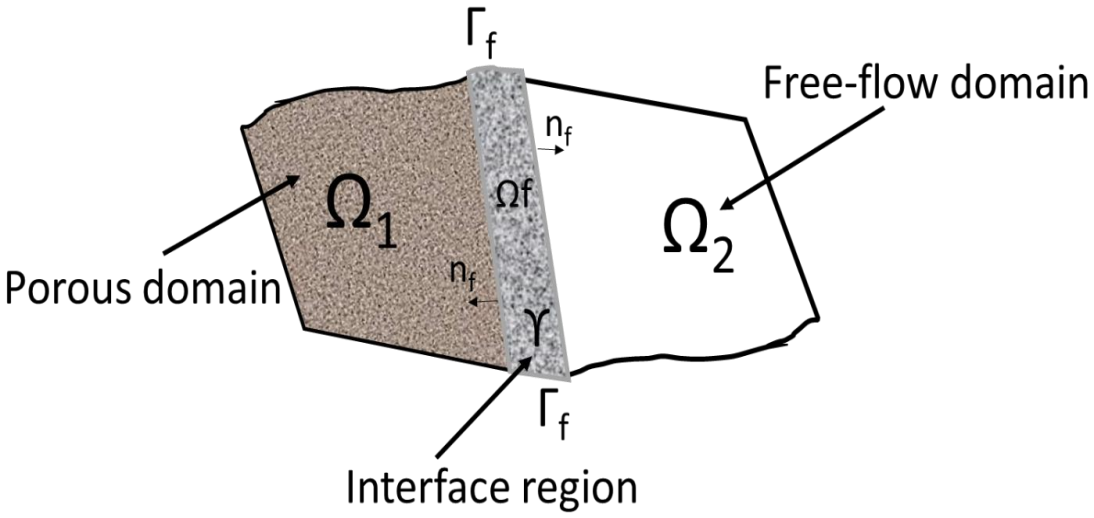

Figure 7: Porous and free-flow domains and interfaces

In 2002, Layton et al. studied mathematically the flow transport between surface water and groundwater by using the Stokes equation for viscous flow and Darcy's law for porous medium as can be seen in Figure 8 (Layton, Schieweck, & Yotov, 2002).

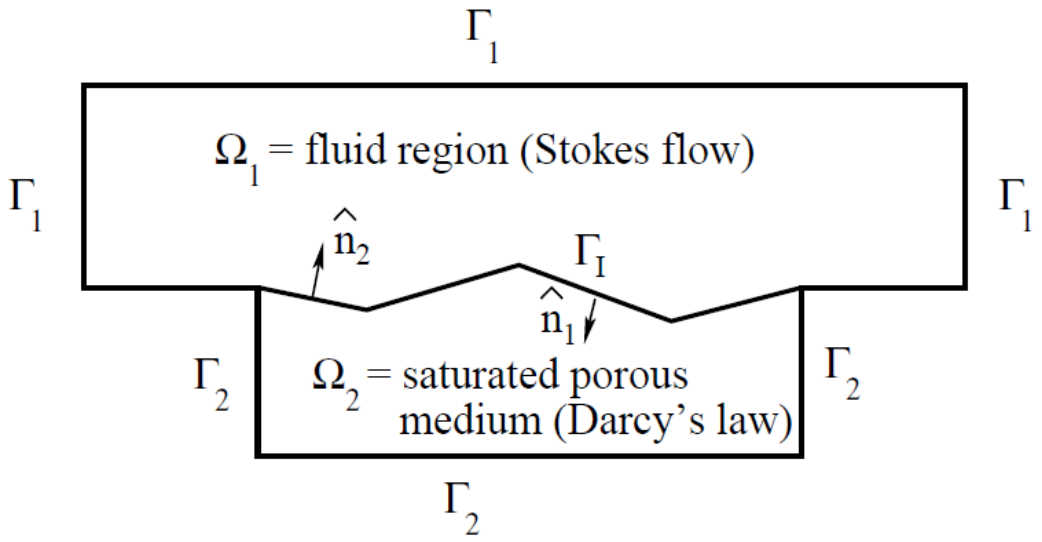

Figure 8: flow of surface water and groundwater as described by Layton et al. mathematical model (Layton et al., 2002)

Layton et al. coupled the Stokes equation and Darcy's law, and they proposed the use of the Beavers-Joseph-Saffman boundary condition to handle the flow behavior across the interface. Layton et al. derived the governing equations and analyzed them theoretically using the FEM to study the discontinuity of the flow between the two regions. Layton et al. concluded: 1) the coupling must occur across the interface with correct conditions and balance of normal forces to ensure the continuity of mass and fluid volume, and 2) the mathematical difficulties that is involved in the coupling process does not occur in the Brinkman's formulation (Layton et al., 2002). The work of Layton et al. shows mathematically: 1) the necessity of using correct boundary conditions at the interfaces, and 2) some of the mathematical complexity during the coupling process of Stokes equation and Darcy's law can be avoided if Brinkman's equation is used citing the work of Angot and Jäger & Mikelić (Angot, 1999; Jager & Mikelic, 2000).

In 2008, Cao et al. extended the work of Layton et al. for the time-dependent case for the groundwater problem, and their findings were similar to the findings of Layton et al. (Cao,

Gunzburger, Hua, & Wang, 2008). In 2011, Chen et al. further extended the work on the groundwater problem to study the convergence issues, and they concluded that convergence can be achieved regardless of mesh size if appropriate conditions are used during the formulation of the Darcy-Stokes equations (W. Chen, Gunzburger, Hua, & Wang, 2011). It is worthy to mention that the work of Layton et al., Cao et al. and Chen et al. mainly contains theorems and lemmas and without any computational results presented.

Arbogast et al. were among the first to study the Darcy-Stokes model and flow behavior in vuggy carbonate rocks (Arbogast & Lehr, 2006). The work of Arbogast et al. is also pure mathematics. Arbogast et al. studied the flow in the porous domain with Darcy's law on a macroscopic scale, and the flow in the vugs was modeled on a microscopic scale using the Stokes equation. They developed a way to generalize the two-scale medium and ensure convergence at the interface by homogenizing the system and using an effective permeability value, which is an average of the two extremes. Arbogast et al. concluded 1) flow in the direction of the interconnected vugs shows Poiseuille flow behavior with low effective permeability value, and 2) the behavior of the alternating flow from vugs to matrix represents a flow behavior in which the vugs have infinite permeability (Arbogast & Lehr, 2006). In 2007, Arbogast et al. extended the work to solve the model numerically (Arbogast & Brunson, 2007). They used the finite element method with different element types representing the porous and free-flow domains, and they used the discontinuous Galerkin method. Arbogast et al. studied the convergence and the order of error by experimenting with different spaces and different gridding systems. They concluded that modifying the finite element spaces result in simpler implementation; however, it does not appear to change the final solutions (Arbogast & Brunson, 2007). Those studies were conducted numerically supported with lemmas and no computational results were conducted.

In 2009, Peng et al. conducted a computational study using the Darcy-Stokes model to track the flow in a vuggy reservoir as the extended Darcy models failed to capture the rapid water breakthrough (Peng, Du, Liang, & Qi, 2009). Peng et al. used the streamline simulation technique to develop their model instead of cell-based simulation techniques as can be seem in Figure 9. Peng et al. concluded 1) the extended Darcy models and the Darcy-Stokes model gave similar results for flow in the porous region, and 2) the extended Darcy models failed to capture the displacement front in the vuggy reservoir while the Darcy-Stokes model was capable of capturing the displacement front, and the model better explained the early water breakthrough as can be seen in Figure 10 (Peng et al., 2009).

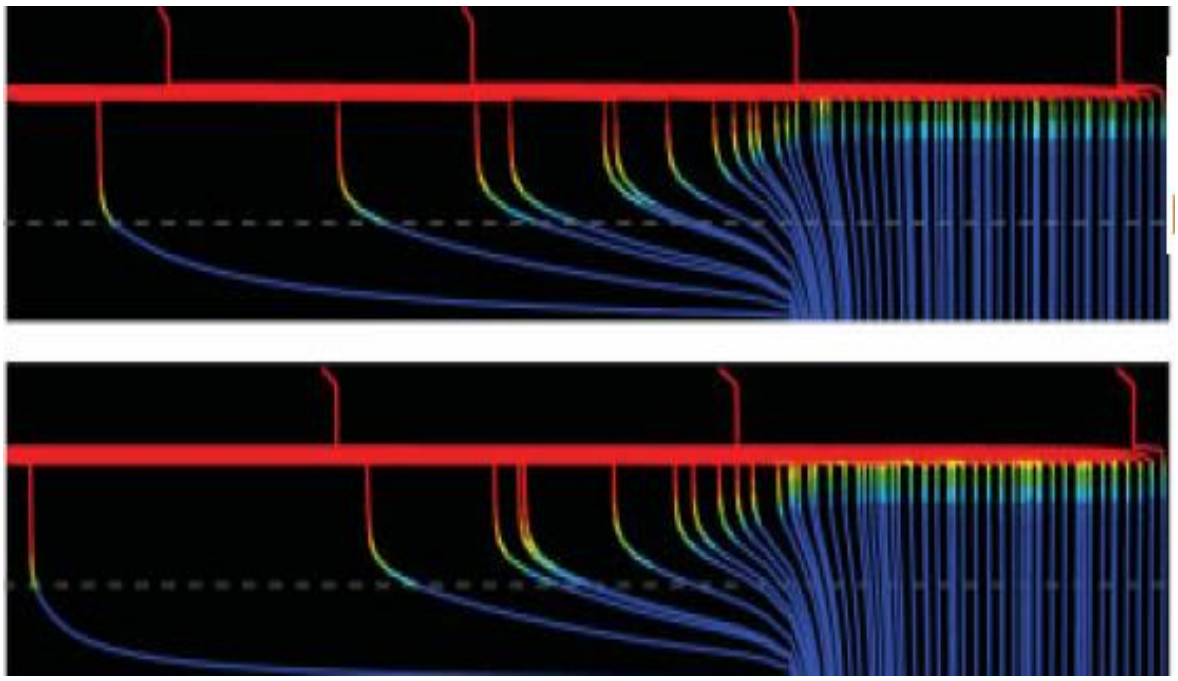

Figure 9: Peng et al. streamline model for Darcy-Stokes (top) and extended Darcy (bottom) (Peng et al., 2009)

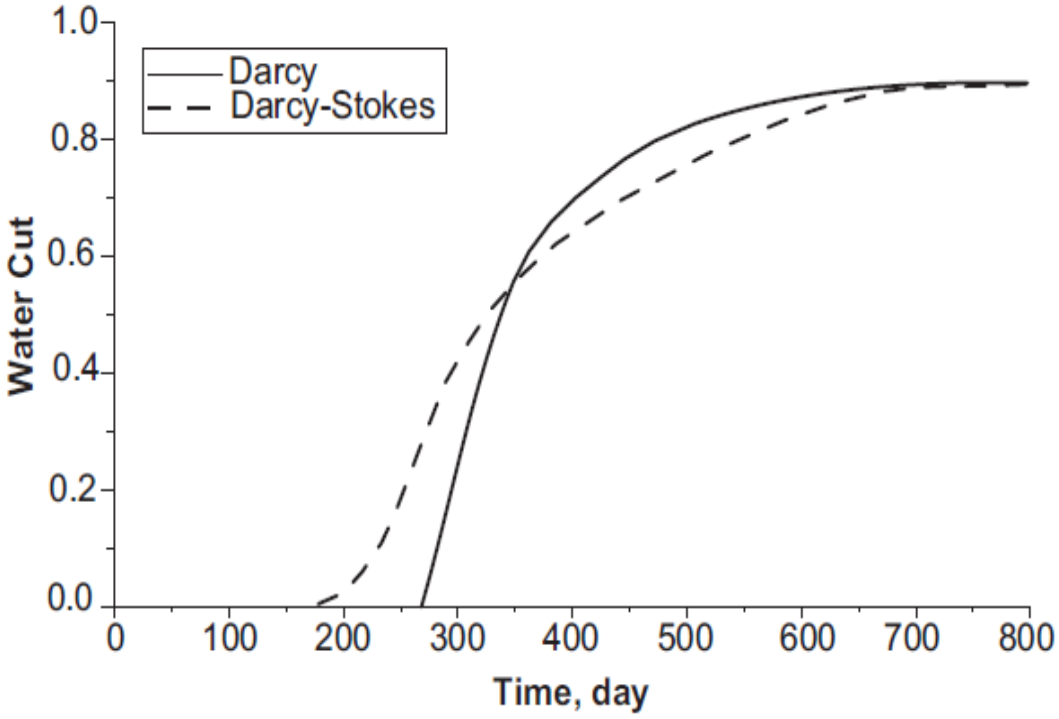

Figure 10: water breakthrough of Peng et al. model (Peng et al., 2009)

To test their model, Peng et al. used unfilled large-scale vugs to simulate the flow in the free-flow region; in reality, the vugs are in microscale and could be filled with fluid. They also used the streamline simulation technique which has serious issues of mass conservation in fine-scale heterogeneous systems such as fractured-vuggy carbonate formations (Thiele, Batycky, & Fenwick, 2010).

In 2010, Yao et al. developed a discontinuous model that consists of macro fractures and vugs and porous matrix system as can be seen in Figure 11 (Yao et al., 2010).

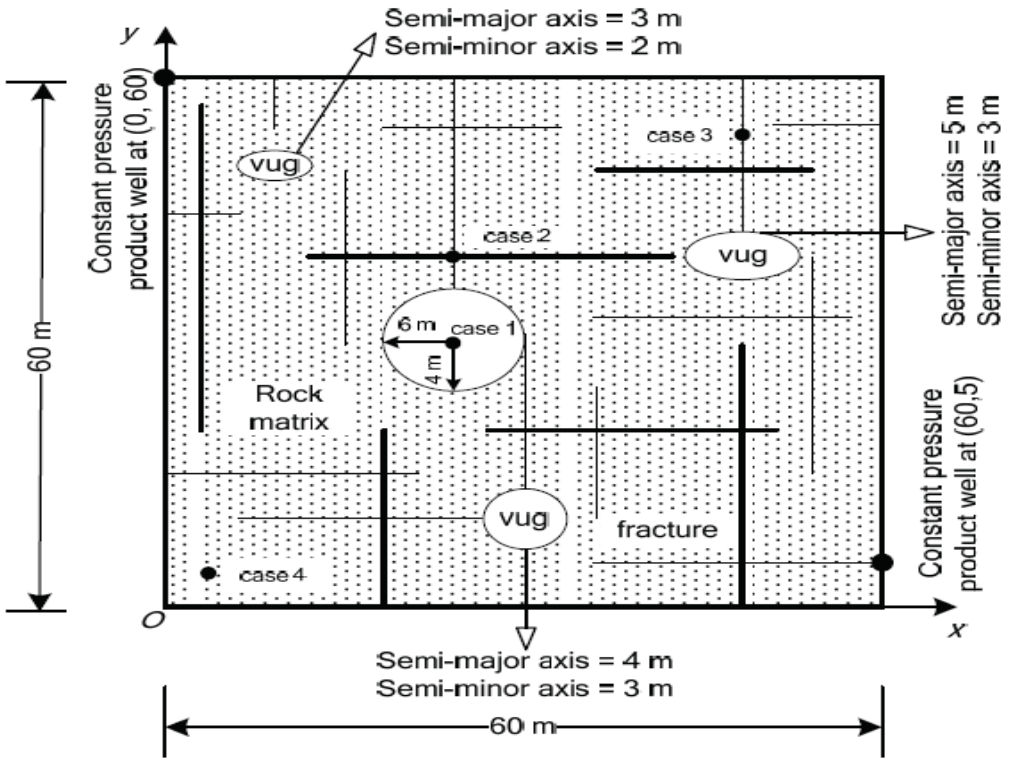

Figure 11: Yao et al. geometry (Yao et al., 2010)

Yao et al. used the Navier-Stokes equations to model the flow in the fractures and vugs, and the flow in the porous matrix was modeled by Darcy's law, and the Beavers-Joseph-Saffman condition was implemented at the interface as can be seen in Figure 11. Yao et al. ran a numerical simulation, and they concluded from their preliminary results that: 1) the flow behavior in the free-flow domain cannot be captured by the use of the continuum approach, 2) the free-flow domain dictates the overall flow behavior as can be seen in Figure 12, and 3) the pressure transmits fast through the vugs (Yao et al., 2010). The Yao et al. model was developed as a discontinuous model; however, they used the finite element method with the standard Galerkin method, which does not perfectly capture the physics of the open regions, instead of the discontinuous Galerkin method, and they also modeled the vugs as macro system instead of fine-scale system, and their porous matrix system was homogeneous.

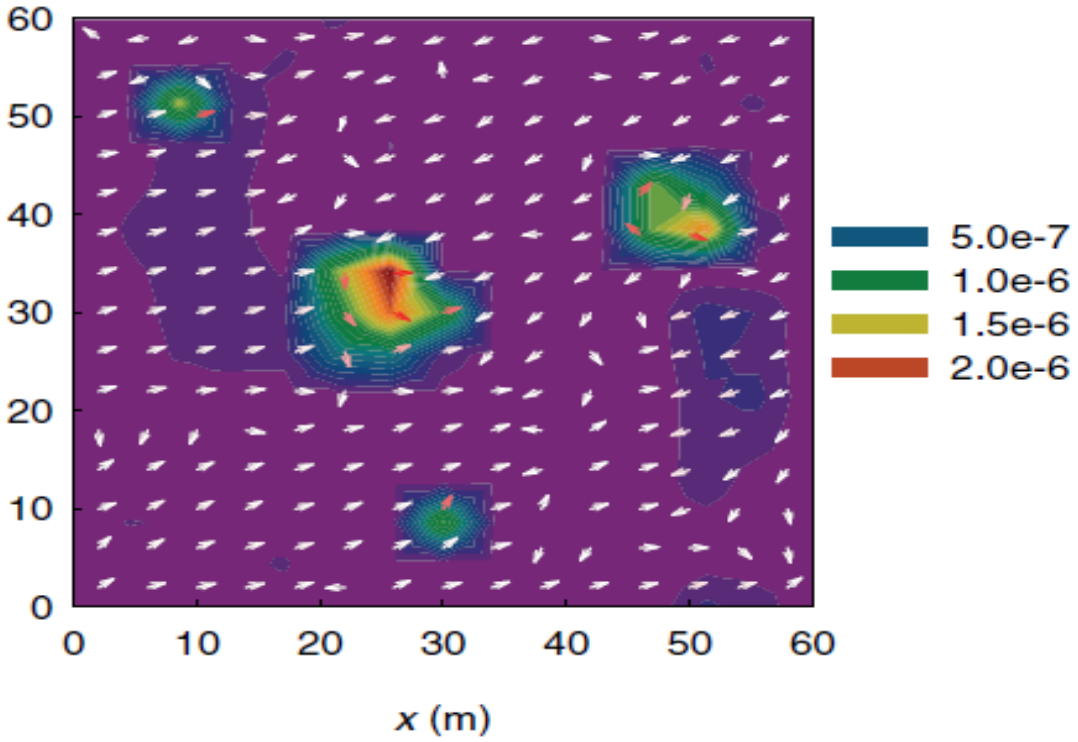

Figure 12: Velocity profile of Yao et al. model (Yao et al., 2010)

The slip and jump conditions on the interface between the two flows in the Darcy-Stokes model as shown in Figure 13 and the coupling of the two equations is an active area of research, especially from the mathematical point of view, to justify the usage of boundary conditions such as the Beavers-Joseph-Saffman boundary condition (Morales, 2013; Morales & Showalter, 2017).

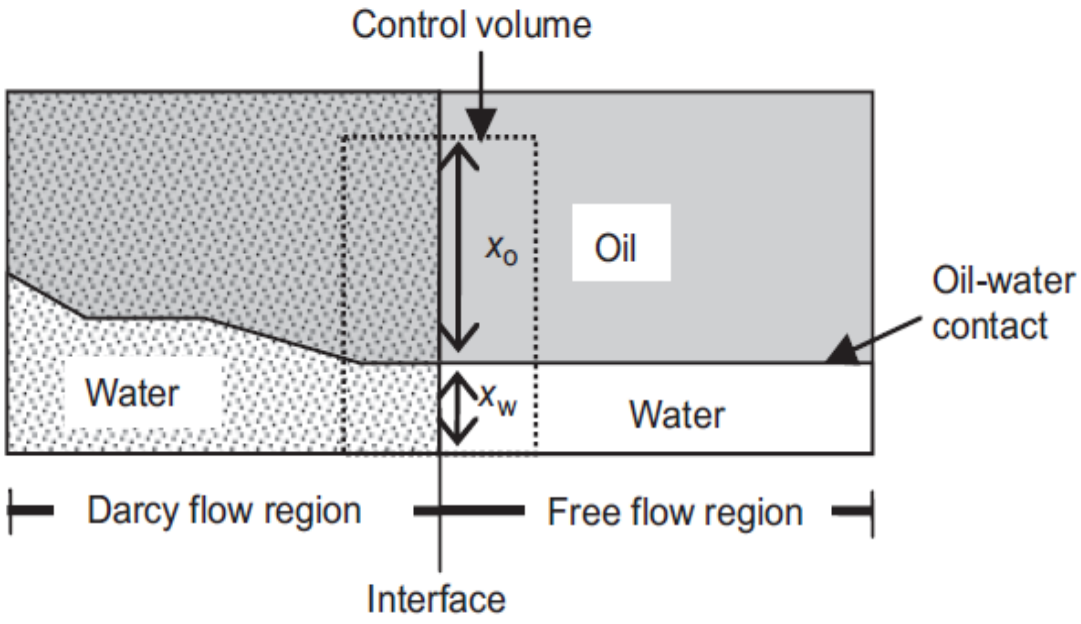

Figure 13: Porous and free-flow domains and interfaces (Peng et al., 2009)

2.1.3 Stokes-Brinkman Model

The Stokes-Brinkman model, which is also known as the Brinkman equation and the Darcy-Stokes-Brinkman model, was developed in 1947 by Brinkman who was an engineer at Royal Dutch Shell, Eq. 2 (Brinkman, 1947). Brinkman combined Darcy's law and Stokes equation into one equation by introducing a term called the effective viscosity (μ^*). Eq. 2 reduces to Darcy's law by making the effective viscosity (μ^*) equal to zero. It also converges to Stokes equation by making the effective viscosity (μ^*) equal to the fluid viscosity (μ) and applying a large permeability value (k➔∞) for fractures and vugs. Brinkman, after comparing results from experiments and analytical solutions, recommended to make the value of the effective viscosity equal to the normal fluid viscosity value (i.e., $\mu^* = \mu$) (Brinkman, 1947). The work of Brinkman provided an approach to model the two flow behaviors with a single equation; hence, the complexities in the Darcy-Stokes model due to the coupling process and the interface interaction

boundary conditions are avoided in the Stokes-Brinkman model (Gulbransen et al., 2010; Popov et al., 2009; Salinger et al., 1994).

$$u + \frac{k}{\mu}(\nabla p - \rho g - \mu^* \Delta u) = 0 \qquad \textit{Eq. 2}$$

where u is the velocity vector, k is the permeability tensor, μ is the fluid viscosity, ρ is the fluid density, g is the gravity vector, p is the pore pressure and μ^* is the effective viscosity

The Stokes-Brinkman model has been compared against the Darcy-Stokes model, and for the tested cases, it gave similar results as the Darcy-Stokes model (Popov et al., 2009; Salinger et al., 1994). In addition to the discussed models in the previous section, there are three publications using the Stokes-Brinkman model that are worthy of mentioning.

In 2007, Popov et al. were among the first to use the Stokes-Brinkman model to simulate the fluid flow behavior in naturally fractured vuggy carbonate reservoirs (Popov et al., 2007). Popov et al. developed the model with steady-state flow and used the finite element method to solve the equations numerically. First, they used a simple 3D geometry to test the model with a single large-scale vug in the center of the geometry as can be seen in Figure 14. Then, they tested the model in structures with fractures and vugs. Popov et al. concluded: 1) Stokes-Brinkman model provides a unified approach to model the flow behavior in porous and free-flow regions, 2) geometries with large-scale isolated vugs can be modeled with Darcy's law providing an effective permeability value, and 3) geometries with fractures and connected vugs significantly affect the flow behavior (Popov et al., 2007, 2009). The model of Popov et al. was developed with steady-state flow, and upscale homogenization procedures were practiced; hence, the findings could be different in systems with fine-scale heterogeneities.

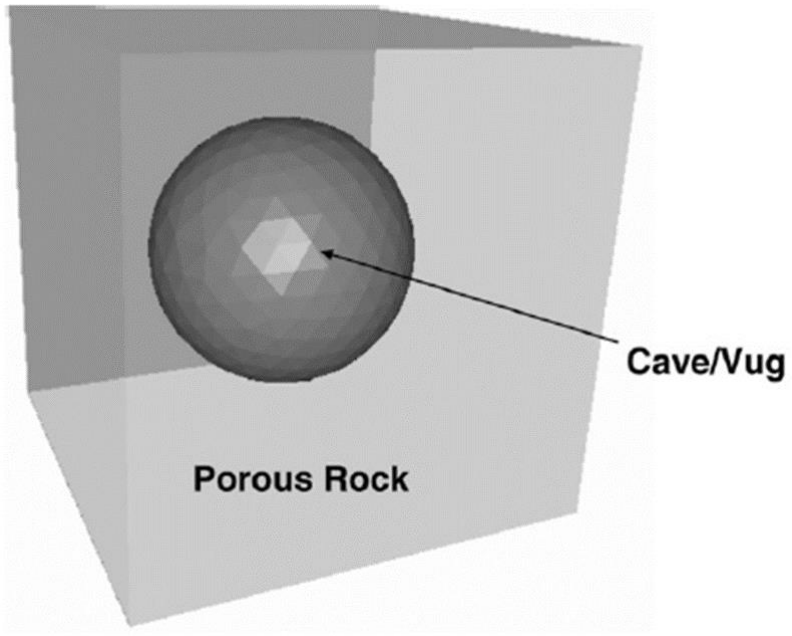

Figure 14: Simple geometry of Popov et al. model (Popov et al., 2009)

In 2010, Gulbransen et al. developed a multi-scale model using multi-scale mixed finite element to study the flow behavior in fractured-vuggy formations (Gulbransen et al., 2010). Gulbransen et al. concluded that: 1) fine-scale heterogeneities can be captured using Darcy's law if multi-scale elements are used, 2) the Stokes-Brinkman model results in accurate solutions but requires high number of degrees of freedom to capture fine-scale heterogeneities in large geometries, and 3) the combination of Stokes-Brinkman model and multi-scale mixed finite element is a promising and more efficient technique to model the flow behavior with high-resolution (Gulbransen et al., 2010). The Gulbransen et al. model is based on steady-state flow and also requires solving the Stokes-Brinkman model first to get accurate basis functions for the mixed finite element method.

In 2015, He et al. developed a transient flow model using the Stokes-Brinkman model and the finite difference method (He et al., 2015). He et al. concluded: 1) the transient Stokes-Brinkman

model accurately describes the fluid flow behavior in both the porous and free-flow regions, and 2) the connected vugs and fractures significantly change the fluid flow pattern while isolated vugs do not interfere that much with the fluid flow pattern (He et al., 2015). He et al. also studied the pressure profiles of a homogeneous system with no fractures and vugs and a heterogeneous system with fractures and vugs. To examine the pressure profiles, they introduced an injection well and a production well at opposite corners of the two-dimensional geometry as can be seen in Figure 15. Figure 15 shows the radial flow pattern and the pressure profile for the homogeneous system.

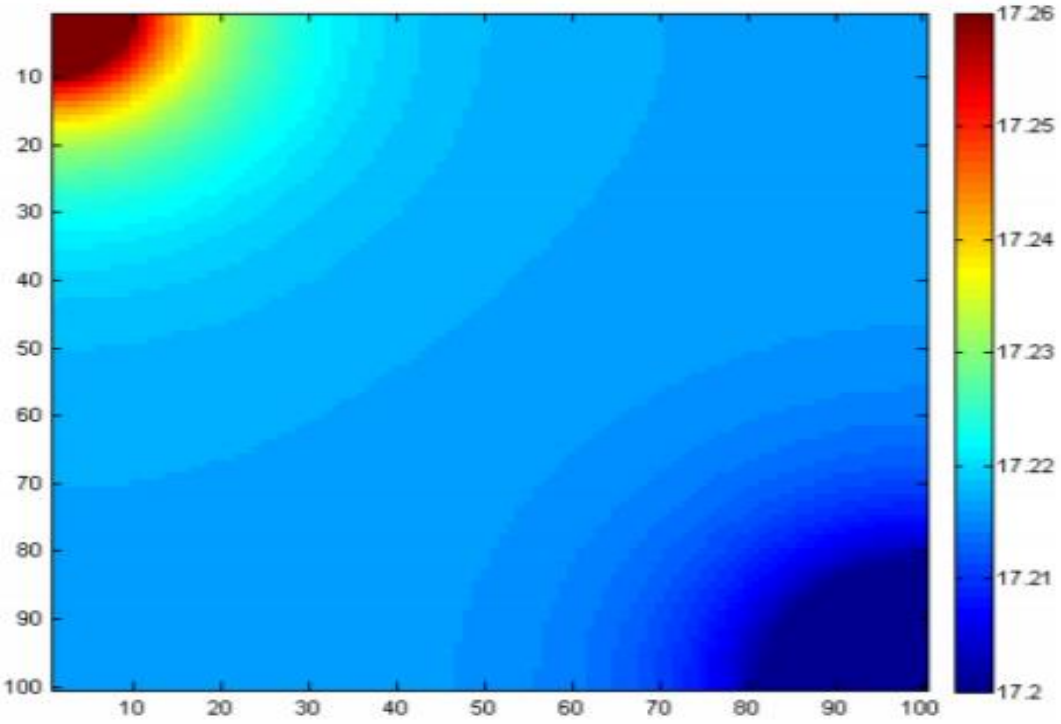

Figure 15: pressure profile of homogeneous test of He et al. model (He et al., 2015)

For the heterogeneous test, He et al. introduced fractures and vugs to their two-dimensional model as can be seen in Figure 16. He et al. concluded that the free-flow regions significantly change the pressure profile as can be seen in Figure 17 (He et al., 2015).

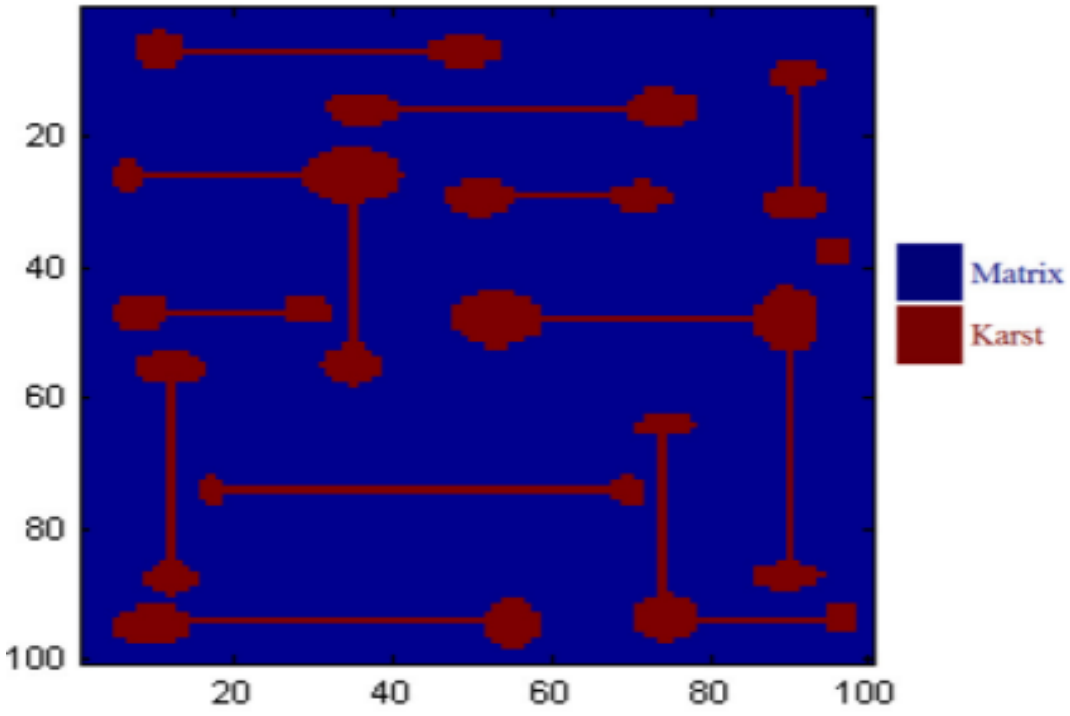

Figure 16: Heterogeneous geometry of He et al. model (He et al., 2015)

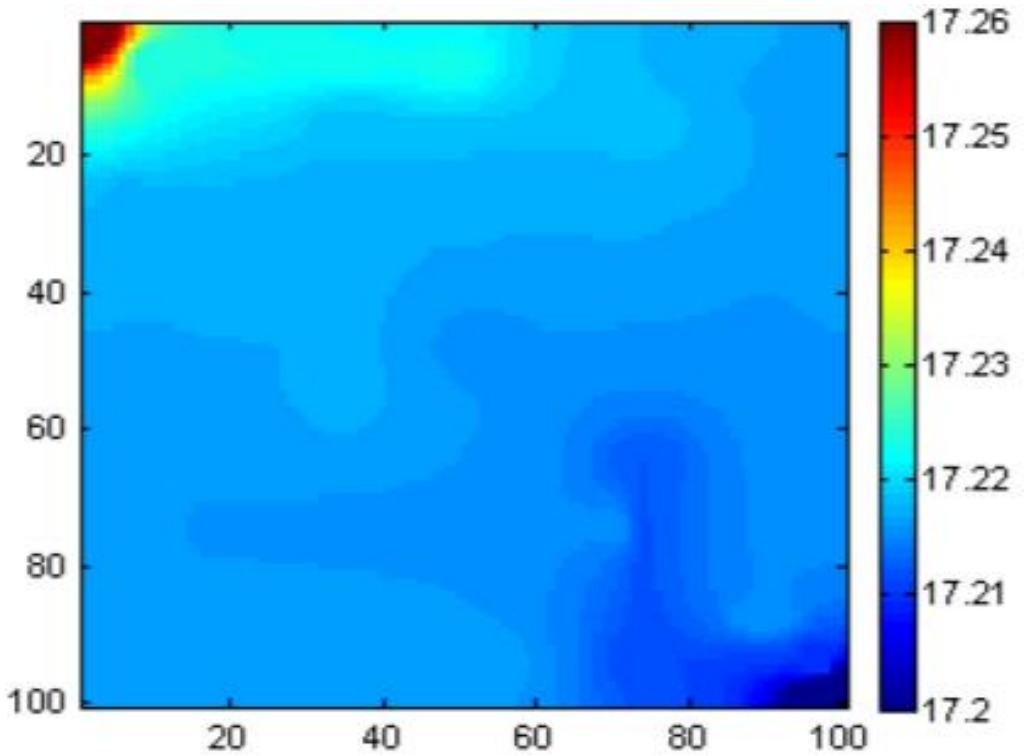

Figure 17: pressure profile of heterogeneous geometry of He et al. model (He et al., 2015)

He et al. model was a two-dimensional model developed by the finite difference method, and they suggested reformulating the finite difference scheme to optimize the process and to make the model more efficient as the model was computationally intensive even though a relatively simple two-dimensional geometry was used to test the model.

2.2 Recent Models

Developing sophisticated models to simulate the fluid flow in karst reservoirs to predict the flow behavior and to estimate the properties of those reservoirs (e.g., porosity and permeability) has become a reality due to the advancement of the computational power and the improvements in the numerical techniques. One of the challenges of simulating the fluid flow in fractured-vuggy carbonate rocks is the complex variety of the parameters' values (e.g., permeability) in the reservoir domain (Benner, Dolgov, Onwunta, & Stoll, 2016). For example, extremely high permeability in the fractures and extremely low permeability values in the matrix system; this significant spatial variation in permeability make the numerical models unstable as they become stuck in local minimum points; thus, they lead to unrealistic results. To overcome this challenge, the numerical models must be developed with 1) proper preconditioner methods and 2) they need to be constructed with stable numerical techniques. The preconditioners assist in solving the system of the linear equations, which are achieved after the governing PDEs are put in a numerical form.

Due to the computational challenges in developing the Brinkman model numerically, Youssef et al. developed a model to simulate the fluid flow in karst formations using an estimated-distributed permeability approach with Darcy's model (Youssef & Awotunde, 2019). Their approach is based on calculating the permeability in the free-flow regions using analytical methods and then the calculated permeability is distributed in the free-flow regions and near the boundary

of the porous region and free-flow region. After that, Darcy's law is used to simulate the flow in the entire domain. Their model is abbreviated as DMEPD, which is Darcy Model with Estimated Permeability Distribution. Youssef et al. compared their model against two-dimensional models and found out that the results are in excellent agreement as can be seen in Figure 18 (Youssef & Awotunde, 2019).

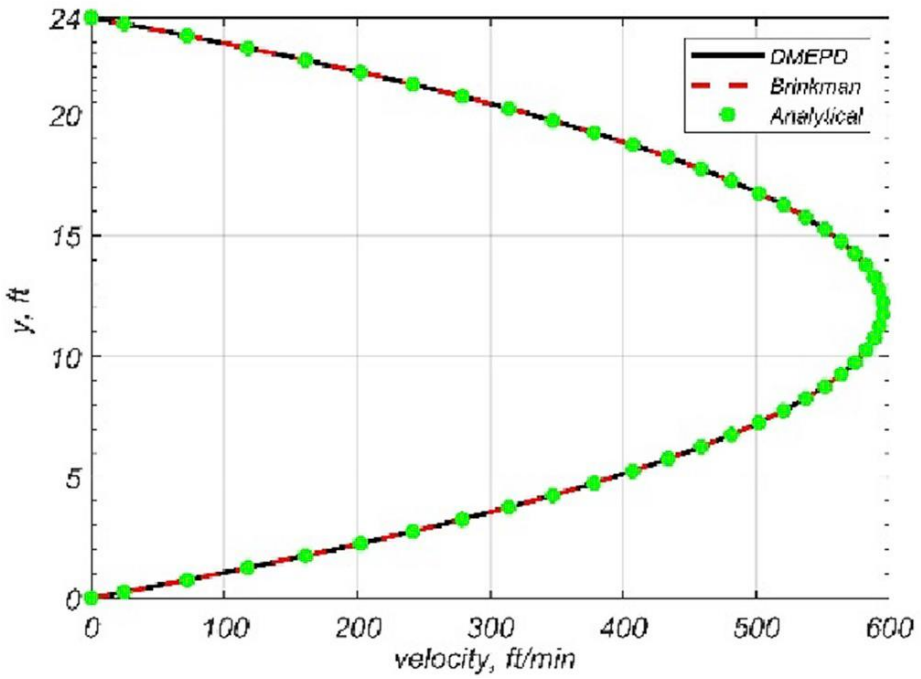

Figure 18: DMEPD model comparison (Youssef & Awotunde, 2019)

The advantages of Youssef et al. model are: 1) the need of dealing with flow in the boundaries of porous region and free-flow region is eliminated and 2) the model require limited computational power to solve. However, the main disadvantages of their model are: 1) the model does not yield accurate results if the flow in the free-flow regions and porous regions is changed rapidly as the calculated and distributed permeability would not be accurate, 2) the model is only applicable for two-dimensional flow problems as the analytical approach to obtain the permeability

becomes complicated for three-dimensional problems, 3) the model should be used only if the open regions (i.e., vugs and fractures) are parallel with the porous region and 4) for certain cases, small time-step is needed to ensure convergence and stability (Youssef & Awotunde, 2019).

In 2020, Hallack et al. developed one-dimensional and two-dimensional single-phase and two-phase models using Darcy's law and the Brinkman formulation (Hallack, de Araujo Cavalcante Filho, & Couto, 2020). They used the finite difference method (FDM) to develop the model numerically. Hallack et al. developed their model in one-dimensional and two-dimensional to compare it against analytical solutions, and they found the models' results are in good agreement against the analytical solutions as can be seen in Figure 19.

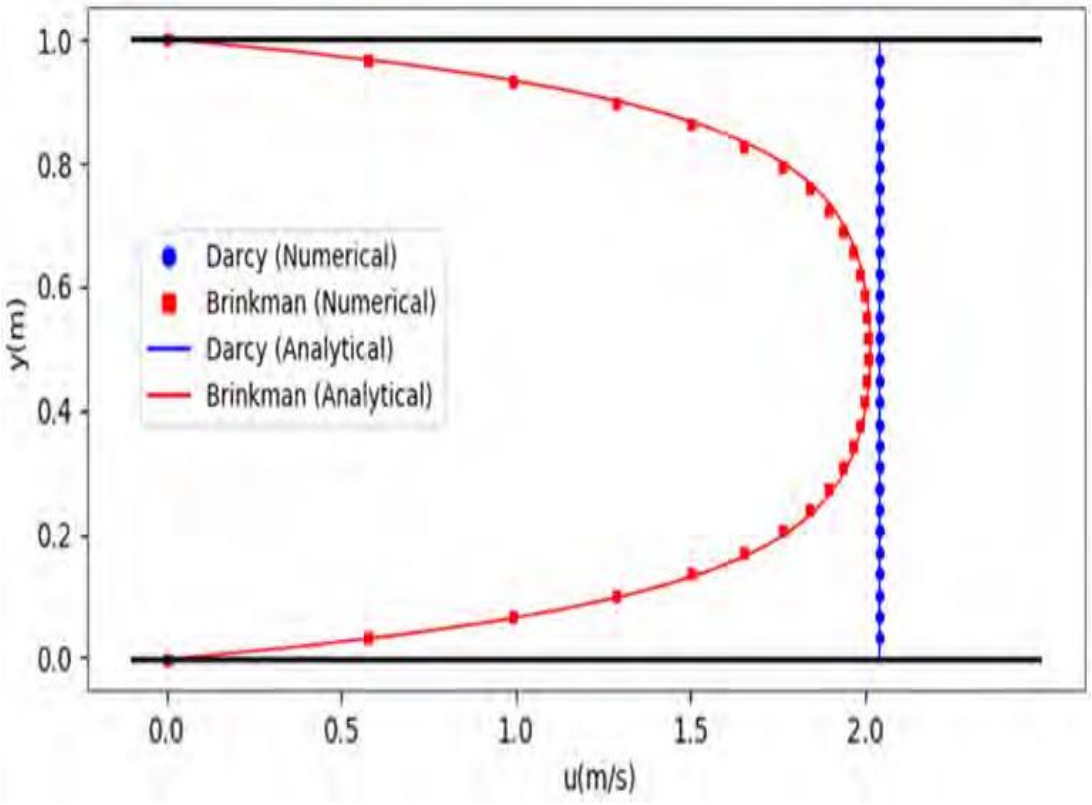

Figure 19: Hallack et al. model (Hallack et al., 2020)

Hallack et al. concluded that the velocity profile of both Darcy's law and the Brinkman formulation is consistent and accurate for the porous region; however, they differ in the free-flow regions as can be seen in Figure 20 (Hallack et al., 2020).

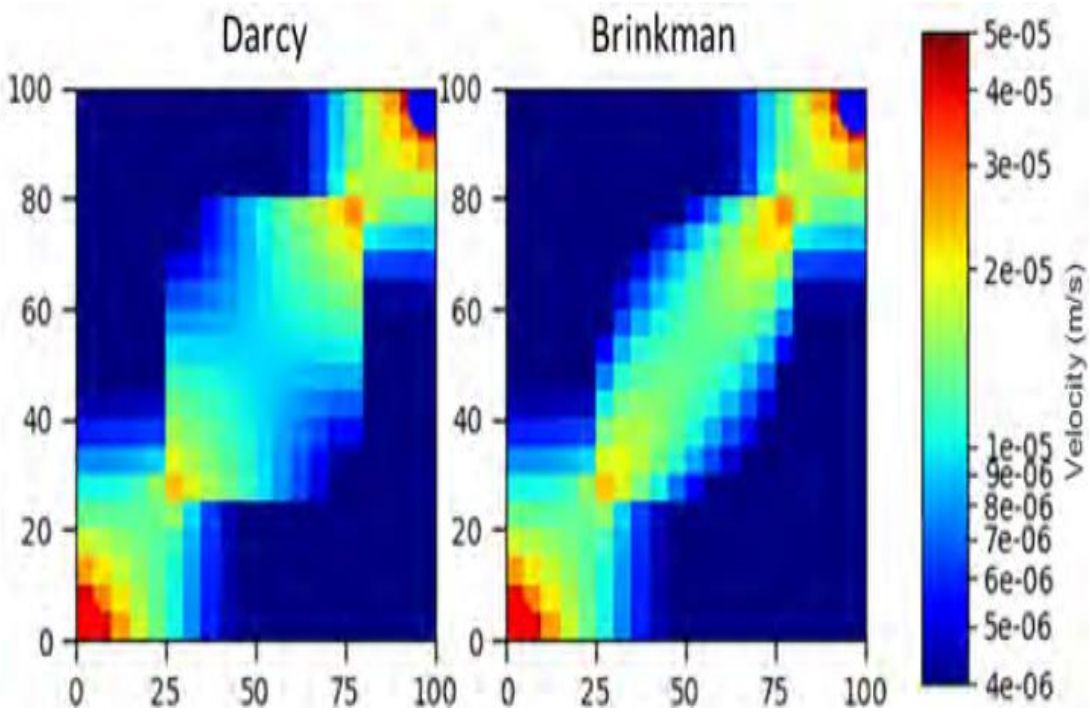

Figure 20: Velocity profile of Hallack et al. model (Hallack et al., 2020)

Hallack et al. also studied the saturation profiles and concluded that the Brinkman formulation provides better results for the displacement efficiency, and they also saw different recovery factor estimations when Darcy's law is used and when the Brinkman formulation is used as can be seen in Figure 21.

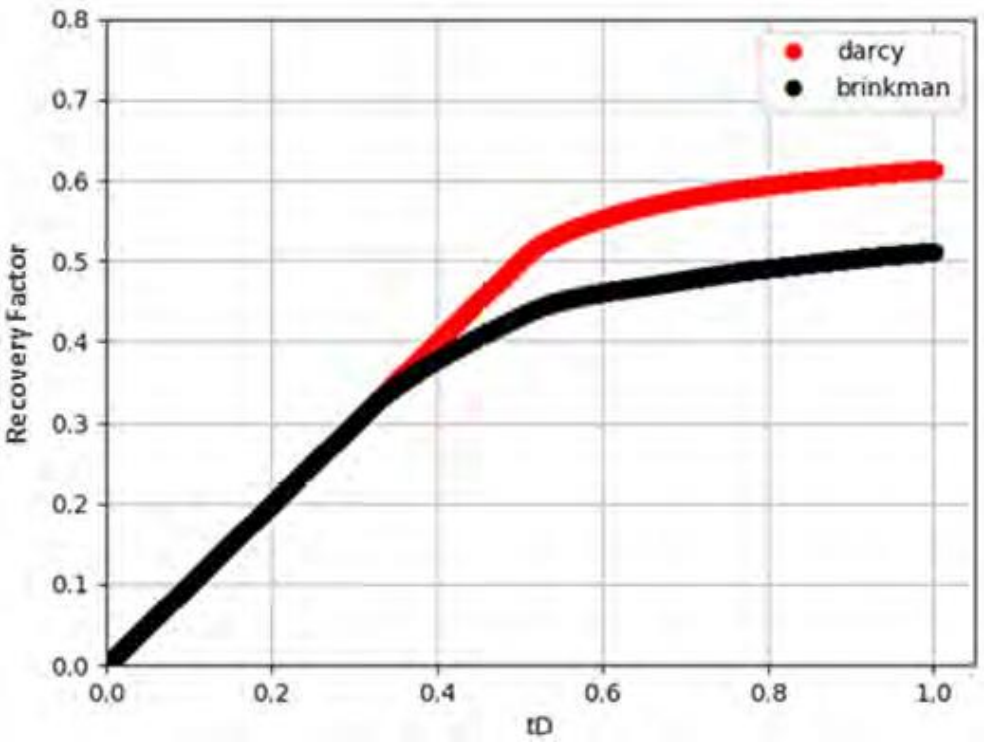

Figure 21: Recovery factor of Hallack et al. study (Hallack et al., 2020)

The Hallack et al. model is a valuable addition to the literature as it provides numerical results of both the Darcy formulation and the Brinkman formulation for single-phase and two-phase. However, their model is designed for basic one-dimensional and two-dimensional geometries (Hallack et al., 2020); hence, further work would be needed to adapt this model and incorporate it in the advanced simulators.

There are also recent proposed methods that consider the coupling of the Brinkman models and the chemical transport models to estimate both the flow and the concentration profiles for when chemical reactions are involved (Rathish Kumar & Chowdhury, 2019).

Yuan et al. developed a three-dimensional model of radial flow to examine the matrix acidizing process with wormholes' effects by using the Brinkman equations in cylindrical coordinates coupled with a reactive transport model that considered only one mineral (i.e., calcite)

(Yuan & Qin, 2020). In their study, Yuan et al. focused on the reactive transport model to examine the dissolution patterns that are caused by the radial flow while injecting acid and by experimenting with different Damköhler number and Peclet number values (Yuan & Qin, 2020). Yuan et al. geometry is synthetic with only one dominant mineral; hence, it does not represent actual core samples or carbonate formations. However, their model provides a roadmap to develop advanced matrix acidizing models.

Carrillo et al. developed a model using the software package OpenFOAM to predict the flow pattern through and around the free-flow regions as can be seen in Figure 22 (Carrillo & Bourg, 2019).

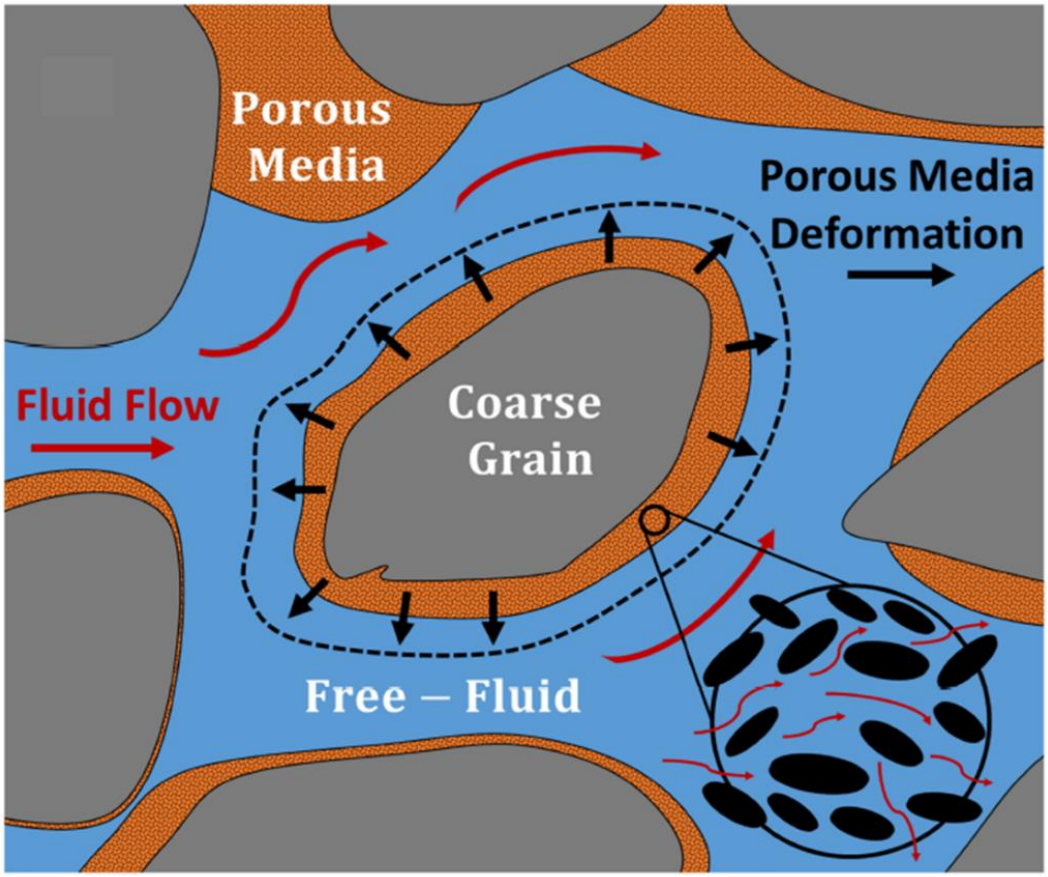

Figure 22: Conceptual representation of Carrillo et al. model (Carrillo & Bourg, 2019)

Carrillo et al. utilized the Brinkman equation with geomechanical effects using a volume averaging technique. Carrillo et al. tested the model and verified its applicability in a porous media with clay-rich formations. However, the limitations of their model are: 1) the model require accurate description of the permeability and rheology in the free-flow regions, 2) the model can be used only if the pores are significantly large as it is a requirement for the volume averaging technique, 3) the model works only for single-phase fully saturated system and 4) their model does not capture the fine scale deformations in heterogeneous matrix system (Carrillo & Bourg, 2019).

Formulating the Brinkman equation to get accurate fluid flow patterns in heterogeneous complex systems require the use of high number of degrees of freedom (DOFs) which means intensive computational powers would be needed to run the simulations.

Williamson et al. proposed an adaptive mesh refinement approach to capture the flow behavior around an obstacle in porous media using the Brinkman formulation as can be seen in Figure 23 (Williamson, Burda, & Sousedík, 2019). They experimented with several mesh refinements as can be seen in Figure 24.

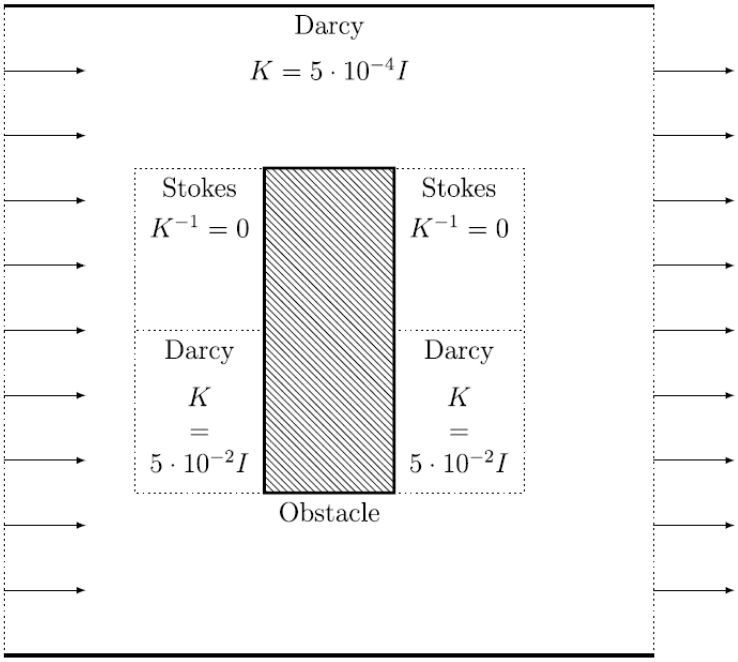

Figure 23: Williamson et al. geometry (Williamson et al., 2019)

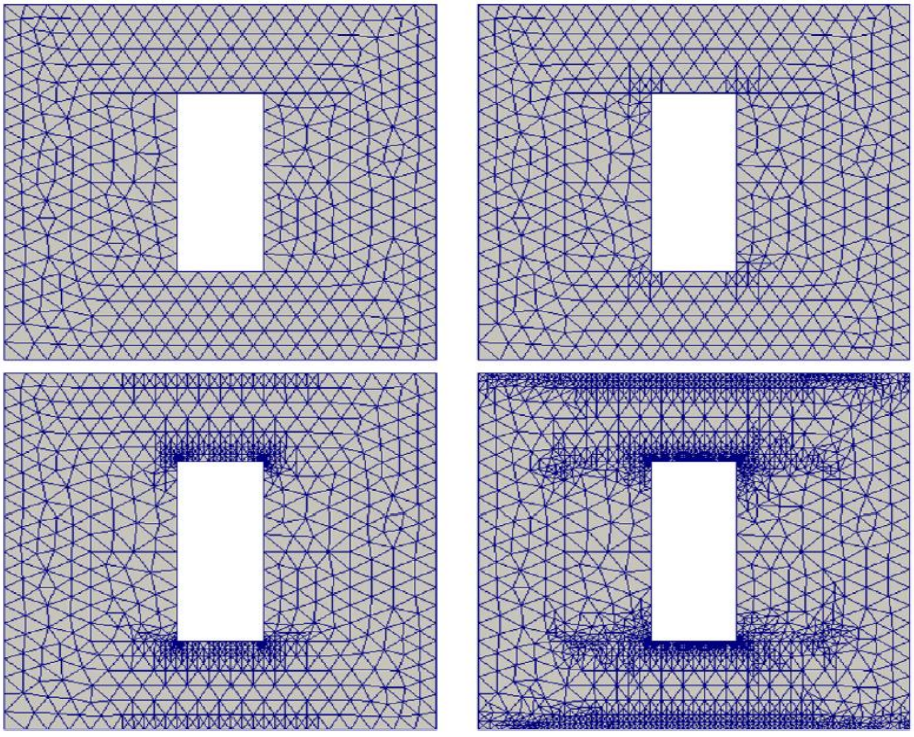

Figure 24: Mesh refinement around the obstacle for Williamson et al. model (Williamson et al., 2019)

Williamson et al. concluded that the mesh refinement significantly improved the results of the flow pattern around the obstacle as can be seen in Figure 25; however, they reported that mesh refinement substantially increased the number of iterations required for the model to converge (Williamson et al., 2019). Thus, the mesh should be refined while considering the computational time.

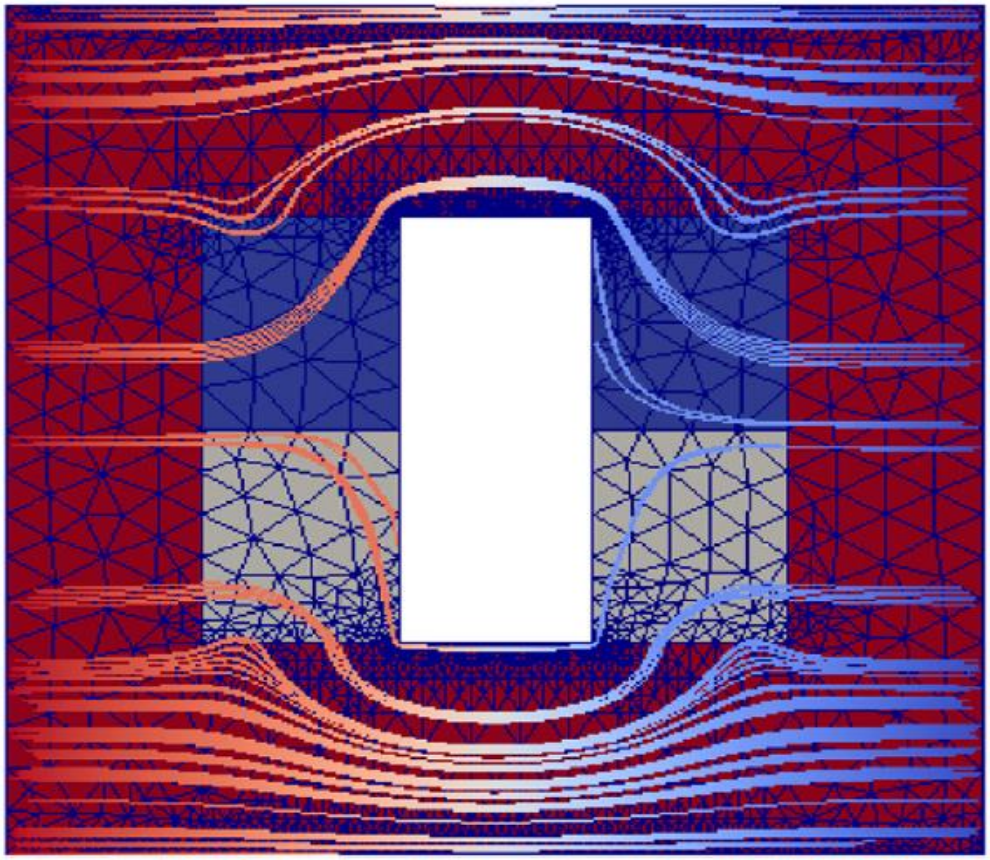

Figure 25: Flow pattern around the obstacle for Williamson et al. model (Williamson et al., 2019)

Zhao et al. recently proposed a method to overcome the need of intensive computational power to formulate the Brinkman equation by the use of discontinuous Galerkin method with specific mesh types as shown in Figure 26 (Zhao, Chung, & Lam, 2020).

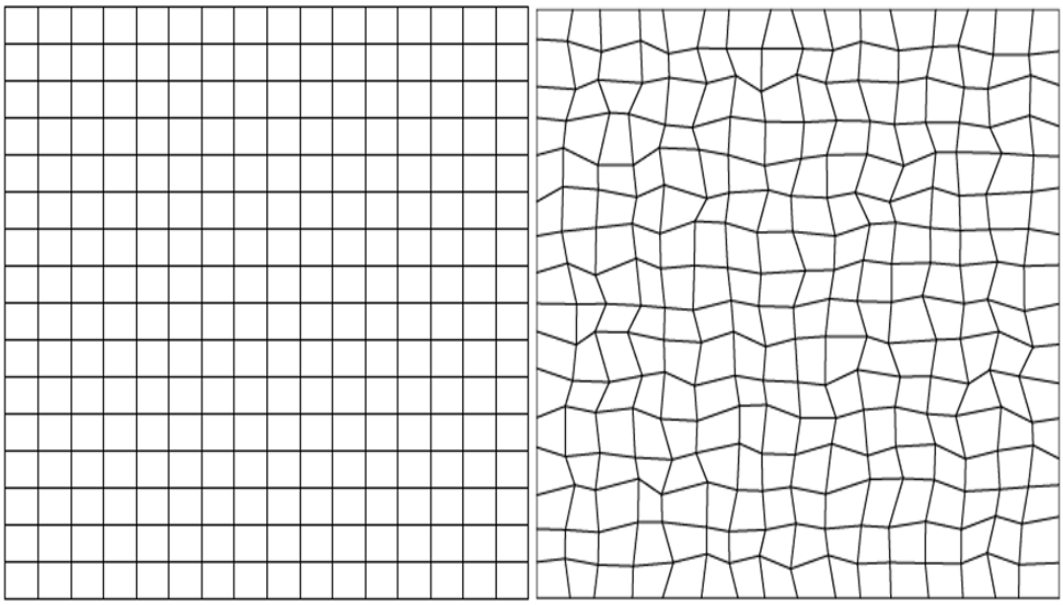

Figure 26: Square mesh type (left) distorted mesh type (right) (Zhao et al., 2020)

Zhao et al. studied mathematically the convergence rate of the Brinkman formulation when the flow becomes Darcy dominant, and they reported that their model yields accurate results (Zhao et al., 2020). Zhao et al. did not provide comprehensive numerical studies for complex carbonate formations with fine scale heterogeneities to support their findings.

Menke et al. used a stokes model and the Brinkman model to examine the permeability in the microporous regions of core samples (H. Menke, Gao, Linden, & Andrew, 2019; H. P. Menke, Gao, & Andrew, 2018). First, they captured the microporous regions by the use of X-Ray nano tomography (nano-XRM) and micro-CT images. Then, they built a porous network and estimated the porosity. Next, they estimated the permeability using the Kozeny-Carman porosity-permeability relationship as can be seen in Figure 27 (H. Menke et al., 2019)

To compare the results from the built microporous network and the Kozeny-Carman relationship, they used both the Stokes model as well as the Brinkman model to estimate the permeability.

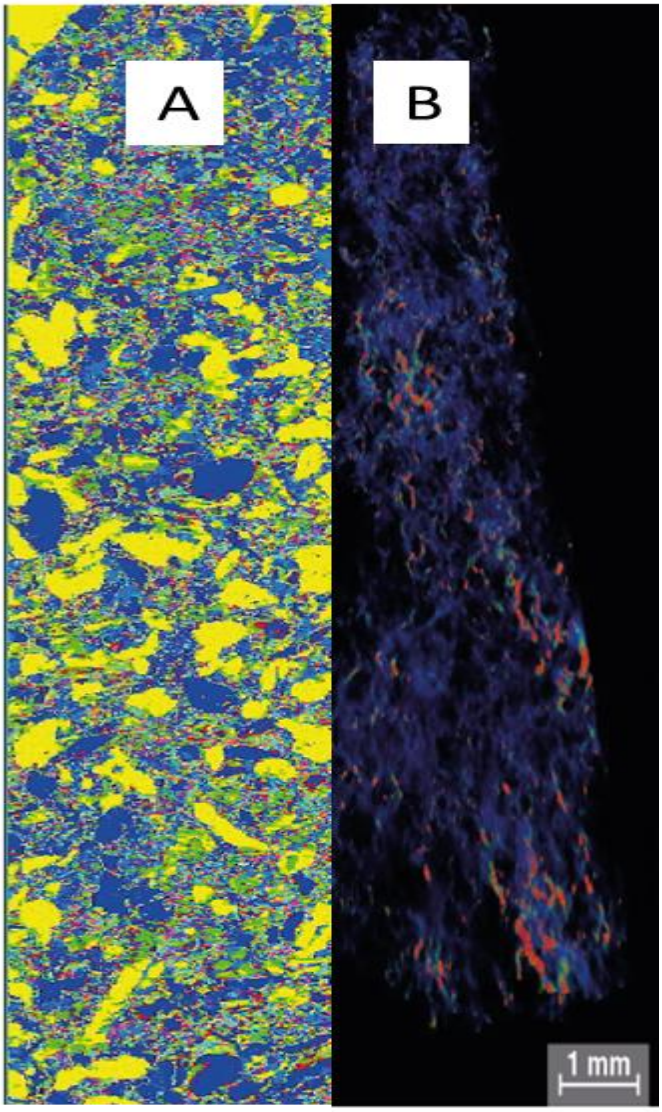

Figure 27: Menke et al. microporous network of grains and pores (A) and velocity profile (B) (H. Menke et al., 2019)

Menke et al. concluded that: 1) the Stokes model underestimated the permeability by about 50%, and 2) the relative permeability curve that was measured experimentally is in good agreement with the estimated relative permeability from the Brinkman model. However, they found out that the Brinkman model overestimates the permeability compared to the measured permeability from the built microporous network. They argued that the overestimated permeability occurred as the

microscopic network that was used to test the Brinkman flow over predicted the connectivity of the pores (H. Menke et al., 2019). The work of Menke et al. adds to the literature as it shows the potential of coupling lab experiments with the advanced flow models and the imaging techniques. However, their work was focused on flow in microporous regions, and they did not consider the fluid flow in both porous regions and free-flow regions. Furthermore, they used commercial software packages (i.e., Math2Market GeoDict) that are developed by the finite volume method to conduct their simulations.

Brinkman flow models have become promising techniques due to the advancement in the numerical methods and the computational powers over the years. Nowadays, the Brinkman models are being used in several different disciplines including the medical sector. For example, Ebenbeck et al. utilized a model that incorporate the Brinkman model to describe the velocity for tumor growth studies (Ebenbeck & Garcke, 2019).

In summary, the extended Darcy's models are considered to be the most convenient models to use as they are already implemented in the existing commercial simulators. However, they require representative effective values as inputs, which are difficult to find. This issue makes the extended Darcy models impractical to use in fractured-vuggy carbonate formations. On the other hand, formulating the Darcy-Stokes model is a complicated process, and the model is difficult to solve due to the flow interface interactions between the two models. The Darcy-Stokes model also requires detailed knowledge of the interface locations to implement the boundary conditions, which have to be obtained prior to solving the model. Furthermore, the Darcy-Stokes model requires that the vugs are free of obstacles in order to get accurate flow behavior (Popov et al., 2009). Consequently, the Brinkman model is the best available option to model the fluid flow behavior in complex and heterogeneous fractured-vuggy carbonate formations. Table 1 provides

a summary of the existing fluid flow models. It is important to mention that all the above discussed models do not fully consider the effects of geomechanics.

Table 1: Summary of fluid flow models

Method	Dual permeability	Averaged permeability	Darcy-Stokes	Brinkman
Description	Multiple values for porosity and permeability are assigned, and Darcy's law is used in the entire domain	A single effective value is assigned, and Darcy's law is used in the entire domain	Utilize Darcy's law for porous regions and Stokes model for free-flow regions	Combines Darcy's law and Stokes model into one equation
Advantages	Convenient models	The most basic models	Captures the flow in both the free-flow regions and porous regions	Eliminate the complexity of the flow interface interactions
Limitations	Results in misleading outcomes	Results in misleading outcomes	Requires the free-flow regions to be free of obstacles	Require high number of DOFs to capture effects of fine-scale heterogeneities

Challenges	Finding the representative values	Finding the single representative value	Complicated due to the interactions near the boundary	Computationally demanding
Comment	Do not accurately capture the fluid flow profile	Do not accurately capture the fluid flow profile	Accurately capture the flow profiles but complex to formulate	The computational time can be improved by using mixed-finite element

2.3 Poromechanics Models

Poromechanics is the study of fluid-rock interaction, which is governed by the theory of poroelasticity. Modeling the fluid-rock interaction requires rigorous coupling of the equations that govern the stress response in porous media and the fluid-flow equations. The mathematical complexity in deriving and coupling the fluid-rock interaction equations along with the limited computational power and the limited knowledge of poromechanics importance back then resulted in a very limited number of modeling studies in the subject (Rice & Cleary, 1976). However, with growing interest in understanding the fluid-rock interaction in the petroleum industry and the realization of its importance, especially in fractured reservoirs, and also to better manage the reservoirs, more modeling work has been conducted in the coupling of the fluid-rock interaction

(H. Chen, Teufel, & Lee, 1995; Olson, Laubach, & Lander, 2004; Philip, Jennings, Olson, Laubach, & Holder, 2005). After all, the petroleum reservoirs consist of two elements; fluid and rock.

In 1976, Rice and Cleary conducted a study by formulating the rock-fluid equations based on Biot's linearized elasticity theory (Rice & Cleary, 1976). They studied saturated porous media with basic stress solutions. Rice and Cleary worked on linear isotropic homogeneous models with fully compressible fluids, and they realized the complexity of the coupling process and the discontinuity in the regions. They also stated that the difficulties and challenges in the heterogeneous geometries are unavoidable. Rice and Cleary recommended to solve such problems numerically using the finite element method (Rice & Cleary, 1976).

In 1995, Chen et al. coupled the fluid flow equations with geomechanics to study the reservoir behavior (H. Chen et al., 1995). Chen et al. derived the governing equations for deformable porous medium and illustrated theoretically that symmetrical fluid flow modeling is the way to model the geomechanics in complex reservoirs. Chen et al. concluded that: 1) the effective stress equation is essential in the coupling process of fluid flow equations and geomechanics, 2) the fluid flow is governed by the same set of equations in the deformable and nondeformable geometries, and 3) the boundary conditions of the problem affect the rock compressibility (H. Chen et al., 1995). The Chen et al. model was derived for simple homogeneous systems, and they did not present any computational results.

In 2000, Wang, in his book titled "Theory of Linear Poroelasticity with Applications to Geomechanics and Hydrogeology" derived the principle partial differential equations (PDEs) for displacement in porous domains with stress, strain and pore pressure components (Wang, 2000).

Wang also demonstrated how Darcy's law is coupled with the displacement equations. The work of Wang was theoretical without any computational results.

In 2007, Silbernagle developed a general poroelastic model by coupling the fluid flow and geomechanics (Silbernagel, 2007). The goal of Silbernagle's work was to demonstrate the coupling process of the fluid flow equations and the geomechanical equations using COMSOL, which is a finite element based software. At that time, COMSOL did not support poroelastic simulations; hence, Silbernagle modified the existed modulus to couple the two set of equations. Silbernagle used Darcy's law to model the fluid flow behavior, and the geometry was homogeneous.

In 2017, Zhang et al. modeled the reservoir depletion process by coupling the fluid flow equations and the displacement equations (F. Zhang et al., 2017). Zhang et al. included vugs and fractures in their geometry as can be seen in Figure 28, and they used Darcy's law to model the fluid flow in the porous medium. Zhang et al. also studied the change of the vugs' shape due to depletion, and they concluded: 1) the fluid flow equations are the dominant factor in the depletion, and 2) the displacement equations (i.e., geomechanics) contribute to the overall deformation and change the volume of the vugs (F. Zhang et al., 2017). Zhang et al. used Darcy's law to model the fluid flow in both the porous and free-flow regions as they used a commercial software package (i.e., FLAC3D.)

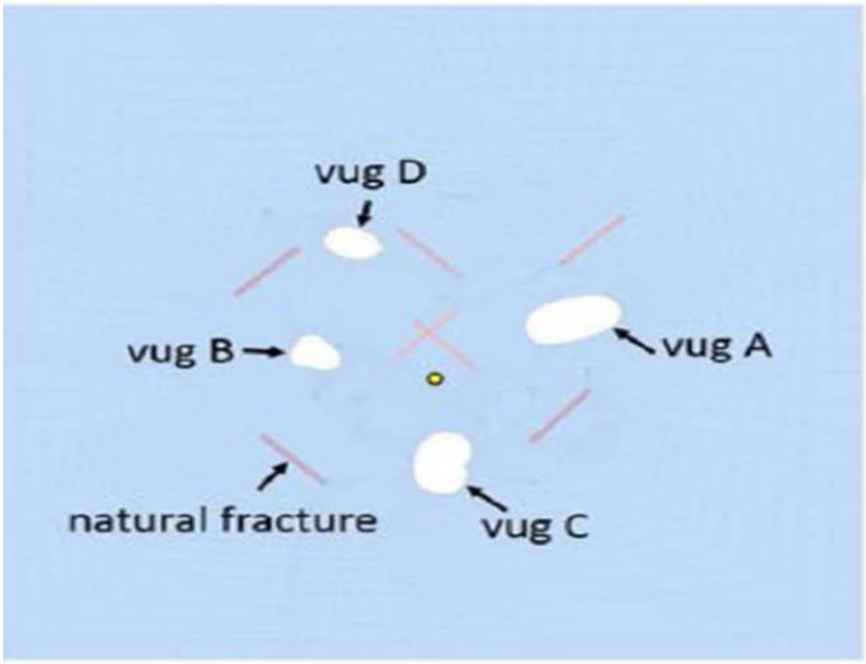

Figure 28: Zhang et al. geometry (Zhang, An, Yan, & Wang, 2017)

In summary, the existing models that couple the fluid flow and geomechanics are not capable of modeling the fluid flow behavior that is encountered in the fractured-vuggy carbonate rocks. The main reason of this limitation is the complexity in the mathematical formulation of the displacement equations. Also, the previous studies clearly show that the finite element method (FEM) is the recommended numerical scheme that should be used to formulate the Brinkman model for the fractured-vuggy carbonate rocks. Several studies have demonstrated that FEM with mixed formulation is a powerful technique, and it accurately capture the fine details in complex geometries (M.M. Alhubail, Misra, & Barati, 2017; Mustafa M. Alhubail, Misra, Maulianda, & Barati, 2020; Reddy, 2004, 2014; Surana & Reddy, 2016; Vassilevski & Villa, 2014).

2.4 High-order Gradient Approach

Capturing and describing the geomechanical effects of the granular materials such as soil can be achieved mathematically by the use of the continuum theory. However, the classical

continuum theory approach does not accurately capture the geomechanical effects in specific problems where deformation occurs due to concentrated forces (Yang & Misra, 2012). The existence of singularities in the solution of those problems result in inaccurate description of deformation and consequently unstable models (Dell'Isola, Sciarra, & Vidoli, 2009). Several studies have been conducted to improve the classical continuum theory approach by improving their capability of handling complex systems to increase the stability of the models. For example, the available techniques include: 1) the viscoplastic theory, 2) the nonlocal theory and 3) the gradient theory (Yang & Misra, 2012).

The viscoplastic theory considers the classical continuum theory models and adds to them the effects of viscous forces (Nemes & Spéciel, 1996). This approach makes the models mesh insensitive; however, it is applicable only for specific problems that are highly rate-dependent (Nemes & Spéciel, 1996).

The nonlocal approach is based on averaging the tensors (e.g., stress and strain) for specific regions and applying them to a particular point similar to the upscaling process, which was discussed in section 1.3 (Bažant & Pijaudier-Cabot, 1988). The issue of this approach is the complexity of implementing it in the numerical models.

The gradient theory approach, which will be used in developing the model, improves the classical continuum theory by accounting for higher-order stress-strain gradients. This technique significantly improves the convergence and accuracy of the models as it makes them mesh independent and apparently unconditionally stable. The higher-order gradient approach is more feasible to be used compared to the other techniques as it does not require knowledge of the weak zones nor the rate-dependency of the problem (Yang, Ching, & Misra, 2011). The mathematical

formulation of the classical rock mechanical equations and the high-order gradient approach will be illustrated in section 3.1.

In summary, the existing models fail to accurately capture the geomechanical effects especially in fractured-vuggy formations as they only consider the classical continuum theory (Yao et al., 2010). The higher order gradient provides more accuracy to the geomechanical models by accounting for non-locality, which makes the models mesh insensitive, and also by eliminating singularities in the solutions (Dell'Isola et al., 2009; Misra & Poorsolhjouy, 2016; Placidi, Misra, & Barchiesi, 2018).

3 Chapter III: Methods

The development of a simulator that is capable of accurately simulating fluid flow with the effects of geomechanics in heterogeneous fractured-vuggy carbonate reservoirs requires the use of a comprehensive and fully integrated poromechanical model. A comprehensive poromechanical model is formed by the coupling of the rock mechanical equations, fluid flow equations and the evolution of porosity and permeability equations.

3.1 Rock Mechanical Equations

The governing equations for rock deformation can be achieved by analyzing the stress. The force equilibrium equations can be obtained by analyzing the stress on a representative elementary volume (REV) as can be seen in Figure 29. The main idea here is that if a change in pore pressure or stress applied on a poroelastic body, then displacements instantaneously occur within the REV to maintain the force equilibrium.

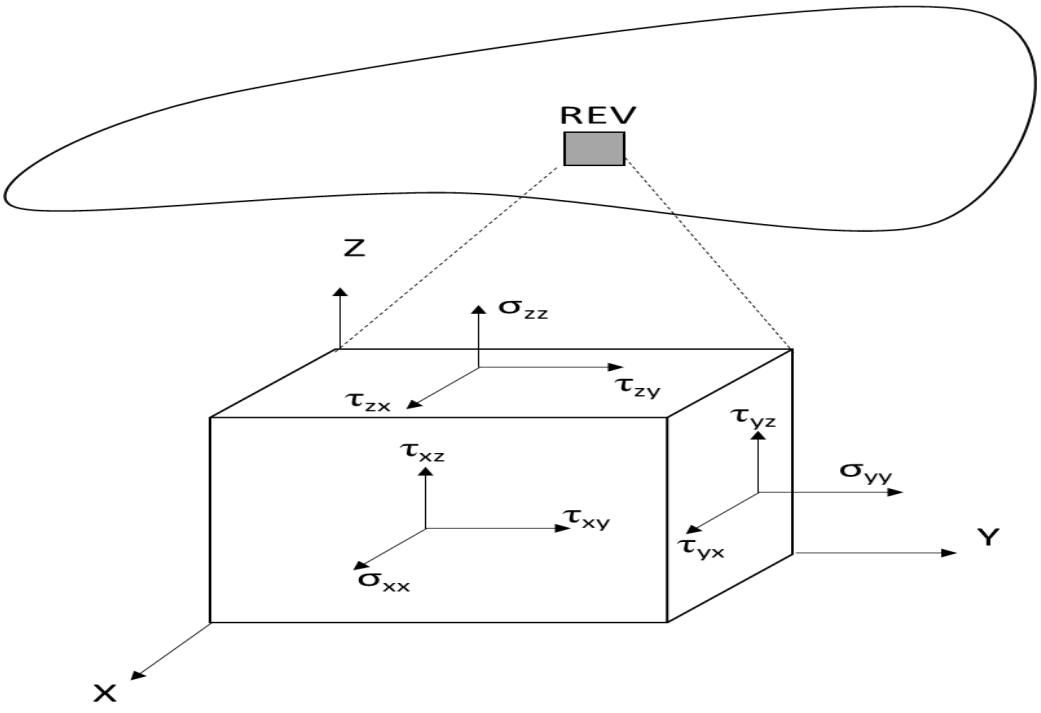

Figure 29: Infinitesimal REV

The tensor components (σ_{ij}) are shown in Figure 29 and Eq. 3.

$$\sigma_{ij} = \begin{bmatrix} \sigma_{xx} & \tau_{xy} & \tau_{xz} \\ \tau_{yx} & \sigma_{yy} & \tau_{yz} \\ \tau_{zx} & \tau_{zy} & \sigma_{zz} \end{bmatrix} \qquad Eq.\ 3$$

where $\sigma_{xx}, \sigma_{yy}, \sigma_{zz}$ are the normal stress components and the τ_{ij} are the shear stress components

Note that the stress tensors are symmetrical (i.e., $\sigma_{ij} = \sigma_{ji}$) for rotational equilibrium. Now, for each principle direction, the net forces are as shown in Eq. 4-Eq. 6:

$$\frac{\partial \sigma_{xx}}{\partial x} + \frac{\partial \tau_{yx}}{\partial y} + \frac{\partial \tau_{zx}}{\partial z} + F_x = 0 \qquad Eq.\ 4$$

$$\frac{\partial \tau_{xy}}{\partial x} + \frac{\partial \sigma_{yy}}{\partial y} + \frac{\partial \tau_{zy}}{\partial z} + F_y = 0 \qquad Eq.\ 5$$

$$\frac{\partial \tau_{xz}}{\partial x} + \frac{\partial \tau_{yz}}{\partial y} + \frac{\partial \sigma_{zz}}{\partial z} + F_z = 0 \qquad Eq.\ 6$$

where F= (F_x, F_y and F_z) represents the applied loads, and in case of no applied loads, only the gravity weight force is considered

Now, for infinitesimal deformation, the strains are defined as shown in Eq. 7:

$$\varepsilon_{ij} = \frac{1}{2}\left(\frac{\partial u_i}{\partial x_j} + \frac{\partial u_j}{\partial x_i}\right) \qquad Eq.\ 7$$

where ε_{ij} are the strain components and u_i are the displacement components (i.e., u, v and w for x, y and z directions, respectively)

The strain components can be written explicitly from Eq. 7 as follow:

$$\varepsilon_{xx} = \frac{\partial u}{\partial x} \qquad \textit{Eq. 8}$$

$$\varepsilon_{yy} = \frac{\partial v}{\partial y} \qquad \textit{Eq. 9}$$

$$\varepsilon_{zz} = \frac{\partial w}{\partial z} \qquad \textit{Eq. 10}$$

$$\varepsilon_{xy} = \frac{1}{2}\left(\frac{\partial u}{\partial y} + \frac{\partial v}{\partial x}\right) \qquad \textit{Eq. 11}$$

$$\varepsilon_{xz} = \frac{1}{2}\left(\frac{\partial u}{\partial z} + \frac{\partial w}{\partial x}\right) \qquad \textit{Eq. 12}$$

$$\varepsilon_{yz} = \frac{1}{2}\left(\frac{\partial v}{\partial z} + \frac{\partial w}{\partial y}\right) \qquad \textit{Eq. 13}$$

The volumetric strain, which is the sum of strains in the longitudinal direction, is defined as follow:

$$\varepsilon_{kk} = \varepsilon_{xx} + \varepsilon_{yy} + \varepsilon_{zz} = \frac{\partial u}{\partial x} + \frac{\partial v}{\partial y} + \frac{\partial w}{\partial z} = \frac{\partial u_k}{\partial x_k} \qquad \textit{Eq. 14}$$

where ε_{kk} is the volumetric strain where k is index notation

By utilizing the constitutive equation, the stress-strain components can be written as shown in Eq. 15. Refer to Appendix A for the detailed derivation.

$$\sigma_{ij} = 2G\ \varepsilon_{ij} + 2G\frac{\upsilon}{1-2\upsilon}\varepsilon_{kk}\ \delta_{ij} - \alpha p\delta_{ij} \qquad \textit{Eq. 15}$$

where E is Young's modulus, G is shear modulus, υ is Poisson's ratio, α is the poroelastic constant, p is pore pressure and δ_{ij} is the Kronecker delta

$$G = \frac{E}{2(1-\upsilon)} \qquad \textit{Eq. 16}$$

$$\delta_{ij} = \begin{cases} 1 & if\ i = j \\ 0 & if\ i \neq j \end{cases} \qquad \textit{Eq. 17}$$

The stress components can be written explicitly from Eq. 15 as follow:

$$\sigma_{xx} = 2G\ \varepsilon_{xx} + 2G\frac{\upsilon}{1-2\upsilon}\varepsilon_{kk} - \alpha p \qquad \textit{Eq. 18}$$

$$\sigma_{yy} = 2G\ \varepsilon_{yy} + 2G\frac{\upsilon}{1-2\upsilon}\varepsilon_{kk} - \alpha p \qquad \textit{Eq. 19}$$

$$\sigma_{zz} = 2G\ \varepsilon_{zz} + 2G\frac{\upsilon}{1-2\upsilon}\varepsilon_{kk} - \alpha p \qquad \textit{Eq. 20}$$

$$\tau_{xy} = 2G\ \varepsilon_{xy} \qquad \textit{Eq. 21}$$

$$\tau_{xz} = 2G\ \varepsilon_{xz} \qquad \textit{Eq. 22}$$

$$\tau_{yz} = 2G\ \varepsilon_{yz} \qquad \textit{Eq. 23}$$

Finally, the classical poroelastic governing equations for infinitesimal deformation can be achieved by substituting the stress equations (Eq. 18-Eq. 23) and the strain equations (Eq. 8-Eq. 13) into the net force equations (Eq. 4-Eq. 6):

$$G\ \Delta u + \frac{G}{1-2\upsilon}\left[\frac{\partial^2 u}{\partial x^2} + \frac{\partial^2 v}{\partial x \partial y} + \frac{\partial^2 w}{\partial x \partial z}\right] = \alpha\frac{\partial p}{\partial x} - F_x \qquad \textit{Eq. 24}$$

$$G\ \Delta v + \frac{G}{1-2\upsilon}\left[\frac{\partial^2 u}{\partial y \partial x} + \frac{\partial^2 v}{\partial y^2} + \frac{\partial^2 w}{\partial y \partial z}\right] = \alpha\frac{\partial p}{\partial y} - F_y \qquad \textit{Eq. 25}$$

$$G\ \Delta w + \frac{G}{1-2\upsilon}\left[\frac{\partial^2 u}{\partial z \partial x} + \frac{\partial^2 v}{\partial z \partial y} + \frac{\partial^2 w}{\partial z^2}\right] = \alpha\frac{\partial p}{\partial z} - F_z \qquad \textit{Eq. 26}$$

where Δ is the Laplace differential operator

$$\Delta u \;=\; \nabla^2 u = \left[\frac{\partial^2 u}{\partial x^2} + \frac{\partial^2 u}{\partial y^2} + \frac{\partial^2 u}{\partial z^2}\right] \qquad \textit{Eq. 27}$$

The poroelastic governing equations for infinitesimal deformation (Eq. 24-Eq. 26) can be written in a compact form using index notation as can be seen in Eq. 28:

$$G\,\Delta u_i + \frac{G}{1-2\upsilon}\frac{\partial^2 u_k}{\partial x_i \partial x_k} \;=\; \alpha\frac{\partial p}{\partial x_i} - F_i \qquad \textit{Eq. 28}$$

By utilizing the volumetric strain definition (Eq. 14), the poroelastic governing equation can be expressed as follow:

$$G\,\Delta u_i + \frac{G}{1-2\upsilon}\frac{\partial \varepsilon_{kk}}{\partial x_i} = \alpha\frac{\partial p}{\partial x_i} - F_i \qquad \textit{Eq. 29}$$

Eq. 28 can also be written in compact form and in terms of the effective stress for infinitesimal deformation as shown in Eq. 30.

$$\nabla\sigma'_{ij} \;=\; \alpha\frac{\partial p}{\partial x_i} - F_i \qquad \textit{Eq. 30}$$

$$\sigma'_{ij} = E_{ijkl}\,\varepsilon_{kl} \qquad \textit{Eq. 31}$$

where E_{ijkl} is the fourth-rank elasticity tensor and ε_{kl} is the strain components

The above equations are the traditional equations for poroelastic domains. However, the developed model is unique as it is further improved by accounting for the second gradient in the equations using the second gradient continuum theory. This addition improves the model as it makes it more responsive to the geomechanical effects by accounting for the nonlocality while

improving the convergence (Dell'Isola et al., 2009; Placidi et al., 2018; Yang & Misra, 2012). Thus, Eq. 30 is modified to account for the second gradients of displacements as follow:

$$\nabla\sigma_{iq}^{eff} = \left(\sigma_{iq}^{0} + \sigma_{ijq,j}^{1}\right)_{,q} = \alpha\frac{\partial p}{\partial x_i} - F_i \qquad \textit{Eq. 32}$$

The effective stress is considered in the model as follow:

$$\nabla\sigma_{iq}^{eff} = \left(\sigma_{iq}^{0} + \sigma_{ijq,j}^{1}\right)_{,q} = \frac{\partial}{\partial x_q}\left(\sigma_{iq}^{eff} + \frac{\partial}{\partial x_j}\,\sigma_{ijq}^{eff}\right) \qquad \textit{Eq. 33}$$

$$\frac{\partial}{\partial x_q}\left(\sigma_{iq}^{eff} + \frac{\partial}{\partial x_j}\,\sigma_{ijq}^{eff}\right) = \frac{\partial}{\partial x_q}\,\sigma_{iq}^{eff} + \frac{\partial^2}{\partial x_q \partial x_j}\,\sigma_{ijq}^{eff} \qquad \textit{Eq. 34}$$

$$\frac{\partial}{\partial x_q}\,\sigma_{iq}^{eff} = \frac{1}{2}\,E_{iqkl}\,\frac{\partial}{\partial x_l}\left(\frac{\partial u_k}{\partial x_q} + \frac{\partial u_q}{\partial x_k}\right) \qquad \textit{Eq. 35}$$

$$\frac{\partial^2}{\partial x_q \partial x_j}\,\sigma_{ijq}^{eff} = \frac{1}{2}D_{ijqklr}\,\frac{\partial^3}{\partial x_r \partial x_j \partial x_q}\left(\frac{\partial u_k}{\partial x_l} + \frac{\partial u_l}{\partial x_k}\right) \qquad \textit{Eq. 36}$$

where E_{iqkl} is the fourth-rank elasticity tensor and D_{ijqklr} is the sixth-rank elasticity tensor where ijqklr are the index notations

The elasticity tensor is defined as shown in Eq. 37, and it can be simplified for isotropic and linear elastic material as shown in Eq. 38.

$$E_{ijkl} = \begin{bmatrix} E_{1111}E_{1122}E_{1133}E_{1123}E_{1131}E_{1112} \\ E_{2211}E_{2222}E_{2233}E_{2223}E_{2231}E_{2212} \\ E_{3311}E_{3322}E_{3333}E_{3323}E_{3331}E_{3312} \\ E_{2311}E_{2322}E_{2333}E_{2323}E_{2331}E_{2312} \\ E_{3111}E_{3122}E_{3133}E_{3123}E_{3131}E_{3112} \\ E_{1211}E_{1222}E_{1233}E_{1223}E_{1231}E_{1212} \end{bmatrix} \qquad \textit{Eq. 37}$$

$$E_{ijkl} = \begin{bmatrix} \lambda+2G & \lambda & \lambda & 0 & 0 & 0 \\ \lambda & \lambda+2G & \lambda & 0 & 0 & 0 \\ \lambda & \lambda & \lambda+2G & 0 & 0 & 0 \\ 0 & 0 & 0 & G & 0 & 0 \\ 0 & 0 & 0 & 0 & G & 0 \\ 0 & 0 & 0 & 0 & 0 & G \end{bmatrix} \qquad \textit{Eq. 38}$$

where λ is first Lame's constant and G is the shear modulus

The first Lame's constant (λ) and the shear modulus (G) are functions of Young's modulus (E) and Poisson's ratio (ν), and they can be calculated by the use of Eq. 39 and Eq. 40, respectively.

$$\lambda = \frac{E\nu}{(1+\nu)(1-2\nu)} \qquad \textit{Eq. 39}$$

$$\mathrm{G} = \frac{E}{2(1+\nu)} \qquad \textit{Eq. 40}$$

The sixth-rank elasticity tensor D_{ijklpq} for isotropic material can be obtained by using Eq. 41 (Dell'Isola et al., 2009).

$$\begin{aligned} D_{ijklpq} = {} & c2\left(\delta_{ik}\delta_{kl}\delta_{pq} + \delta_{ij}\delta_{kp}\delta_{lq} + \delta_{ik}\delta_{jq}\delta_{lp} + \delta_{iq}\delta_{jk}\delta_{lp}\right) + c3\left(\delta_{ij}\delta_{kq}\delta_{lp}\right) \\ & + c5\left(\delta_{ik}\delta_{jl}\delta_{pq} + \delta_{ik}\delta_{jp}\delta_{lq} + \delta_{il}\delta_{jk}\delta_{pq} + \delta_{ip}\delta_{jk}\delta_{lq}\right) \\ & + c11\left(\delta_{il}\delta_{jp}\delta_{kq} + \delta_{ip}\delta_{jl}\delta_{kq}\right) \\ & + c15\left(\delta_{il}\delta_{jq}\delta_{kp} + \delta_{ip}\delta_{jq}\delta_{kl} + \delta_{iq}\delta_{jl}\delta_{kp} + \delta_{iq}\delta_{jp}\delta_{kl}\right) \end{aligned} \qquad \textit{Eq. 41}$$

where δ is the Kronecker delta

For three-dimensional systems, Eq. 41 yields a matrix with 729 components, which is a 27x27 matrix. However, the matrix contains many zero components, and the non-zero components

are represented by only five constants (i.e., c2, c3, c5, c11 and c15) (Dell'Isola et al., 2009; Misra & Poorsolhjouy, 2016).

3.2 Stokes-Brinkman Flow Equations

The flow of a single-phase slightly compressible fluid in porous media is governed by material balance (Eq. 42) and Darcy's law. However, as was mentioned before, Darcy's law is not valid in the free-flow regions (i.e., vugs and fractures) (Li, Khorsandi, Johns, & Dilmore, 2015). Hence, the Stokes-Brinkman model (Eq. 43) should be used instead of Darcy's law to account for both the porous and free-flow regions.

$$\frac{\partial}{\partial t}(\phi\rho) + \nabla(\vec{u}\rho) = \dot{m} \qquad \textit{Eq. 42}$$

where ϕ is the porosity, ρ is the fluid density, $\vec{u}$ is the velocity vector and $\dot{m}$ is mass flow per unit volume (i.e., production or injection)

$$u + \frac{k}{\mu}(\nabla p - \rho g - \mu^* \Delta u) = 0 \qquad \textit{Eq. 43}$$

where u is the velocity vector, k is the permeability tensor, μ is the fluid viscosity, ρ is the fluid density, g is the gravity vector, p is the pore pressure and μ^* is the effective viscosity

Note that the material balance equation (Eq. 42) also accounts for both the porous and free-flow regions by selecting different porosity values for each region. Basically, the porosity equals to 1 in vugs and fractures. Thus, Eq. 42 and Eq. 43 define the fluid flow behavior in fractured-vuggy carbonate rocks, and they can be written explicitly as shown in Eq. 44-Eq. 47. Note that the z-direction is aligned with the gravity direction.

$$\frac{\partial}{\partial t}(\phi\rho) + \frac{\partial}{\partial \mathrm{x}}(\rho u_x) + \frac{\partial}{\partial \mathrm{y}}(\rho u_y) + \frac{\partial}{\partial \mathrm{z}}(\rho u_z) = \dot{m} \qquad \textit{Eq. 44}$$

$$u_x + \frac{k_x}{\mu}\left[\frac{\partial p}{\partial x} - \mu^*\left(\frac{\partial^2 u_x}{\partial x^2} + \frac{\partial^2 u_x}{\partial y^2} + \frac{\partial^2 u_x}{\partial z^2}\right)\right] = 0 \qquad \textit{Eq. 45}$$

$$u_y + \frac{k_y}{\mu}\left[\frac{\partial p}{\partial y} - \mu^*\left(\frac{\partial^2 u_y}{\partial x^2} + \frac{\partial^2 u_y}{\partial y^2} + \frac{\partial^2 u_y}{\partial z^2}\right)\right] = 0 \qquad \textit{Eq. 46}$$

$$u_z + \frac{k_z}{\mu}\left[\frac{\partial p}{\partial z} - \rho g - \mu^*\left(\frac{\partial^2 u_z}{\partial x^2} + \frac{\partial^2 u_z}{\partial y^2} + \frac{\partial^2 u_z}{\partial z^2}\right)\right] = 0 \qquad \textit{Eq. 47}$$

Finally, to find the fluid flow behavior in fractured-vuggy carbonate system, Eq. 44-Eq. 47, with proper boundary conditions, should be solved simultaneously for the velocity components and pore pressure (u_x, u_y, u_z and p). However, the system of equations becomes more complicated when the coupling of the geomechanical equations are included as will be illustrated in section 3.5.

3.3 Evolution of Porosity

The porosity is usually taken as a constant value; however, the porosity could also be a function of volumetric strain, pore pressure, chemical precipitates and temperature (Z. Chen, Huan, & Ma, 2006; Detournay & Cheng, 1993; Ghabezloo, Sulem, & Saint-Marc, 2009; Nermoen, 2018; Zimmerman, 1984). The evolution of porosity is important in studying the fluid flow behavior especially in fractured-vuggy carbonate rocks because a change in the pore pressure, strain or a chemical reaction of some sort could significantly change the overall structure by producing more vugs or plugging the existing small vugs with precipitated minerals. Consequently, new areas would have porosity values of 1, and the porosity in other areas might decrease to less than 1

resulting in variation of fluid flow pattern. The governing equation for the evolution of porosity is shown in Eq. 48.

$$\frac{\partial}{\partial t}(\phi + M) = \left(\alpha - (\phi + M)\right)\frac{\partial}{\partial t}\left(\varepsilon_{kk} - \beta T + \frac{1-\alpha}{K}p\right) \qquad \textit{Eq. 48}$$

where ϕ is the porosity, M is the concentration of the precipitated minerals, α is the poroelastic constant, β is the thermal expansion coefficient, ε_{kk} is the volumetric strain, T is the temperature, p is the pore pressure and K is the bulk modulus

$$K = \frac{E}{3(1-2\upsilon)} \qquad \textit{Eq. 49}$$

The solution of the porosity evolution equation (Eq. 48) is shown in Eq. 50:

$$\phi + M \ = \alpha + \left(\phi_0 + \ M_{ref} - \alpha\right) e^{\left(\frac{\alpha-1}{K}\left(\ p - p_{ref}\right) - \varepsilon_{kk} + \beta\left(T - T_{ref}\right)\right)} \qquad \textit{Eq. 50}$$

where ϕ_0 is the porosity at the reference points and zero strain

Eq. 50 can be simplified by considering only the terms of interest. For instance, if the problem at hand does not show that the porosity is a function of temperature, then the $\beta\left(T - T_{ref}\right)$ term is removed from Eq. 50. If there are no precipitates due to chemical reactions or dissolution, then the porosity does not depend on the concentration of the precipitated minerals (M), hence, that term is removed from the equation. If the porosity does not depend on mechanical deformation, then the volumetric strain (ε_{kk}) term can be removed. Finally, if the porosity does not depend on change of fluid pressure in pores, then the term $\left(\ p - \ p_{ref}\right)$ is removed from Eq.

50. By considering the geomechanical effects, the evolution of porosity equation is simplified to Eq. 51 (Detournay & Cheng, 1993).

$$\phi = \phi_0 \, e^{\left(\frac{\alpha-1}{K}(p-p_{ref})-\varepsilon_{kk}\right)} \qquad \textit{Eq. 51}$$

3.4 Change of Permeability

The permeability tensor can also be updated after each time step using a permeability-porosity correlation such as the Kozeny-Carman equation as shown in Eq. 52 (Carman, 1938; David, 2003; Kozeny, 1927)

$$k_{ij} = A \, k_{ij}^0 \frac{\phi^n}{(1-\phi)^m} \qquad \textit{Eq. 52}$$

where k is the permeability tensor, $A = b \, d^2$, d is the grain diameter, b, n and m are user-defined fitting constants.

3.4.1 Relative Permeability

For multi-phase flow, the relative permeability can also be calculated and updated after each time step by using the Corey model or the Brooks and Corey relative permeability model as shown in Eq. 53-Eq. 55 (Brooks & Corey, 1966).

$$k_{r,wetting} = S_{eff}^{\frac{(2+3\lambda)}{\lambda}} \qquad \textit{Eq. 53}$$

$$k_{r,nonwetting} = \left(1 - S_{eff}\right)^2 \left(1 - S_{eff}^{\frac{(2+\lambda)}{\lambda}}\right) \qquad \textit{Eq. 54}$$

$$S_{eff} = \frac{S - S_{res}^{\beta}}{1 - \sum_{\beta} S_{res}^{\beta}} \qquad \textit{Eq. 55}$$

where $k_{r,wetting}$ is the relative permeability of wetting phase, $k_{r,nonwetting}$ is the relative permeability of non-wetting phase, S_{eff} is the effective saturation, β is the phase and λ is a user-defined constant.

3.4.2 Capillary Pressure

The capillary pressure is also considered in the model. To take advantage of the framework MOOSE, the van Genuchten capillary pressure, which is already developed in MOOSE, was utilized and coupled in the developed model. The van Genuchten capillary pressure relationship is represented by Eq. 56 (van Genuchten, 1980).

$$P_c = \begin{cases} 0, & S = 1 \\ \frac{1}{a}\left({S_{eff}}^{-\frac{1}{m}} - 1\right)^{1-m}, & S < 1 \end{cases} \qquad \textit{Eq. 56}$$

where Pc is the capillary pressure, S_{eff} is the effective saturation, a and m are user defined parameters.

The user-defined fitting parameters are modified based on the type of formation and rock samples. Thus, in case of tight formations, the parameter "a" is adjusted accordingly, based on laboratory tests, to represent the type of rock to be tested.

3.5 Coupling of Fluid Flow and Geomechanics

The coupling between fluid flow and solid mechanics, which can be expressed by the increment of fluid content, is established by the theory of poroelasticity (Biot, 1941). The theory of poroelasticity states that, in a control volume (i.e., REV), fluid exchange occurs due to 1) the

existence of a sink or a source (i.e., production or injection well), 2) change of fluid pressure, and 3) deformation. The increment of fluid content is expressed by Eq. 57 (Biot & Willis, 1957).

$$\xi = -\phi \nabla \left(U_f - U_s\right) \qquad \textit{Eq. 57}$$

where ξ is the fluid volume content increment, ϕ is the porosity and U_f and U_s are the fluid and solid displacements, respectively

The relative velocity between the fluid and solid can be expressed as shown in Eq. 58 (Wang, 2000):

$$\vec{u} = \frac{1}{\phi} u = \left(U_f - U_s\right) \qquad \textit{Eq. 58}$$

Now, substituting Eq. 58 into Eq. 57 yields:

$$\xi = -\nabla u \qquad \textit{Eq. 59}$$

The next step is taking the time derivative and including the source and sink term to get the material balance constrains. In notation form:

$$\frac{\partial \xi}{\partial t} = -\nabla u + \dot{m} \qquad \textit{Eq. 60}$$

Eq. 60 can be expressed explicitly as follow:

$$\frac{\partial \xi}{\partial t} + \frac{\partial u_x}{\partial \mathrm{x}} + \frac{\partial u_y}{\partial \mathrm{y}} + \frac{\partial u_z}{\partial \mathrm{z}} = \dot{m} \qquad \textit{Eq. 61}$$

Now, Substituting the Stokes-Brinkman equation (Eq. 43) into Eq. 60 yields Eq. 62:

$$\frac{\partial \xi}{\partial t} = \left[\frac{k}{\mu}(\nabla p - \rho g - \mu^* \Delta u)\right] + \dot{m} \qquad \textit{Eq. 62}$$

By utilizing the constitutive equation between strain, pore pressure and fluid content increment, the main governing equation that couples the fluid and effects of geomechanics is achieved as shown in Eq. 63. Refer to Appendix A for detailed derivation of strain, pore pressure and fluid content increment relationship.

$$\frac{1}{\Gamma}\frac{\partial p}{\partial t} + \alpha\frac{\partial \varepsilon_{kk}}{\partial t} = \left[\frac{k}{\mu}(\nabla p - \rho g - \mu^{*}\Delta u)\right] + \dot{m} \qquad \textit{Eq. 63}$$

where Γ is Biot's modulus

$$\frac{1}{\Gamma} = \frac{(1-\alpha)(\alpha-\phi)}{K} + \frac{\phi}{K_f} \qquad \textit{Eq. 64}$$

where K is solid bulk modulus and K_f is fluid bulk modulus

3.6 Two-Phase Flow Model

The importance of the two-phase flow models is to understand the recovery mechanisms in the cases of water or gas injection. By developing two-phase models, the effects of relative permeability, capillary pressure, pore size distribution and the wettability on the flow performance and the overall recovery process can be examined.

Note that Eq. 63 is derived for a single-phase fluid. To consider the two-phase flow in the model, the fluid flow equation, which is a material balance equation, is derived for multiphase flow. Hence, the model's fluid flow equation, Eq. 63, is modified to account for the saturations and density of each phase as well as the relative permeability. Therefore, Eq. 65 is introduced to the model's fluid flow equation to achieve Eq. 66. Eq. 66 is used to simulate the fluid flow of multiple phases while considering the effects of geomechanics. The model's other equations (e.g., rock mechanical equation, porosity and permeability equations) remain the same.

$$\mathrm{P} = \sum_{phase} S_{phase}\, p_{phase} \qquad \textit{Eq. 65}$$

$$\frac{\partial}{\partial t}\, \varphi\, \rho_{phase}\, S_{phase} + \frac{\partial \varepsilon_{kk}}{\partial t}\, \varphi\, \rho_{phase}\, S_{phase} = \left[\frac{k_{ij}\, k_{relative}^{phase}\, \rho_{phase}}{\mu} (\nabla \mathrm{P} - \rho g - \mu^{*} \Delta u) \right] + \dot{m} \qquad \textit{Eq. 66}$$

3.7 Governing Equations of the Model

The fluid flow behavior in fractured-vuggy carbonate rocks including the effects of geomechanics on the vugs' shape and volume and accounting for the evolution of porosity and permeability for single-phase and two-phase flow can be described by solving the system of equations (Eq. 67-Eq. 70) with proper boundary conditions, which are problem dependent.

$$\nabla \sigma_{iq}^{eff} = \left(\sigma_{iq}^{0} + \sigma_{ijq,j}^{1}\right)_{,q} = \alpha \frac{\partial p}{\partial x_i} - F_i \qquad \textit{Eq. 67}$$

$$\frac{\partial}{\partial t}\, \varphi\, \rho_{phase}\, S_{phase} + \frac{\partial \varepsilon_{kk}}{\partial t}\, \varphi\, \rho_{phase}\, S_{phase} = \left[\frac{k_{ij}\, k_{relative}^{phase}\, \rho_{phase}}{\mu} (\nabla \mathrm{P} - \rho g - \mu^{*} \Delta u) \right] + \dot{m} \qquad \textit{Eq. 68}$$

$$\phi = \phi_0\, e^{\left(\frac{\alpha - 1}{K}(p - p_{ref}) - \varepsilon_{kk}\right)} \qquad \textit{Eq. 69}$$

$$k_{ij} = A\, k_{ij}^{0} \frac{\phi^{n}}{(1-\phi)^{m}} \qquad \textit{Eq. 70}$$

3.8 Model Workflow

The proposed model is recommended to be solved as shown in the flowchart, Figure 30. The first step is to create a geometry (REV) of the porous matrix including fractures and vugs. The next step is initialization. Initialization includes imposing the initial and boundary conditions (e.g.,

elastic properties, injection and production conditions). After that, the geomechanical equations (Eq. 67) and the fluid flow equations (Eq. 68) are solved simultaneously. Specifying a tolerance or a number of iterations is critical in this step to ensure that convergence occurs within a reasonable timeframe. After the system of equations is solved, the velocity, displacement, stress and strain values will be calculated. The next step is to update the porosity and permeability using Eq. 69 and Eq. 70, respectively, and then move on to the next time step. This process is repeated until the final time step is reached where the velocity, displacement, stress and strain profiles are achieved; hence, the fluid flow behavior of the created REV can be described.

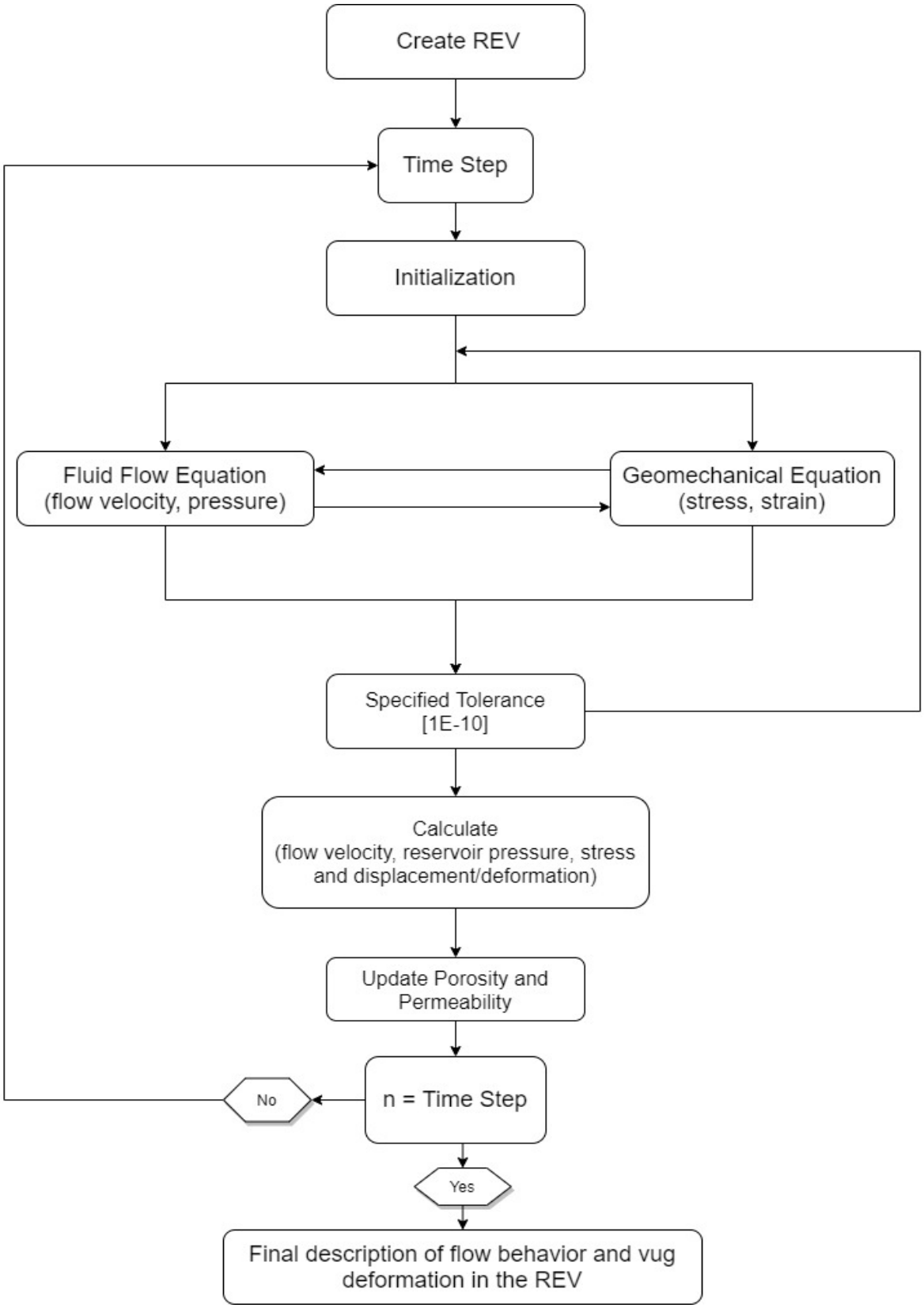

Figure 30: Model flowchart

3.9 Geometry

The first step to run and test the developed model is to create a representative elementary volume (REV) that describes the formation or rock sample of interest. The geometry is created by the use of a preprocessing software. The software package Coreform Trelis was used to create the geometries for both the single-phase and two-phase flow models. Creating computer-aided design (CAD) geometries with fractures and vugs that are imbedded in them is not a simple procedure as the coordinate locations of each fracture and vug in the geometry must be specified beforehand. The matrix, fractures and vugs also need to be specified as separate block sections which is a way to assign them IDs so that each block section (e.g., matrix, spherical vugs etc.) can be assigned distinctive material properties (e.g., porosity, permeability and Young's modulus etc.). Consequently, this procedure could be rather a tedious task without using advanced software packages.

The second step involves meshing of the created geometry. The meshing process is a crucial step and plays an important role in the model's outcome. The model must be meshed so that both the large scale and the fine scale heterogeneities could be captured accurately. However, the geometry should also be meshed considering the available computational power as extremely fine meshes would lead to impractical computational time.

3.9.1 Geometry of the Single-Phase Model

Figure 31 presents a formation geometry with Cartesian coordinate system. The geometry is subdivided into three sections where each subsection has its own properties (e.g., porosity and Young's modulus etc.) as shown in Figure 32. The geometry is meshed with hexagonal elements with 27 nodes (27HEX) element type, and the geometry has 1137 elements. The geometry has two

main fractures and several vugs with different shape and size as shown in Figure 33 and Table 2. Figure 34 shows the meshed geometry.

This geometry is created to conduct the single-phase tests and to examine the flow behavior in the fractures and vugs as well as the vug deformation due to compaction.

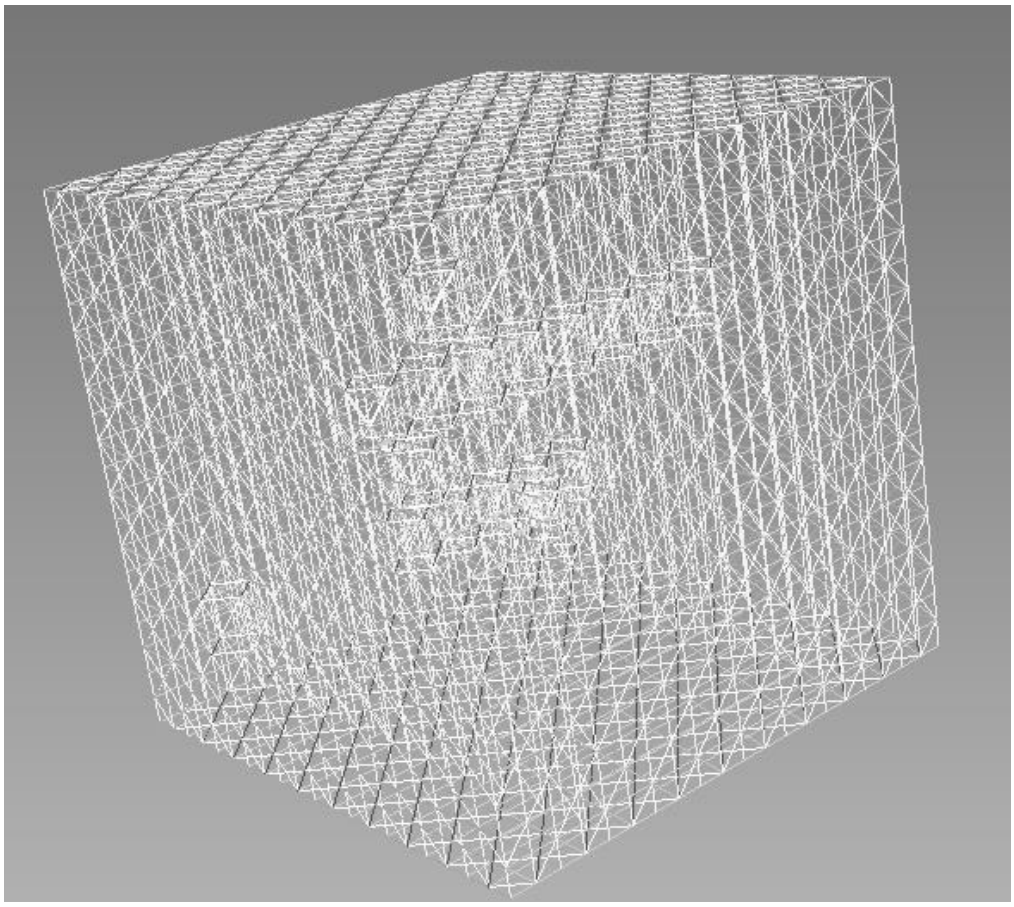

Figure 31: Geometry for single-phase tests

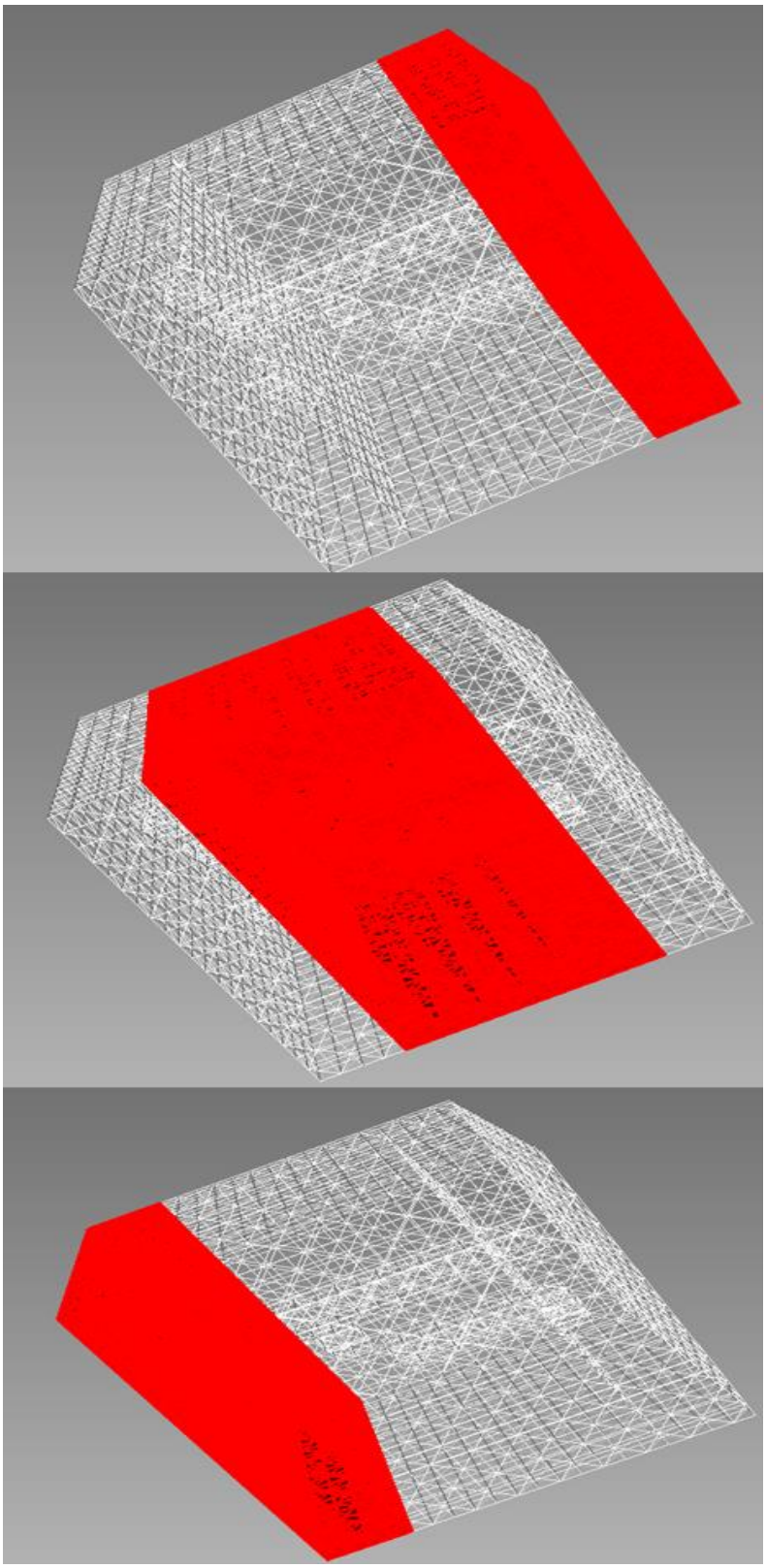

Figure 32: The three subdivided sections of the reservoir domain

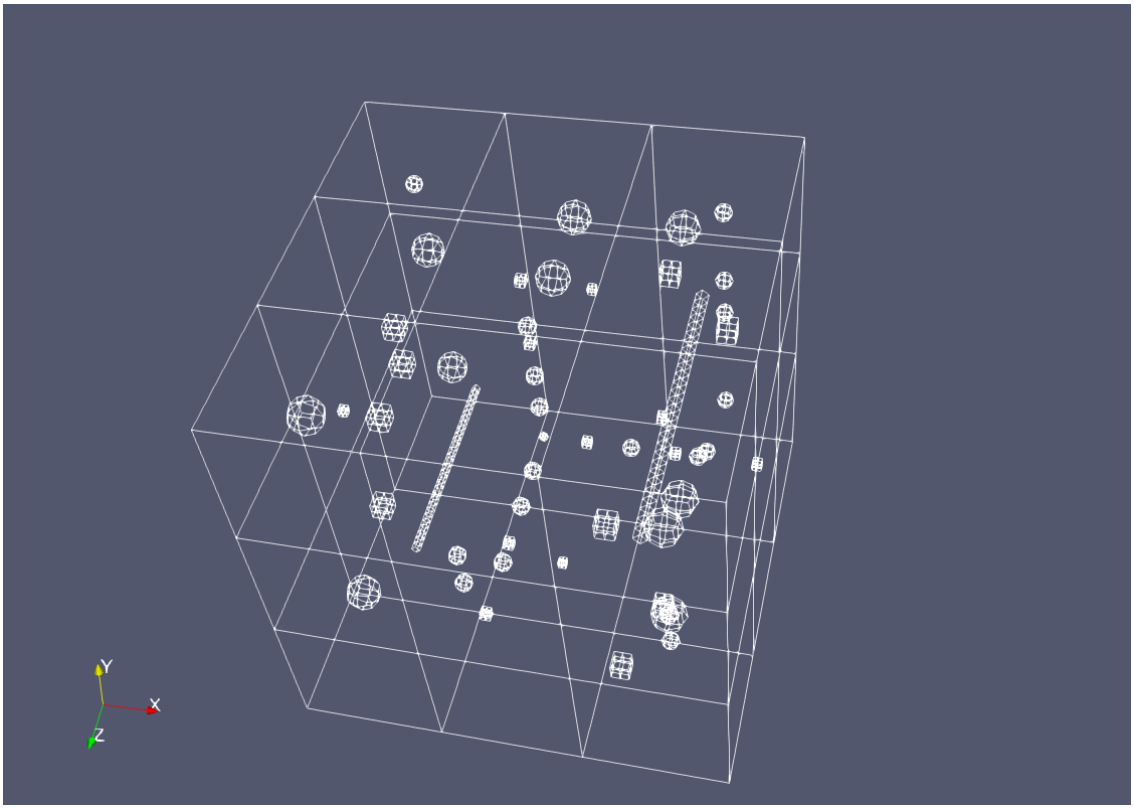

Figure 33: Geometry with different vug shapes for single-phase tests

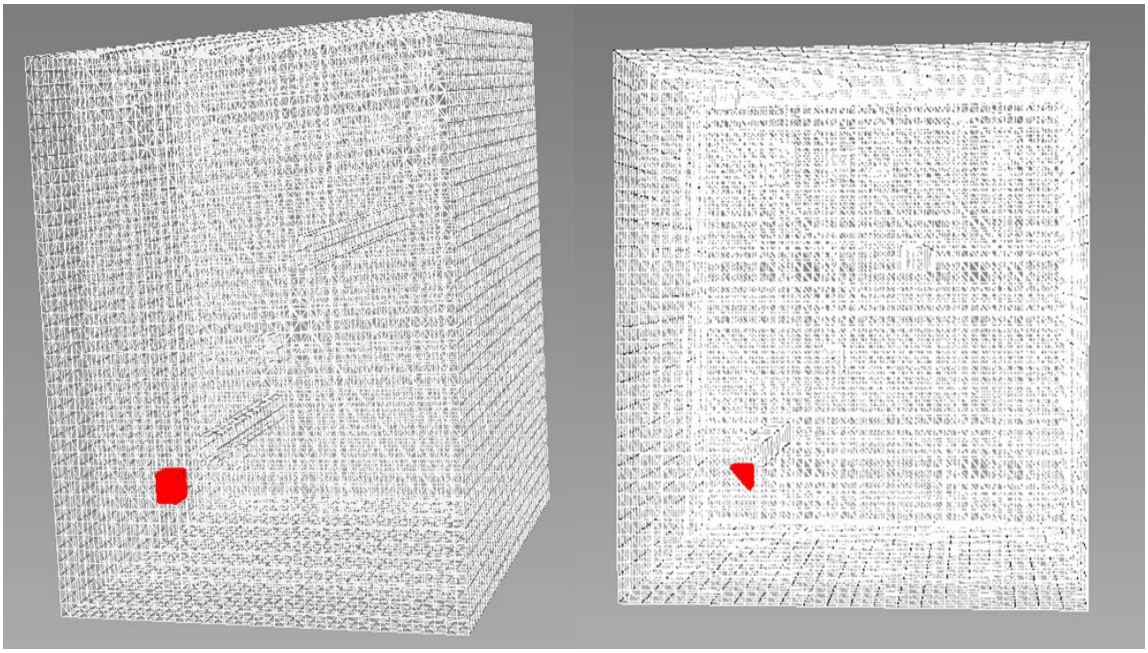

Figure 34: Meshed geometry for single-phase tests

In the single-phase test, one side of the geometry is used as an injection boundary and another side is used as a production boundary where the remaining sides of the geometry are sealed boundaries.

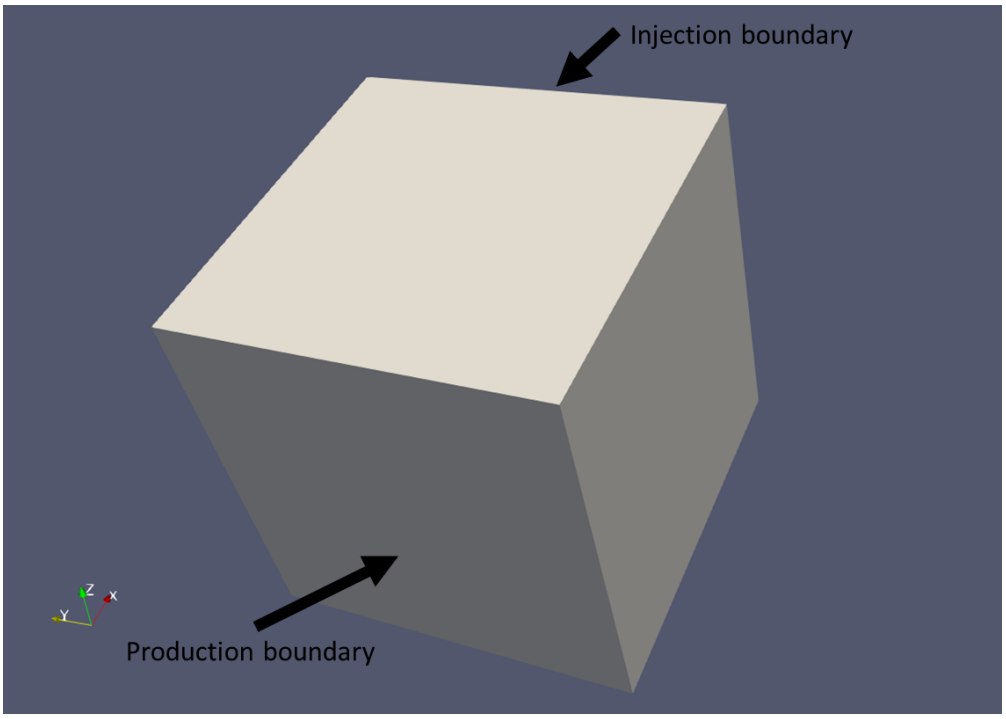

Figure 35: Injection and production boundaries

3.9.2 Geometry of the Two-Phase Flow Model

For the two-phase fluid flow tests, a radial geometry is created to represent the formation rather than a simple cube as in the single-phase tests as shown in Figure 36. The geometry is created this way to mimic the simulation of well testing treatments (e.g., pressure transient tests). The geometry has five fractures and several vugs with different shape and size as shown in Figure 37 and Table 2.

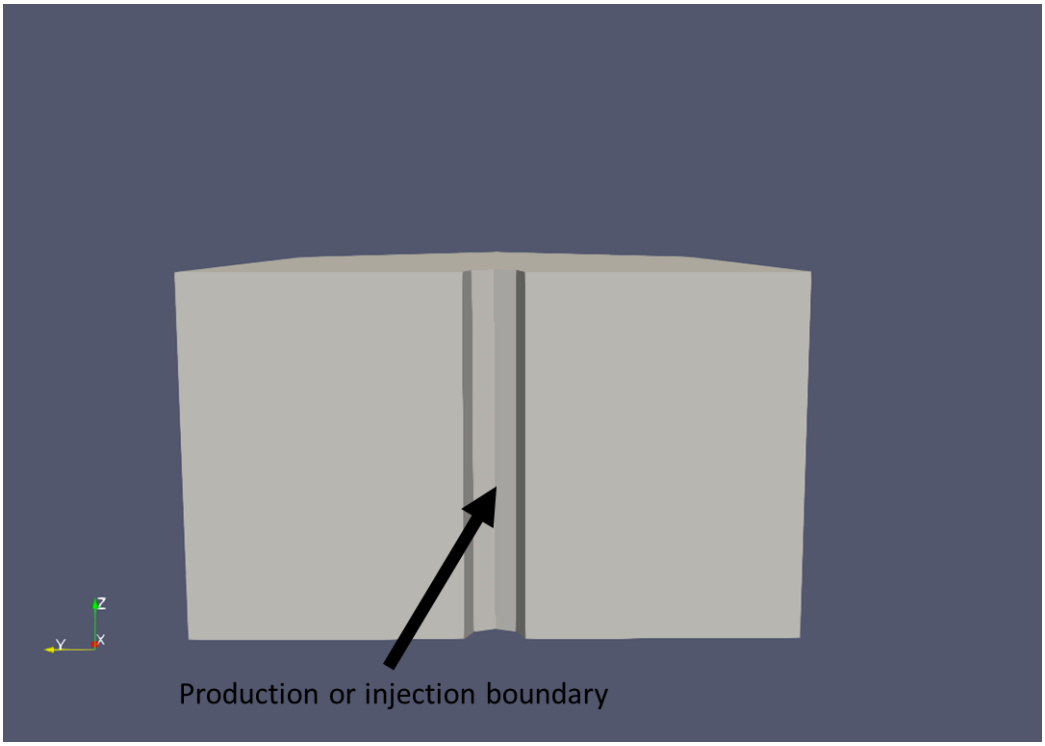

Figure 36: Geometry for two-phase flow tests

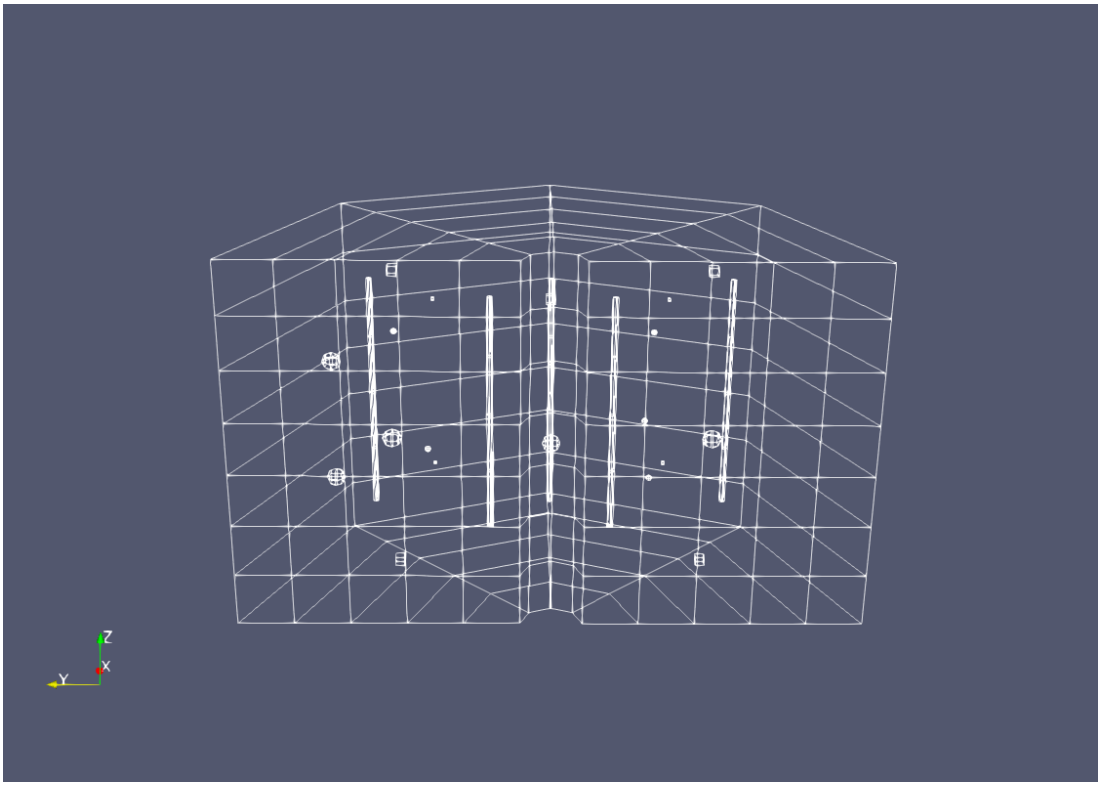

Figure 37: Geometry with different vug shapes for two-phase flow tests

Table 2: Data of geometries

Parameter	Single-phase geometry	Two-phase geometry
Length (m)	10	---
Width (m)	10	---
Height (m)	10	12
Outer radius (m)	---	10
Number of fractures	2	5
Number of vugs	50	20
Main type of elements	HEX27	HEX27
Number of elements before mesh refinement	1173	510
Number of elements after mesh refinement	8000	9375

4 Chapter IV: Results and Discussion

4.1 Single-Phase Flow

In this section, several tests for the single-phase flow model will be conducted to examine different aspects of the fractured-vuggy carbonate rocks. The reservoir pressure, fluid flow, vugs' deformation and elasticity effects will be examined in the following tests.

4.1.1 Reservoir Pressure

The first test is conducted to examine the pressure profile in the reservoir domain after 30 days of continuous injection and production. The reservoir domain is fully saturated with the injected fluid. The fluid (i.e., water) is injected at the injection boundary and produced from the production boundary as shown in Figure 35. The fluid is injected with a pressure of 6960 (psi). The model is capable of handling both fixed-rate and fixed-pressure production constrains. The complete data of the test are provided in Table 3.

Table 3: Data for the fully saturated single-phase model

Parameter	Value
Fracture and vugs porosity	1
Reference permeability (mD)	1
Matrix porosity	0.1
Reference porosity	0.1
Matrix permeability (mD)	1
Initial pressure (psi)	6500
Biot poroelastic coefficient	0.69
Fluid viscosity (cP)	1
Fluid density (kg/m3)	1000

Pressure difference between injection and production (psi)	1160
Young's modulus (GPa)	66
Poisson's ratio	0.18
Stimulation period (Days)	30

At the end of the stimulation period, the final pressure profile of the reservoir domain is shown in Figure 38. The pressure profile of the reservoir domain can be examined at different periods of time by making a cross-section of the domain. The domain was cut through in the middle and the pressure profile after 1, 5 and 30 days is recorded and plotted as can be seen in Figure 39.

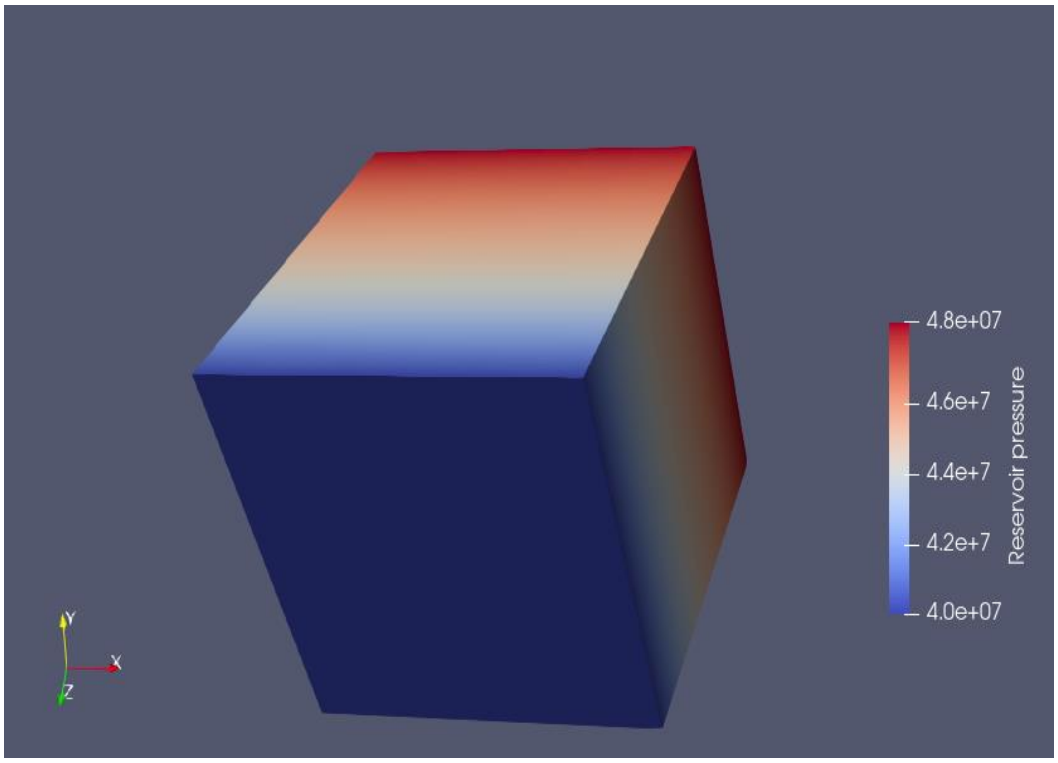

Figure 38: Reservoir pressure for fully saturated single-phase flow model after 30 days of injection and production

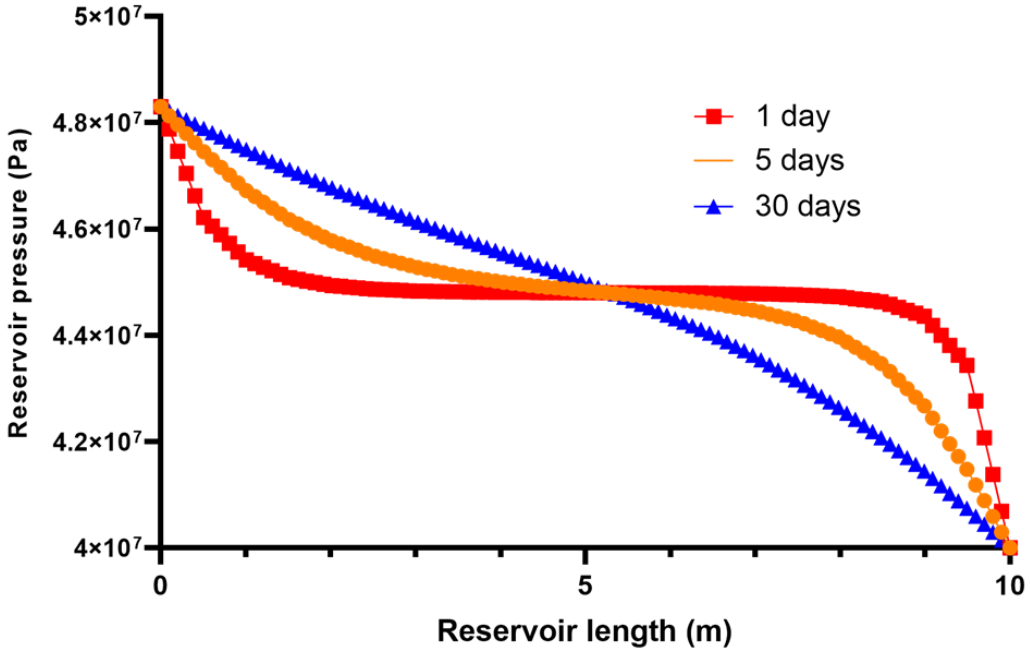

Figure 39: Pressure profile of a cross-section of reservoir domain for fully saturated single-phase flow model

Figure 39 shows the reservoir pressure profile. It is clear from the pressure profile that the pressure increases near the injection boundary with time and decreases near the production boundary due to continues injection and production, respectively. Knowledge of the locations in which the vugs would experience the most compaction can be attained by studying the pressure profile of fractured-vuggy carbonate rocks. Thus, proper characterization of the formation can be conducted, and informed decision can be made to improve the production.

4.1.2 Fluid Flow

The following test is conducted to examine how the cumulative production is affected when the Brinkman's equation is used and compared with the simple dual permeability models. Several case scenarios are tested. The tests are conducted on the single-phase model using the already created geometry for the single-phase fully saturated model where fluid is injected from one

boundary and produced from another boundary, and the remaining boundaries are sealed as can be seen in Figure 40. The data for the tests is provided in Table 4.

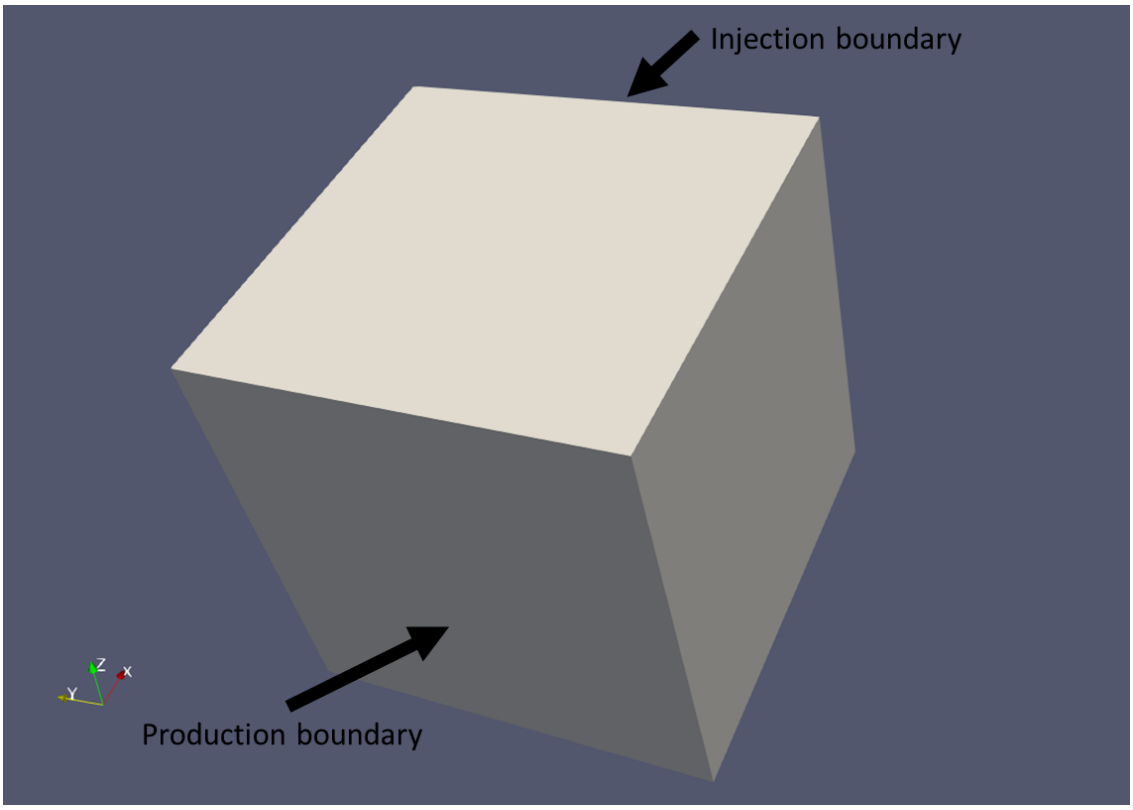

Figure 40: Injection and production boundaries for fluid flow test

Table 4: Data for flow tests of fully saturated single-phase model

Parameter	Value
Pore volume (ft^3)	3530
Matrix porosity	0.1
Matrix permeability (mD)	1
Low averaged permeability for open regions (mD)	100
High averaged permeability for open regions (mD)	1000
Initial pressure (psi)	6500
Biot poroelastic coefficient	0.69

Fluid viscosity (cP)	1
Fluid density (kg/m3)	1000
Effective Young's modulus (GPa)	66
Effective Poisson's ratio	0.18

The first case scenario examines the flow of the matrix without any vugs and fractures. The second case examines the flow of the matrix system with fractures and vugs using Darcy's law with low averaged permeability value (i.e., 1 mD for matrix and 100 mD for open regions). The third case scenario examines the flow of the matrix system with fractures and vugs using Darcy's law with high averaged permeability value (i.e., 1 mD for matrix and 1000 mD for open regions). The final case scenario examines the flow of the developed model using the Brinkman's equation coupled with the rock mechanical equation and evolution of porosity and permeability. 1.5 pore volume is injected in all four cases. The results are shown in Figure 41.

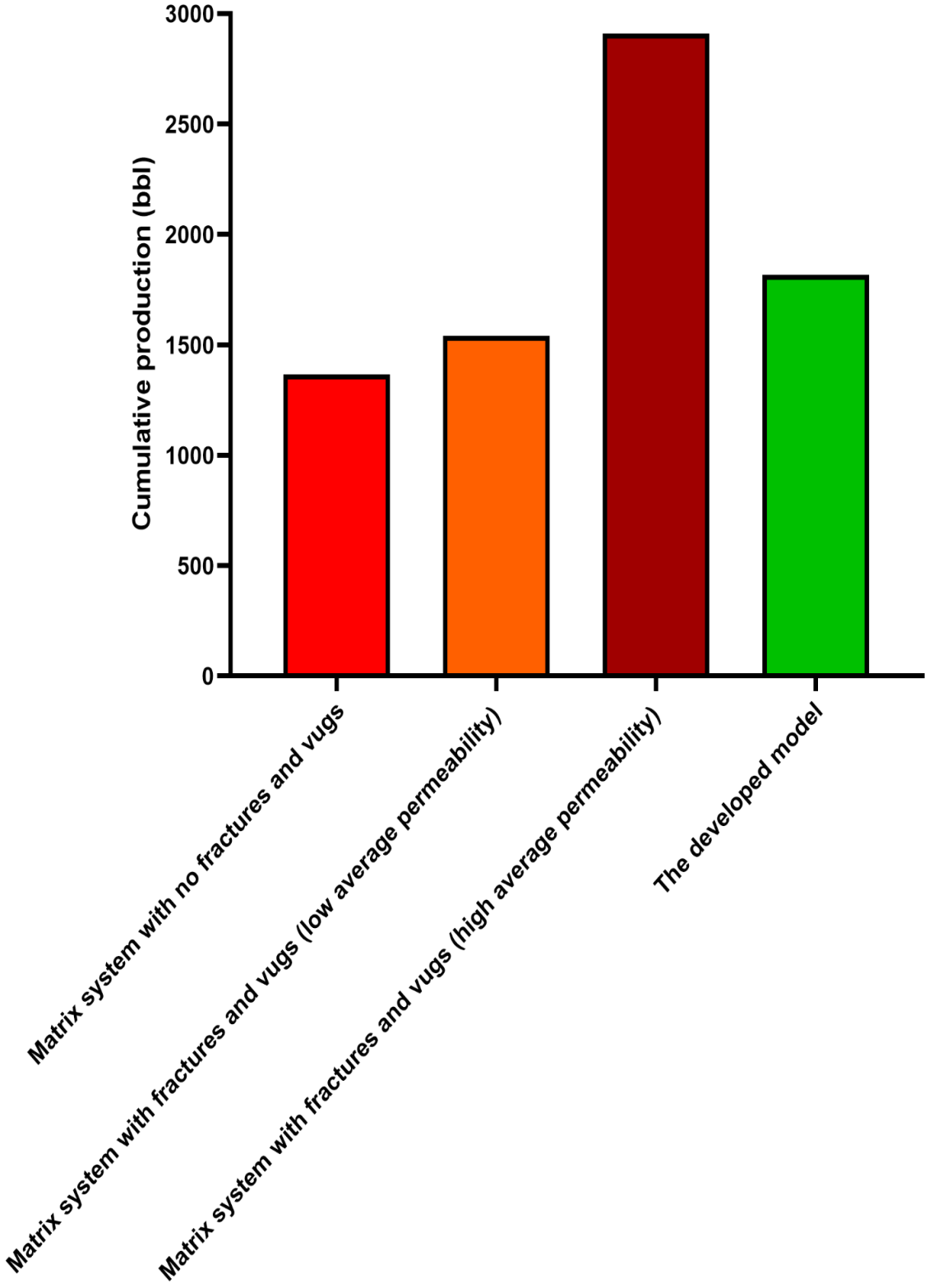

Figure 41: Cumulative production for flow tests after 30 days of production

As it can be seen from the results in Figure 41, for the first test where no fractures and vugs in the matrix system, the cumulative production is the lowest with 1367 bbl after 1.5 pore volume of injection and 30 days of production period. When fractures and vugs (i.e., 2 fractures and 50 vugs with different shape and size) are introduced in the reservoir domain, the production improves to 1542 bbl after 1.5 pore volume of injection and 30 days of production. The third test gave a cumulative production of 2909 bbl after 1.5 pore volume of injection and 30 days of production, and the fractures and vugs were assigned an average permeability value of 1000 mD. The final test was for the developed model which considers the rock mechanical equation and evolution of porosity and permeability, and the fluid flow in the matrix and open regions is captured using the Brinkman's equation. The developed model gave a cumulative production of 1818 bbl after 1.5 pore volume of injection and 30 days of production.

It is clear from the results that assigning an average permeability value for the open regions and using Darcy's law to capture the fluid flow in those regions, as the existing models do, is not an ideal practice. The cumulative production can be underestimated or overestimated if the assigned average permeability value does not properly capture the overall heterogeneities of the reservoir system.

4.1.3 The Effect of Vugs on the Stiffness Modulus

Several researchers have studied the effects of voids and cracks on the geomechanical properties (Ornés, Deisman, & Chalaturnyk, 2013; Walsh, 1965a, 1965b). The objective of the studies was to examine the effects of voids and cracks on the stiffness modulus and Poisson's ratio.

The stiffness modulus is an important parameter as it provides knowledge of the material stiffness. Several studies showed that the voids volume in rocks affect the rocks' geomechanical properties (Martínez-Martínez, Benavente, & García-del-Cura, 2012; Ornés et al., 2013; Walsh,

1965b, 1965a). The studies found the stiffness modulus for rock samples with cracks and voids is less in value than identical rock samples without cracks and voids; hence, the existence of voids and fractures increase the compliance of the rocks (Walsh, 1965b). Ornes et al. found that as the volume of the voids increases, the stiffness modulus decreases below the intrinsic value (Ornés et al., 2013).

Ornes et al. have studied the impact of the vugs volume on the stiffness modulus of carbonate specimens by numerical simulations, and they compared their findings against empirical equations (Ornés et al., 2013). Their findings were in good agreement with the empirical equations, and they established that the stiffness modulus can be estimated in the presence of vugs and cracks by the use of Eq. 71. The Young's modulus (i.e., stiffness modulus) of rocks with vugs and cracks is also called the effective Young's modulus.

$$E_{vuggy} = E_{eff} = E_{intact}\, e^{-3.82 \frac{V_{vugs}}{V_{intact}}} \qquad Eq.\ 71$$

where E_{vuggy} is the modulus in the presence of vugs and cracks, E_{intact} is the modulus without the presence of vugs and cracks, V_{vugs} is the total volume of the voids and V_{intact} is the sample volume without voids

The Young's modulus of the intact sample, E_{intact}, can be found by lab testing of rock samples or by evaluating log measurements. For example, Eq. 72 can be used to calculate the static Young's modulus for carbonate rocks.

$$E_{static} = \frac{1}{3.8\ \alpha^{-0.68}}\ \rho_b\, V_p^2 \frac{(1-2\nu)(1+\nu)}{(1-\nu)} \qquad Eq.\ 72$$

where α is the wave propagation energy lost, ρ_b is the bulk density, Vp is the compression primary sonic wave and ν is Poisson's ratio

In fact, Eq. 72 was found to be valid in the presence of voids and cracks (Martínez-Martínez et al., 2012). Thus, when time and money are not a priority and representative rock samples are available, Eq. 72 would be a valid option to estimate the stiffness modulus for the vuggy-fractured carbonate rocks.

The porosity has been found to be convenient and consistent in estimating certain geomechanical properties of carbonate rocks (Farquhar, Somerville, & Smart, 1994). Hence, the usage of the porosity relationships would be timesaving and cost effective as the porosity data are typically available. Therefore, to predict the stiffness modulus, E_{intact}, the porosity empirical equation for carbonate rocks can be used as shown in Eq. 73 (Farquhar et al., 1994; Ornés et al., 2013).

$$E_{intact}\ (GPa) = 69.05\ e^{-6\,\varphi} \qquad \textit{Eq. 73}$$

where φ is the porosity in fraction

Thus, the intact Young's modulus can be estimated by the use of the porosity empirical equation, Eq. 73, then the effective Young's modulus is calculated by the use of Eq. 71.

4.1.4 The Effects on Poisson's Ratio

Poisson's ratio is a measure of the geometric change of shape under stress. Walsh studied the effect of cracks and voids on Poisson's ratio, and he found that its value decreases for rocks with higher density of vugs and cracks (Walsh, 1965a). Walsh studied the change of Poisson's ratio in rocks with cracks and voids under low stress and high stress. He found that under low stress, the lateral strain rate of rocks with cracks and voids equals to that of intact rocks and showed that the effective Poisson's ratio can be calculated by Eq. 74 (Walsh, 1965a). Eq. 74 indicates

that the effective Poisson's ratio would be zero as the $\frac{E_{eff}}{E}$ approaches zero. However, at high stress, Walsh demonstrated that the effective Poisson's ratio for rocks with cracks and voids should be calculated by Eq. 75 (Walsh, 1965a). The quantity values of the low stress and high stress were not exactly mentioned in the study.

$$\nu_{eff} = \left(\frac{E_{eff}}{E}\right)\nu \qquad \textit{Eq. 74}$$

$$\nu_{eff} = \nu + \frac{1-2\nu}{2}\left(1 - \frac{E_{eff}}{E}\right) \qquad \textit{Eq. 75}$$

where ν_{eff} is the effective Poisson's ratio with vugs and cracks, ν is the intact Poisson's ratio, E_{eff} is the effective Young's modulus with vugs and cracks and E is the intact Young's modulus

4.1.5 Vug Deformation at Different Stiffness Moduli

The developed model is capable of handling different stiffness modulus and Poisson's ratio values for the vugs and fractures that are separate from the matrix. The user-assigned elastic values can be equal, greater or less than the matrix values. Thus, the user has the option of either using Eq. 71 and Eq. 75 to calculate effective values for the stiffness modulus and Poisson's ratio that are representative for the entire domain or assign entirely different stiffness modulus and Poisson's ratio values for the regions hosting vugs and fractures. It is important to mention that finding a representative stiffness modulus for the open regions is a challenging task and complex lab experiments might be required to get reasonable stiffness modulus values for those regions that are separate from the matrix.

In the following tests, the open regions (i.e., vugs and fractures) are assigned different stiffness modulus values than the matrix to study the effect of the stiffness modulus on the overall deformation of the vugs. Six values of stiffness moduli are used; 10, 20, 40 66, 75 and 100 (GPa).

The matrix is assigned a stiffness modulus of 66 GPa. The reservoir domain has multiple vugs and fractures as can be seen in Figure 42; however, post processing is conducted only on three vugs as shown in Figure 43. The first vug is near the injection boundary. The second vug is in the middle of the reservoir domain and the third vug is near the production boundary. The input data for the model is provided in Table 3.

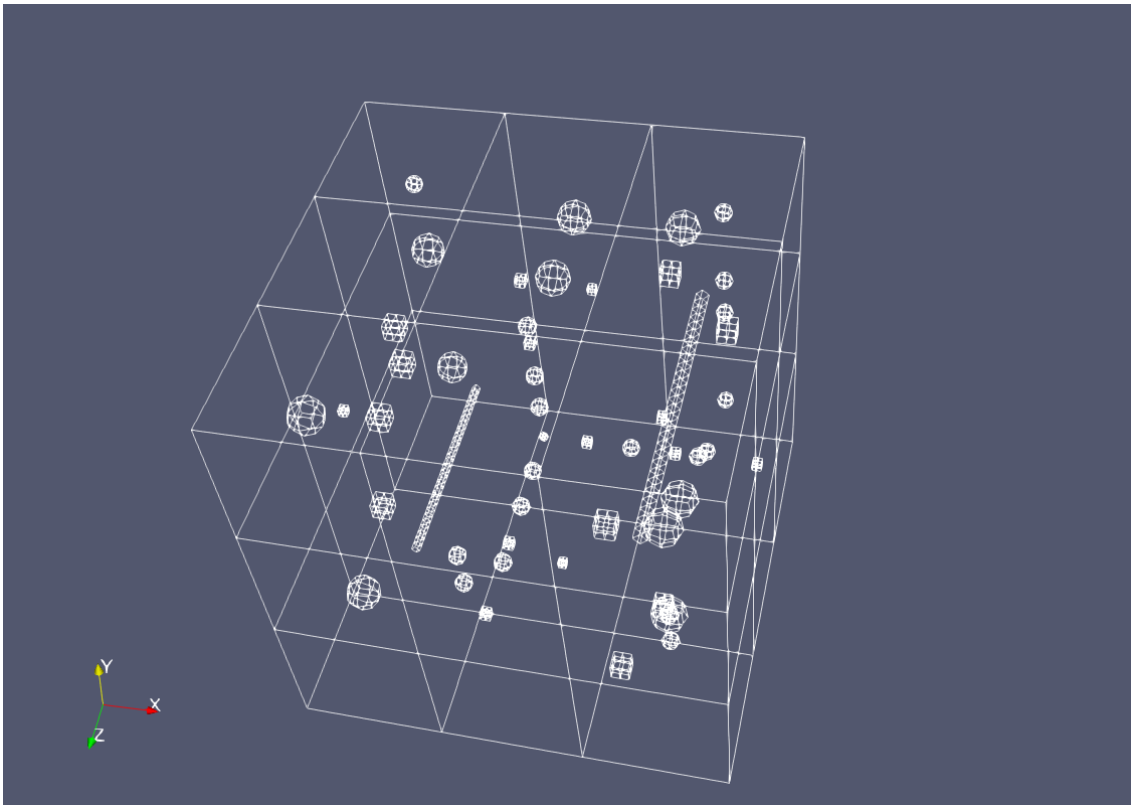

Figure 42: Geometry with different vug shapes for single-phase tests

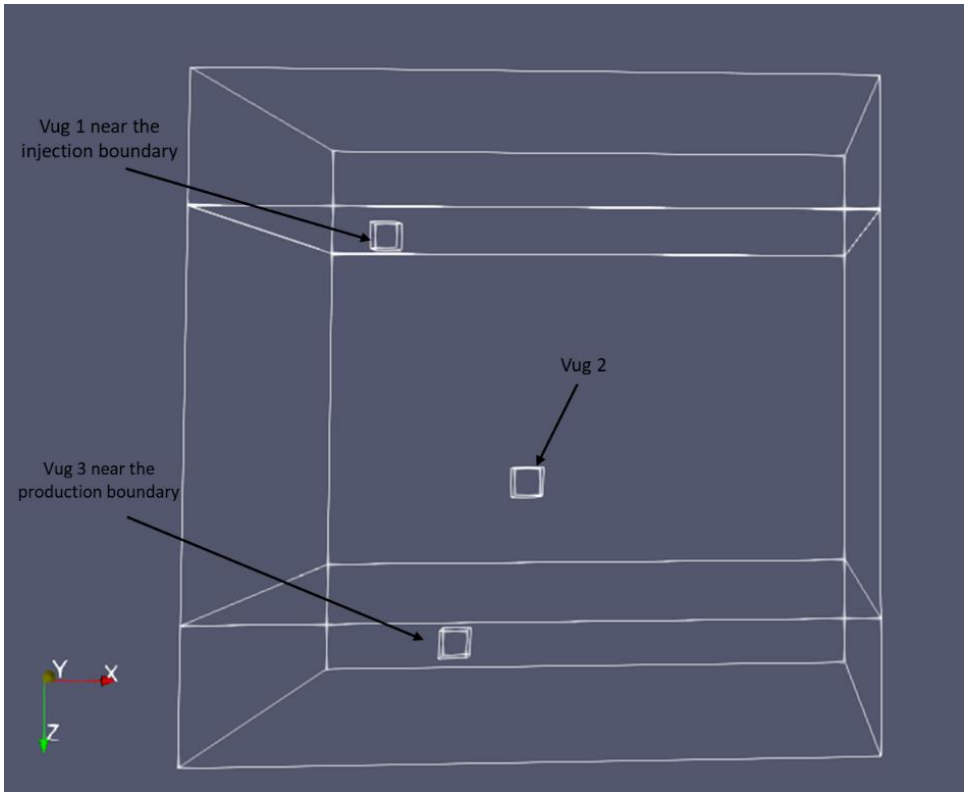

Figure 43: Location of vugs in the reservoir domain

The results of the tests are plotted for each vug as shown in Figure 44, Figure 45 and Figure 46. The results are also tabulated in Appendix B. It is clear from the results that as the stiffness modulus near the vugs' region increases, the vug showed lower deformation as their ability to resist the change of volume due to compaction increases. Furthermore, with continuous production, the deformation increases with time as the reservoir gets depleted and the applied stress on the vugs increases. Hence, the deformation after 30 days production is more than 5 days of production. Furthermore, the results show that more deformation occurs in the vugs that are near the production boundary; this is due to the fact that those vugs experience more compaction compared to the other vugs as can be seen by comparing Figure 44, Figure 45 and Figure 46.

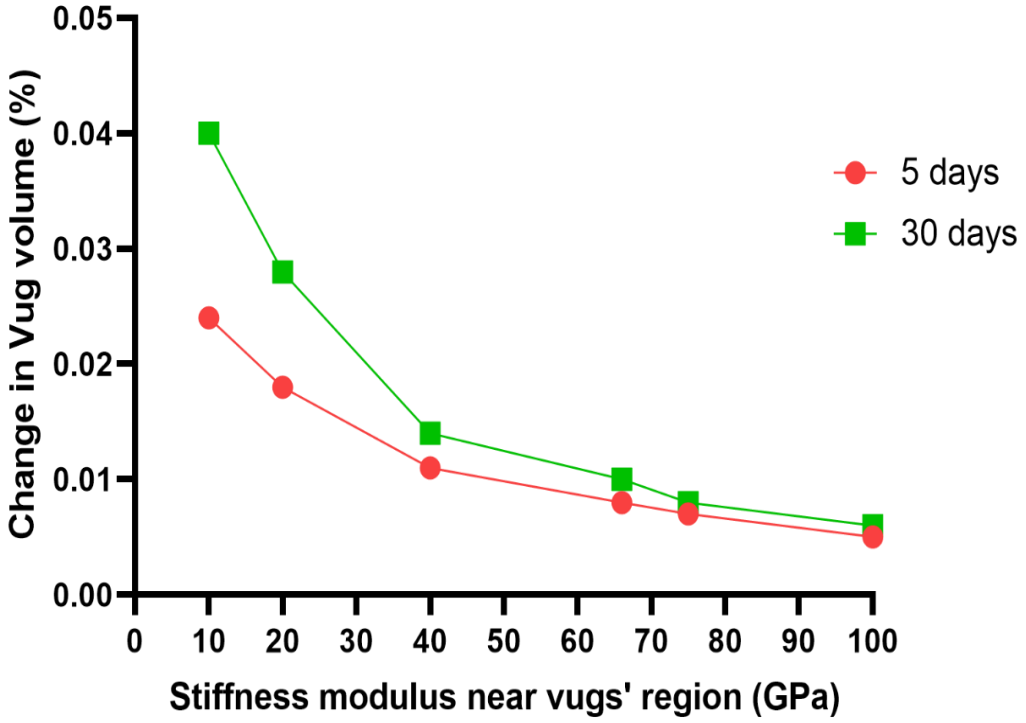

Figure 44: Results of Vug 1 – near injection boundary

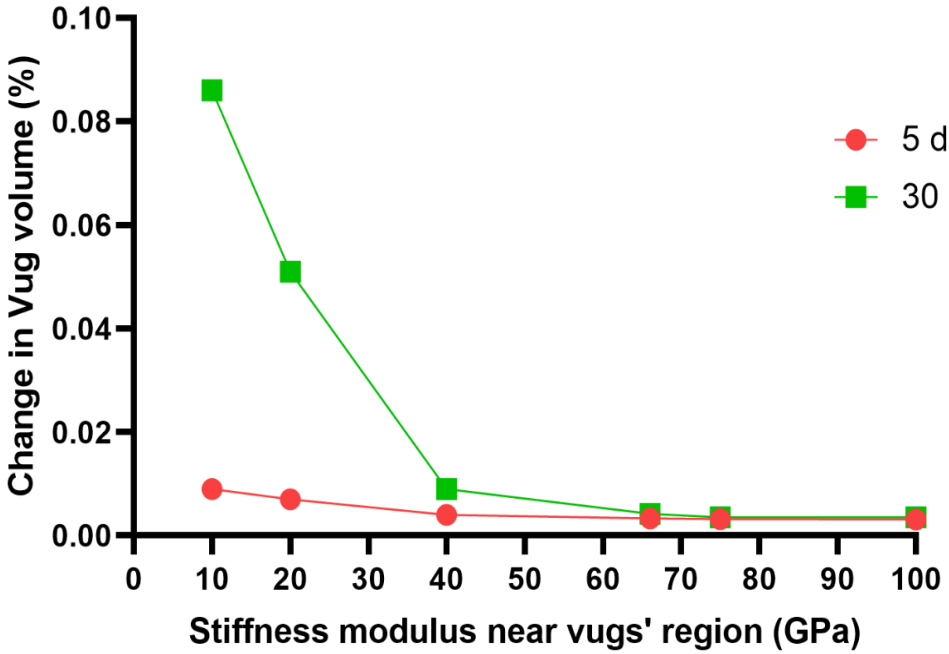

Figure 45: Results of Vug 2

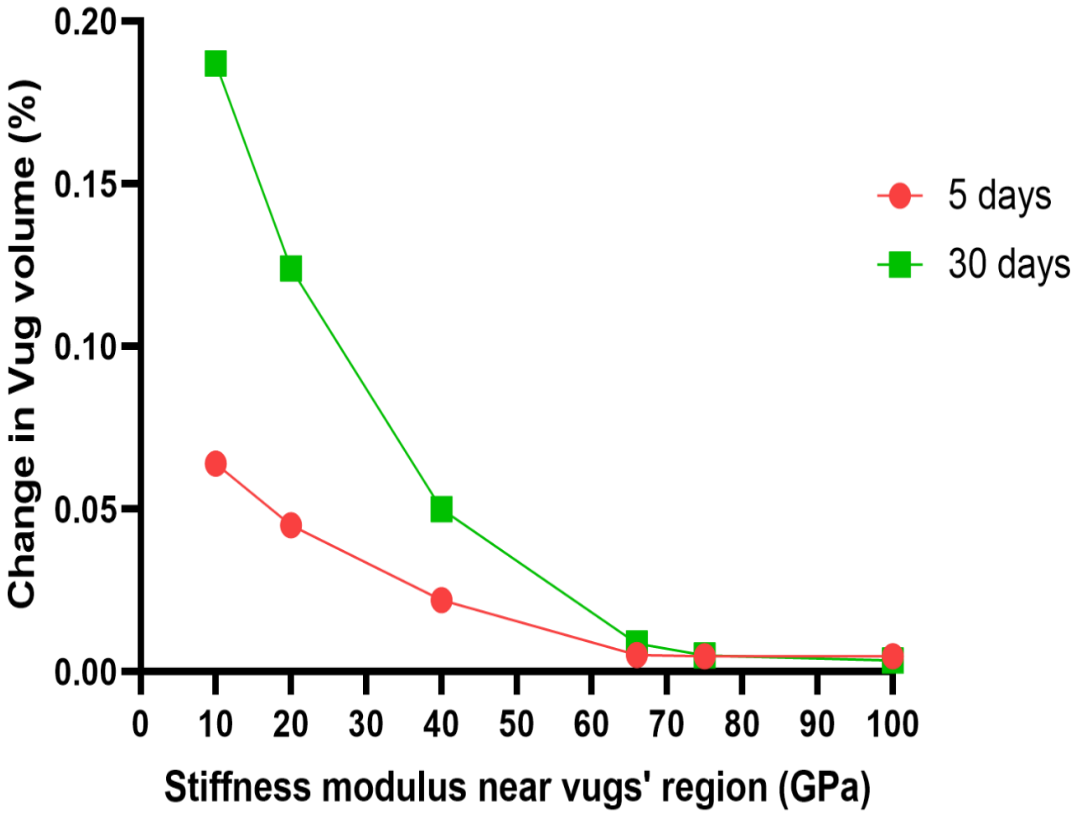

Figure 46: Results of Vug 3 - near production boundary

This study illustrates the significance of the stiffness modulus in the reservoir simulators that consider the geomechanical effects. The developed simulators should be designed in such a way that different stiffness modulus values for the open regions can be entered or calculated than the ones reported for rest of the matrix. The stiffness value of the free-flow regions (e.g., vugs) can be less in value than the stiffness of the matrix if the open regions are fluid-filled. The stiffness of the open regions could also be greater in value than the matrix stiffness if the open regions are sediment-filled. Assigning the same value of stiffness modulus for the open regions and matrix would definitely influence the overall geomechanical behavior and thus the outcome from the simulators as this study showed. While 0.2% of vug deformation might look insignificant, one must note that this is just one vug and the stimulation time is only 30 days; however, the overall

deformation becomes substantial in vuggy carbonate rocks that are set to produce for years. Also, the small percentage in vugs' volume change corresponds to a large amount of fluid in giant fields, which produce tens of thousands of oil barrels per day, such as Ghawar oil field.

4.1.6 Elasticity Effect

This test is conducted to examine how the vug's volume changes during injection and production and after the production is stopped to inspect the effects of elasticity. In this test, fluid is injected from one boundary and produced from another boundary where the other boundaries are sealed as shown in Figure 47. To examine the vugs' deformation with time, the production is halted after 5 days of production while the injection is continued till the end of the simulation period (i.e., 10 days). The test data are provided in Table 5.

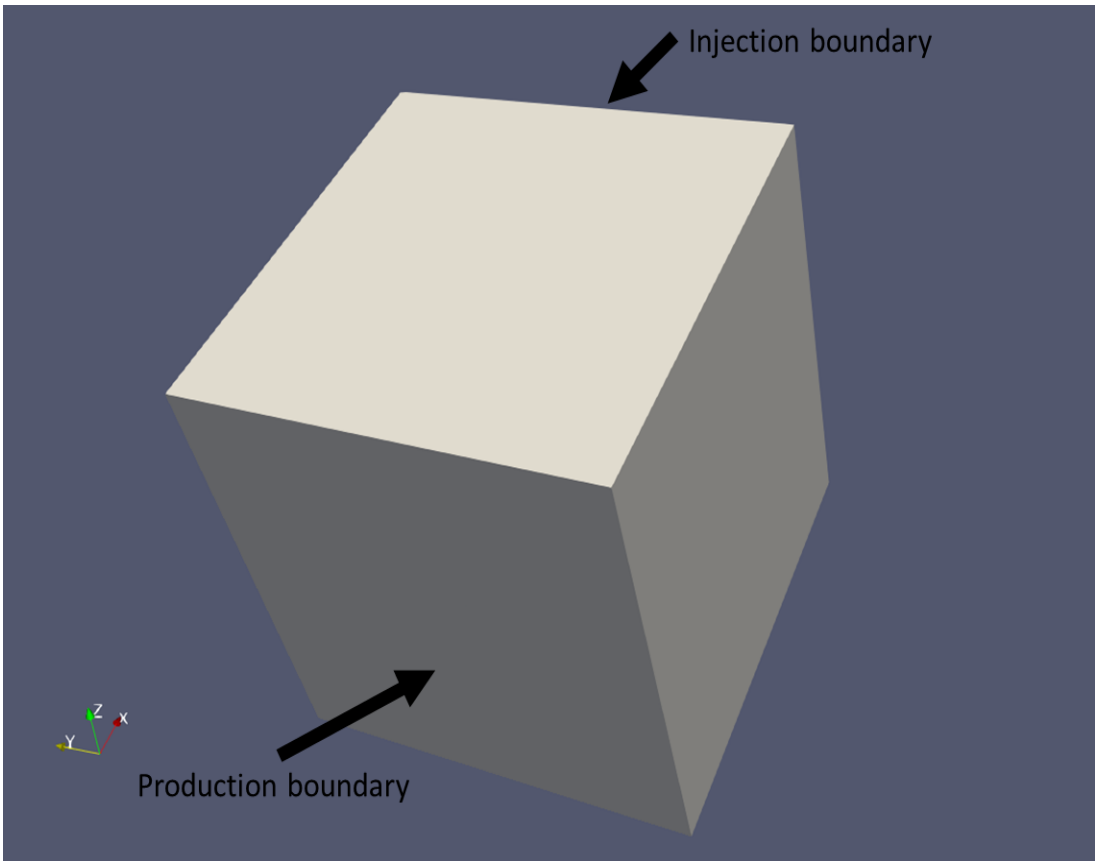

Figure 47: Injection and production boundaries for elasticity effect test

Table 5: Data for Elasticity effect test of single-phase model

Parameter	Value
Fracture and vugs porosity	1
Matrix porosity	0.1
Matrix permeability (mD)	1
Initial pressure (psi)	6500
Biot poroelastic coefficient	0.69
Fluid viscosity (cP)	1
Fluid density (kg/m3)	1000
Young's modulus (GPa)	66
Poisson's ratio	0.18

Young's modulus near vugs' region (GPa)	10
Injection period (Days)	10
Production period (Days)	5

The results of the test can be seen in Figure 48. The results indicate that the vugs deform due to compaction. However, when the production is halted, the vugs would return to their original shape after some time if the injection is continued and if they do not experience fracturing stress. This is due to elasticity as the model is developed for elastic material. The previous tests (e.g., Figure 46) also indicate that the vugs' deformation becomes more difficult as the stiffness modulus near the vugs' region increases. It is also important to note that the rock brittleness increases as the stiffness modulus increases; hence, the possibility of cracking and fracturing the brittle material becomes higher.

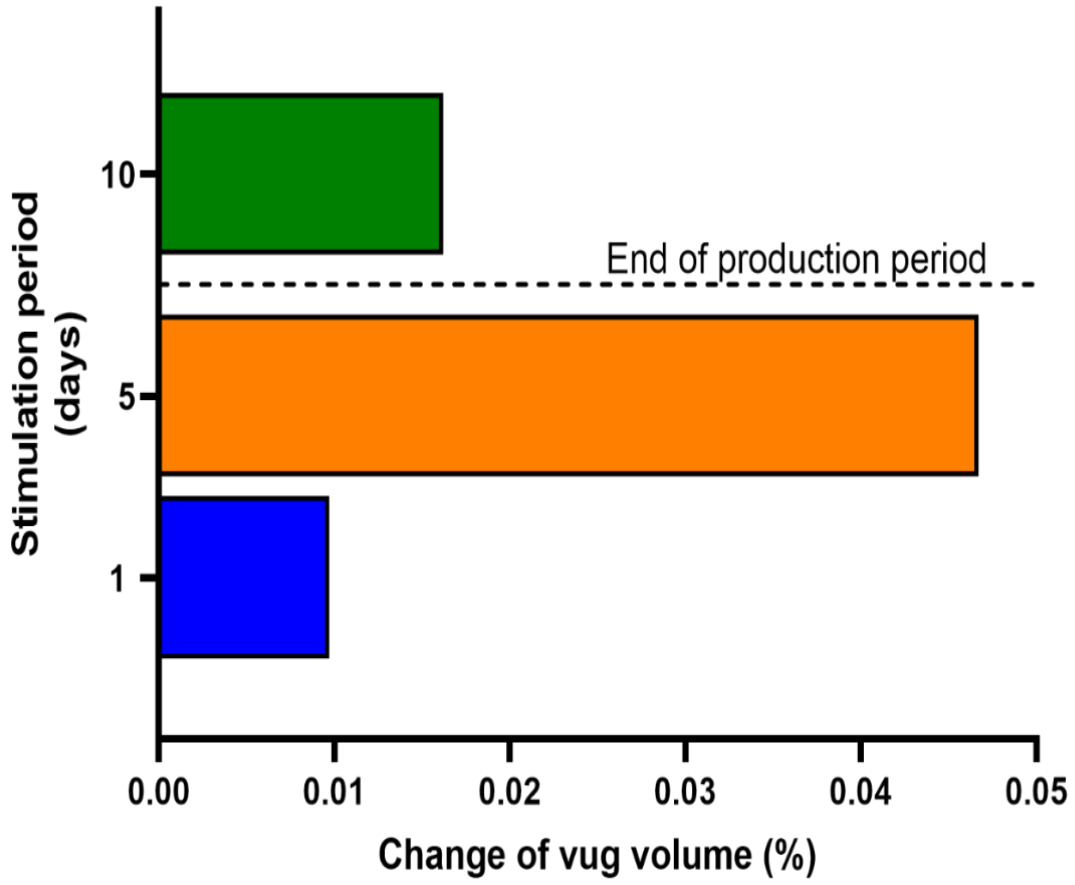

Figure 48: Effect of elasticity test

Figure 48 shows that the vug starts to deform (i.e., change of vug volume) after 1 day of stimulation, and the deformation increases with time as more fluid is produced. Therefore, the reservoir domain becomes more depleted; thus, the stress on the vug increases. However, if the injection is continued and the production is stopped, the pressure in the reservoir domain builds up. It is clear from Figure 48 that the vug slowly start to return to its original shape after the production is halted as can be seen at the 10 days mark.

4.1.7 Convergence Improvement

It was mentioned in the literature review chapter that one of the advantages of using the Brinkman's equation is not having to deal with complex boundary conditions (e.g., the Beavers and Joseph boundary condition or the Beavers-Joseph-Saffman boundary condition) to handle the flow behavior across the interface of the boundaries of the matrix and the open regions (refer to section 2.1.1). However, to capture the effects of the fine-scale heterogeneities using the Brinkman's equation and to ensure convergence and continuity, high number of degrees of freedom is required. This is a challenge as refining the mesh to capture the fine scale heterogeneities makes the model computationally demanding. One way to relax this requirement and to optimize the process is the use of multi-scale mixed finite elements. The following test examine the model's convergence at varying meshes with multi-scale elements where the mesh is refined near the vugs' regions. Table 6 shows the data for the mesh refinement tests.

Table 6: Data for the mesh refinement test for convergence improvement

Parameter	Mesh of Single-phase geometry
Main type of elements	HEX27
Number of elements before mesh refinement	1173
Number of elements after 1st mesh refinement	8000
Number of elements after 2nd mesh refinement	18000

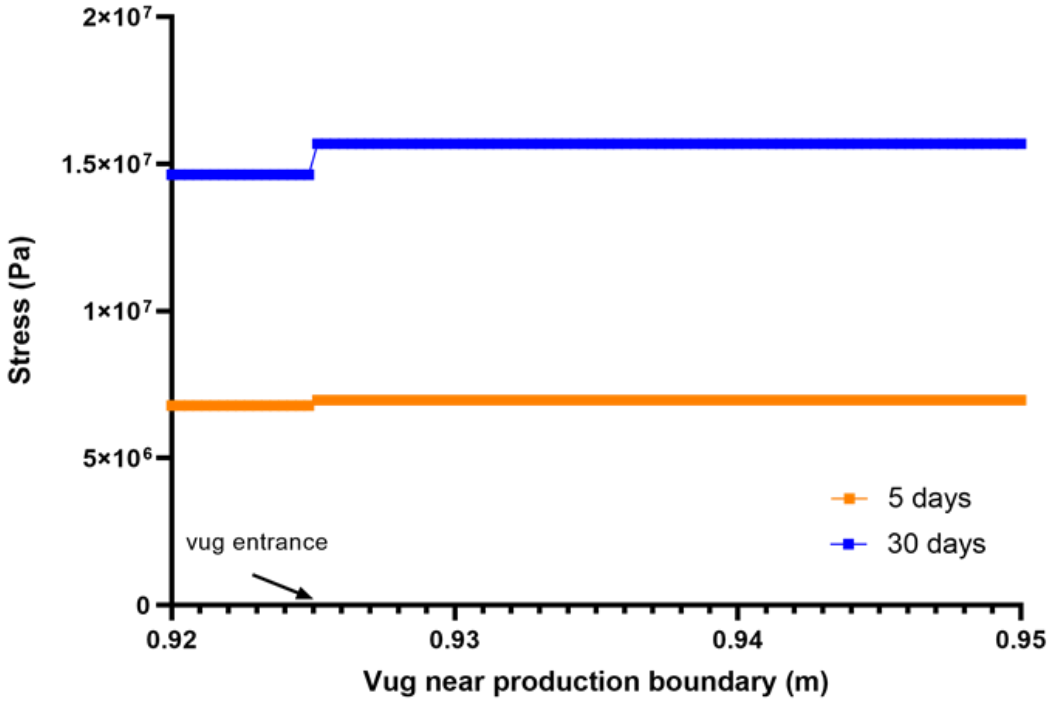

Figure 49: Before mesh refinement

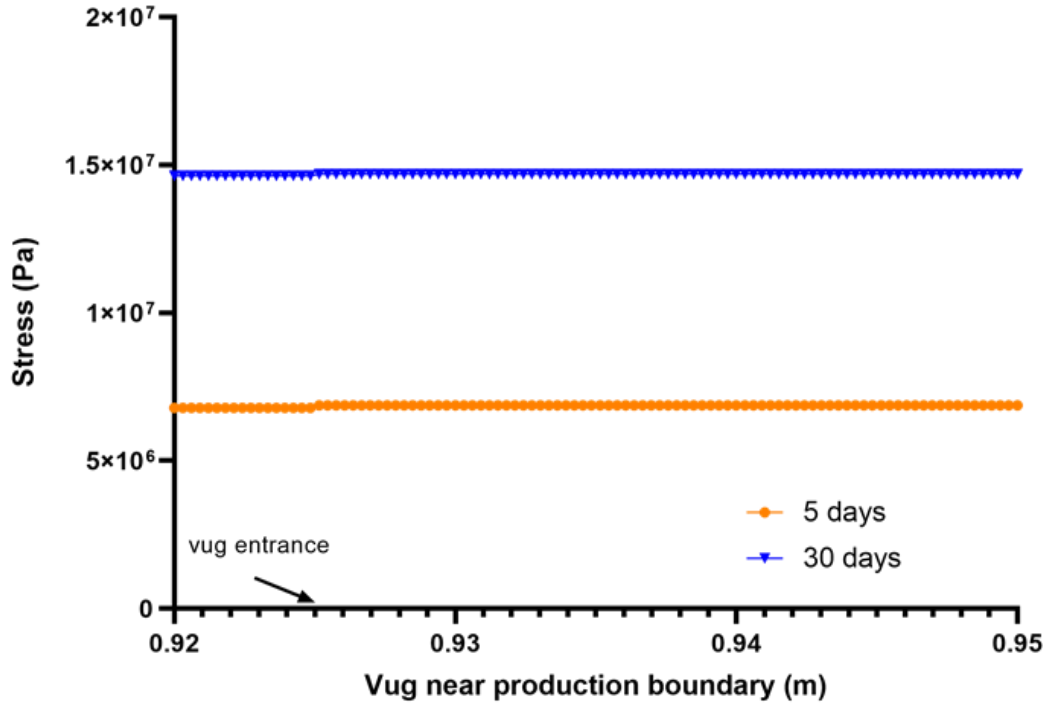

Figure 50: After first mesh refinement

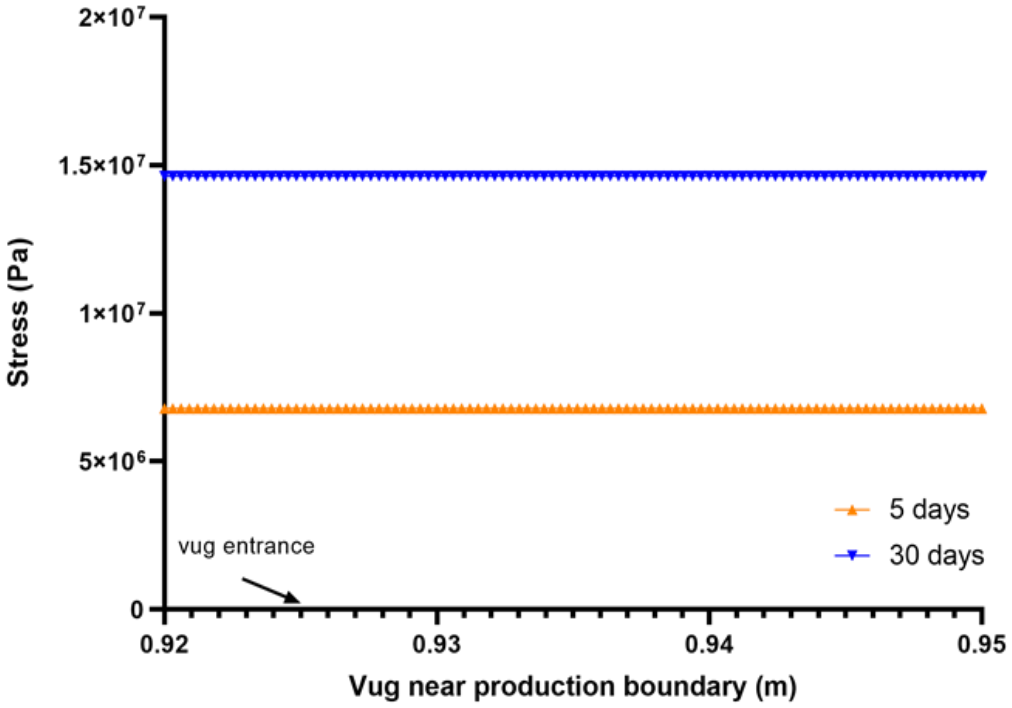

Figure 51: After second mesh refinement

The results in Figure 49, Figure 50 and Figure 51 show the stress profile before the vug entrance and in the vug. It is clear from Figure 49 where no mesh refinement is applied that there is a shift or a discontinuity in the stress profile at the boundary of the vug entrance. This discontinuity occurs due to the different fluid flow behavior before the vug (i.e., Darcy's flow) and in the vug (i.e., free-flow region). It is also clear from Figure 49 that the shift in stress is more after 30 days than 5 days which means the shift becomes higher with time. As mentioned above, the convergence and continuity of the results can be improved without the usage of complex boundary conditions by refining the mesh. After refining the mesh with 8,000 elements, Figure 50 shows improvement in the convergence and continuity. Further mesh refinement is conducted with 18,000 elements, and the results significantly improves as can be seen in Figure 51.

4.2 Two-Phase Flow

In this section, several tests for the two-phase flow model will be conducted to examine different aspects of the fractured-vuggy carbonate rocks. The first test is the simulation of an injection well, and the second test is the simulation of a production well. Note that the two-phase model is an extension of the single-phase model; hence, it handles the flow using the Brinkman's equation, and the geomechanical effects are also included in the model.

4.2.1 Injection Test

In this test, the reservoir domain is initially fully saturated with water and then gas is injected. The water is the wetting phase and the gas is the non-wetting phase. The gas is injected at a user specified boundary and with a user specified injection rate as can be seen in Figure 52. The input data for the test are provided in Table 7.

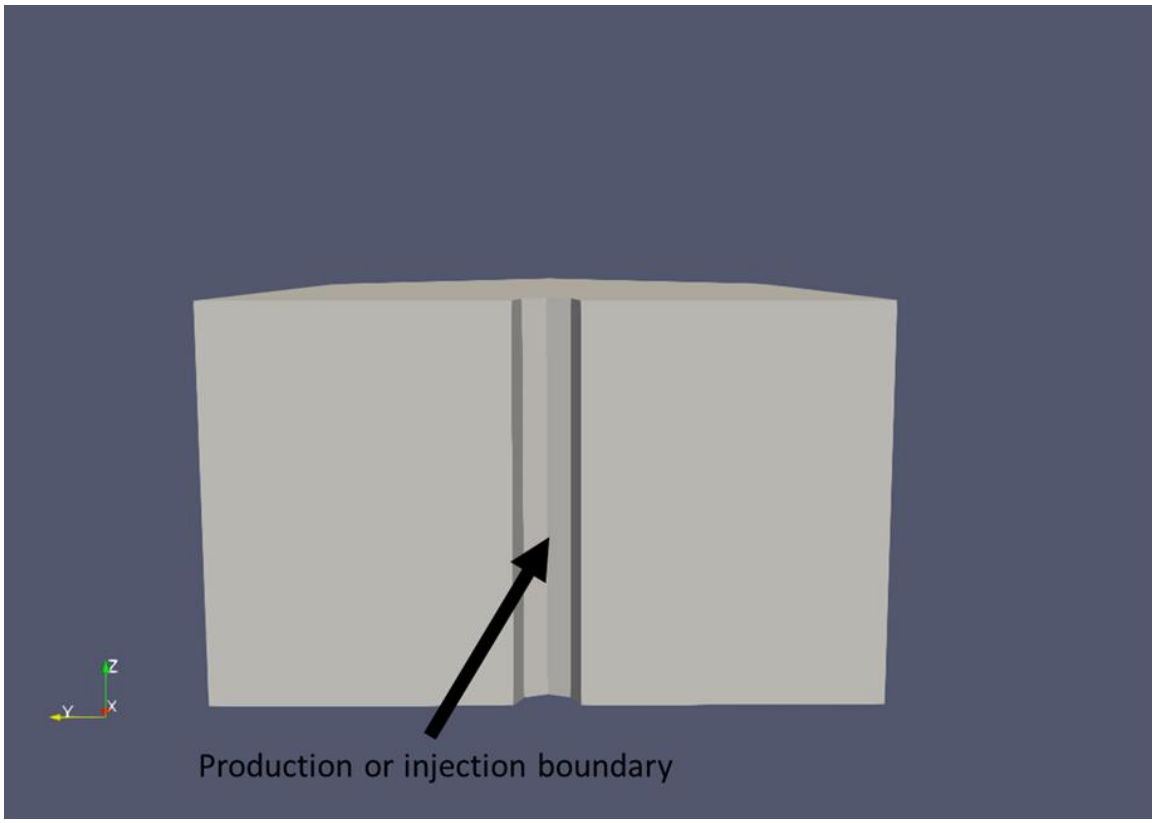

Figure 52: Geometry for two-phase tests

Table 7: Two-phase model data for injection test

Parameter	Value
Reservoir outer radius (m)	10
Reservoir height (m)	12
Fracture and vugs porosity	1
Matrix porosity	0.1
Matrix permeability (mD)	1
Initial pressure (psi)	2900
Injection rate (bbl/min)	1.5
Young's modulus (GPa)	66

Poisson's ratio	0.18
Biot poroelastic coefficient	1
lambda parameter for relative permeability	2
m parameter for capillary pressure	0.6
Residual saturation of liquid phase	0.15
Residual saturation of gas phase	0.1

After an injection period of two days, the water saturation starts to decrease near the injection boundary, and the gas saturation increases as can be seen in Figure 53 and Figure 54, respectively.

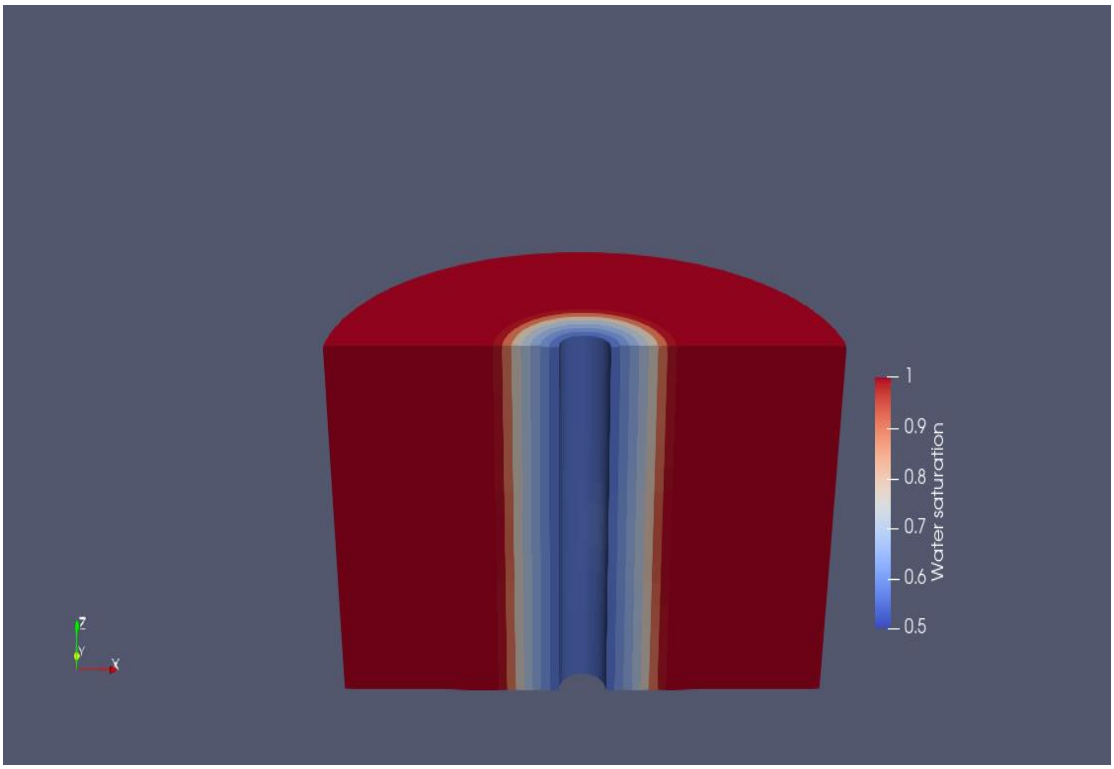

Figure 53: Water saturation for injection test

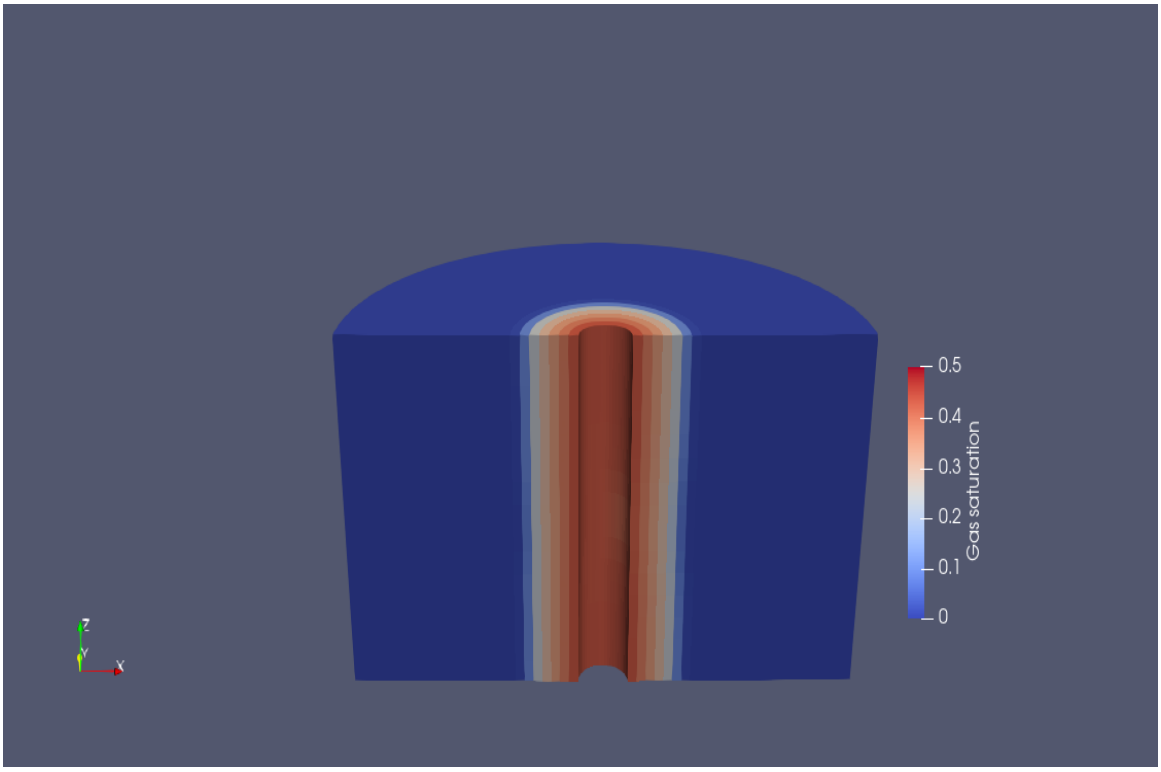

Figure 54: Gas saturation for injection test

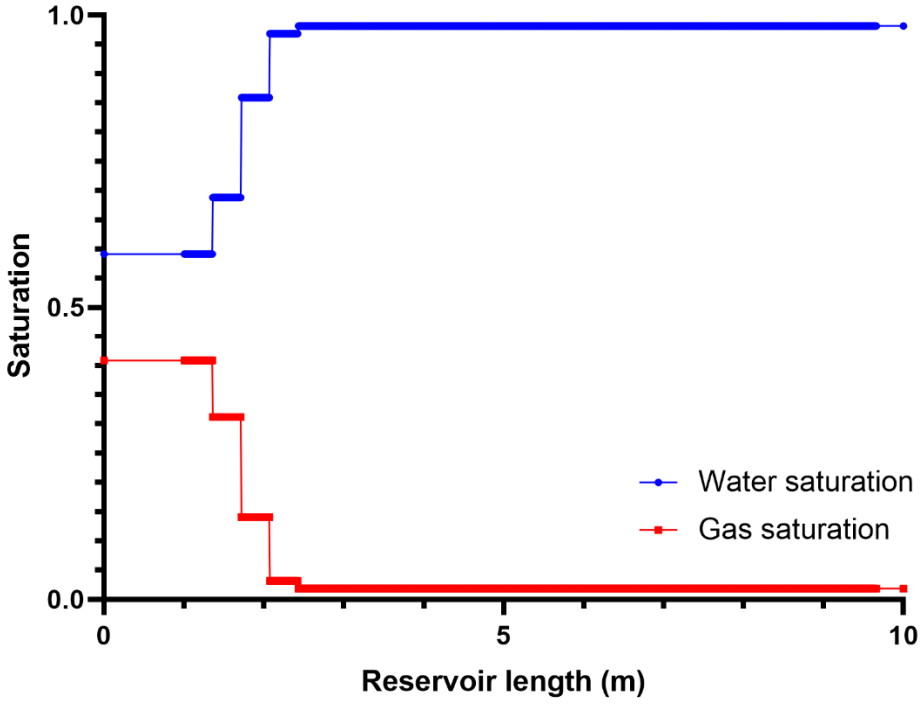

Figure 55: Saturation profile after 1 day of injection

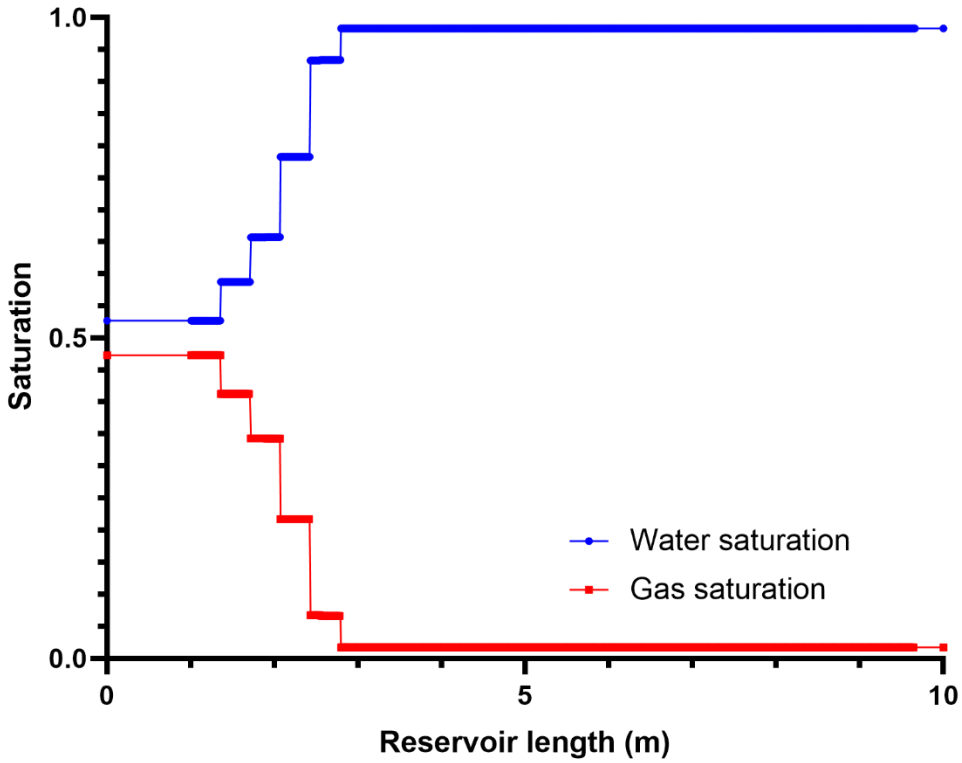

Figure 56: Saturation profile after 2 days of injection

Figure 55 and Figure 56 show the saturation profiles for the water and gas after 1 day and 2 days. It is clear from the figures that the gas saturation increases with time while the water saturation decreases; however, the entire domain is pressurized due to the injection treatment (Appendix C).

After injecting gas for a two-day period, it is clear that the pressure near the injection boundary increases for both the water and gas as can be seen in Figure 57 and Figure 58, respectively. Figure 57 also shows that the pressure near a vug is slightly higher than the matrix. This is expected as it becomes more difficult to inject there due to the wettability effects as the matrix system is water-wet; thus, the water tends to stick to the matrix rocks.

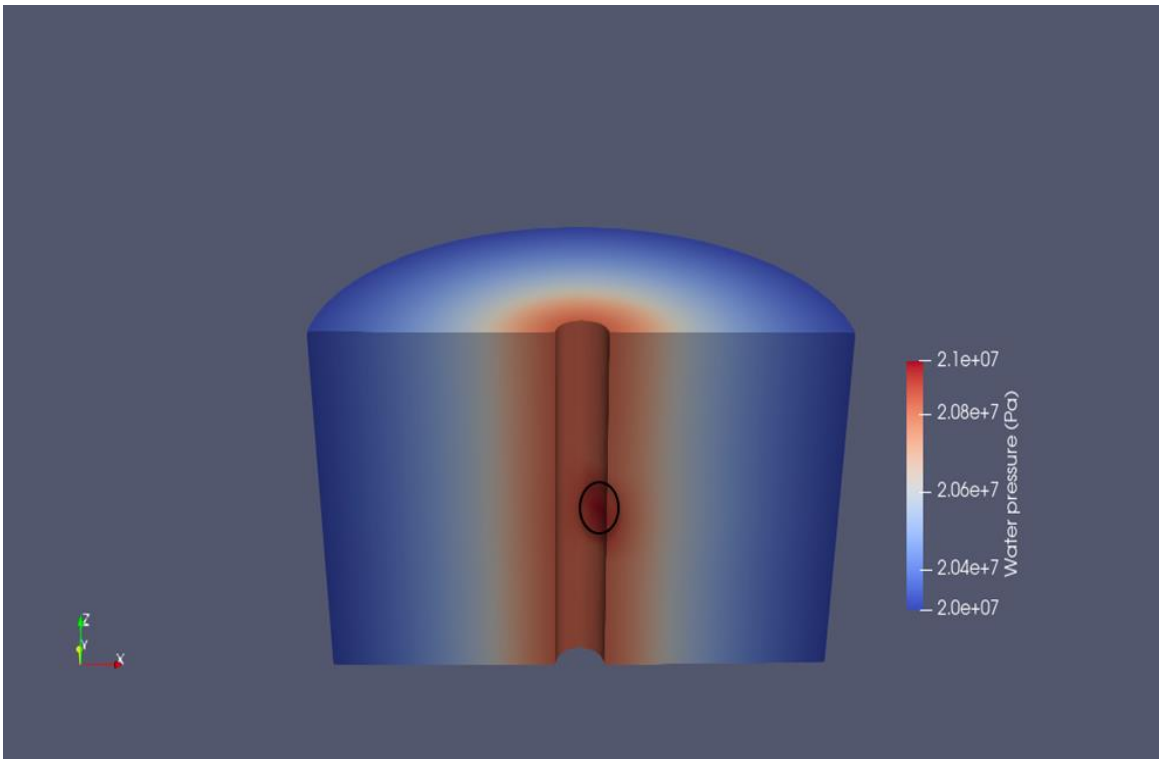

Figure 57: Water pressure for injection test

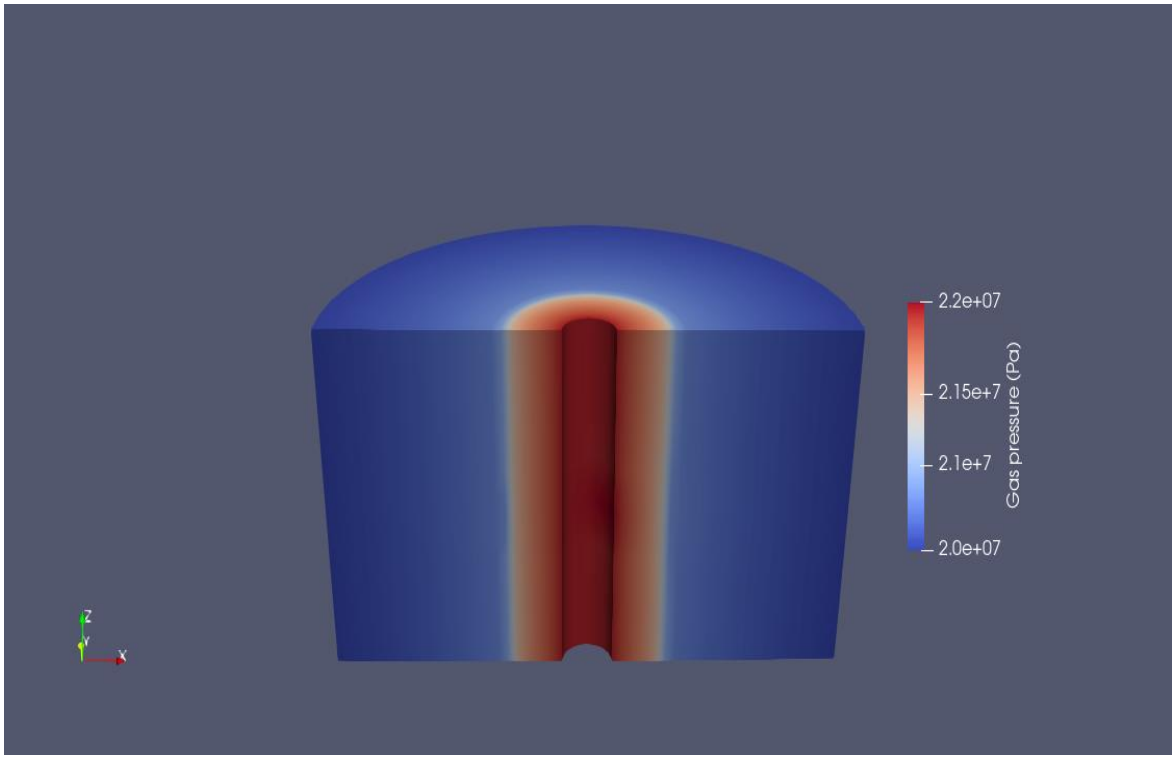

Figure 58: Gas pressure for injection test

4.2.2 Production Test

In this test, the reservoir domain contains both water and gas. The water is the wetting phase, and the gas is the non-wetting phase. The gas is produced at a user specified boundary and with a user specified flow rate as can be seen in Figure 59. The input data for the test are provided in Table 8.

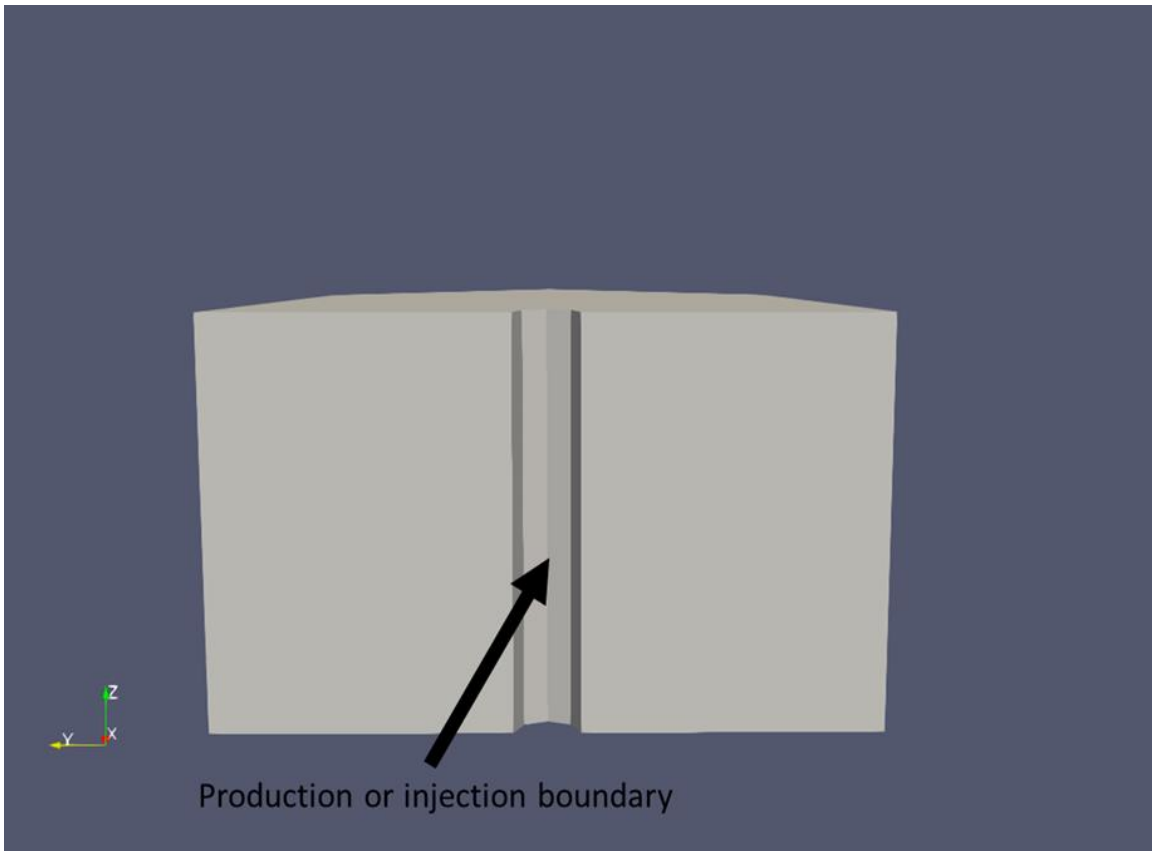

Figure 59: Geometry for two-phase tests

Table 8: Two-phase model data for production test

Parameter	Value
Reservoir outer radius (m)	10
Reservoir height (m)	12
Fracture and vugs porosity	1

Matrix porosity	0.1
Matrix permeability (mD)	1
Initial water pressure (psi)	2900
Initial gas pressure (psi)	2975
Young's modulus (GPa)	66
Poisson's ratio	0.18
Biot poroelastic coefficient	1
lambda parameter for relative permeability	2
m parameter for capillary pressure	0.6
Residual saturation of liquid phase	0.15
Residual saturation of gas phase	0.1

The water and gas saturation profiles after six days of production are provided in Figure 60 and Figure 61, respectively. It is clear from the saturation profiles that the gas saturation is high near the wellbore whereas the water is less there. This occurs as the gas is the phase being produced and because the water is the wetting-phase.

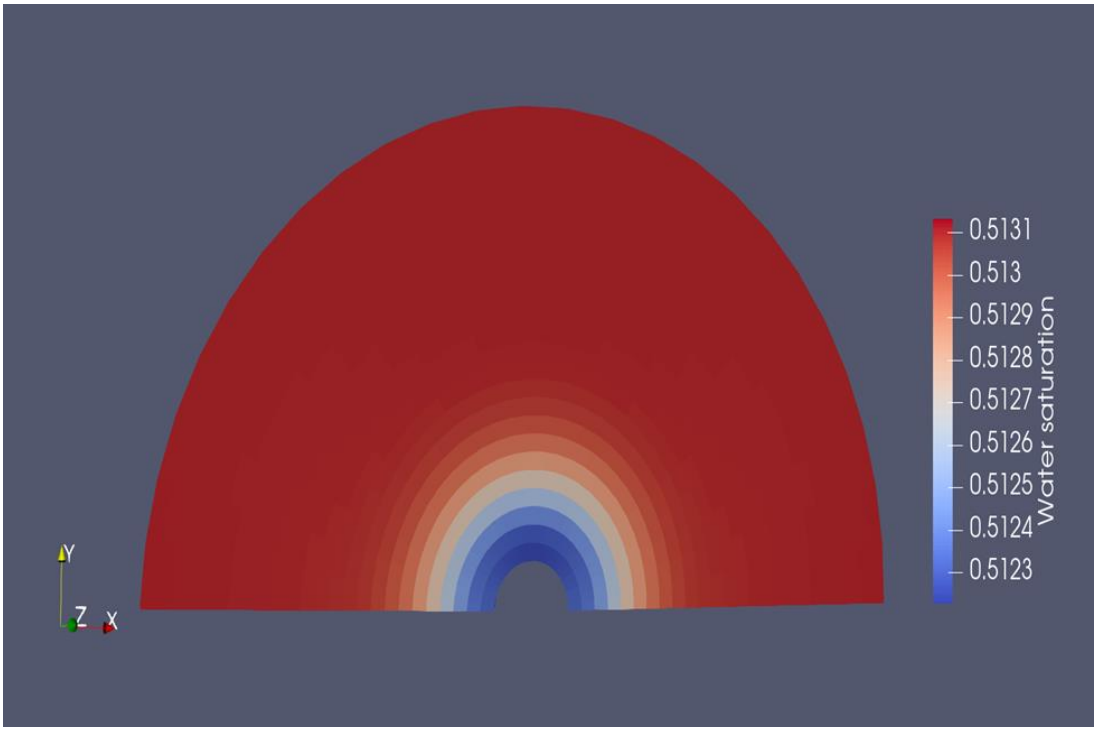

Figure 60: Water saturation for production test

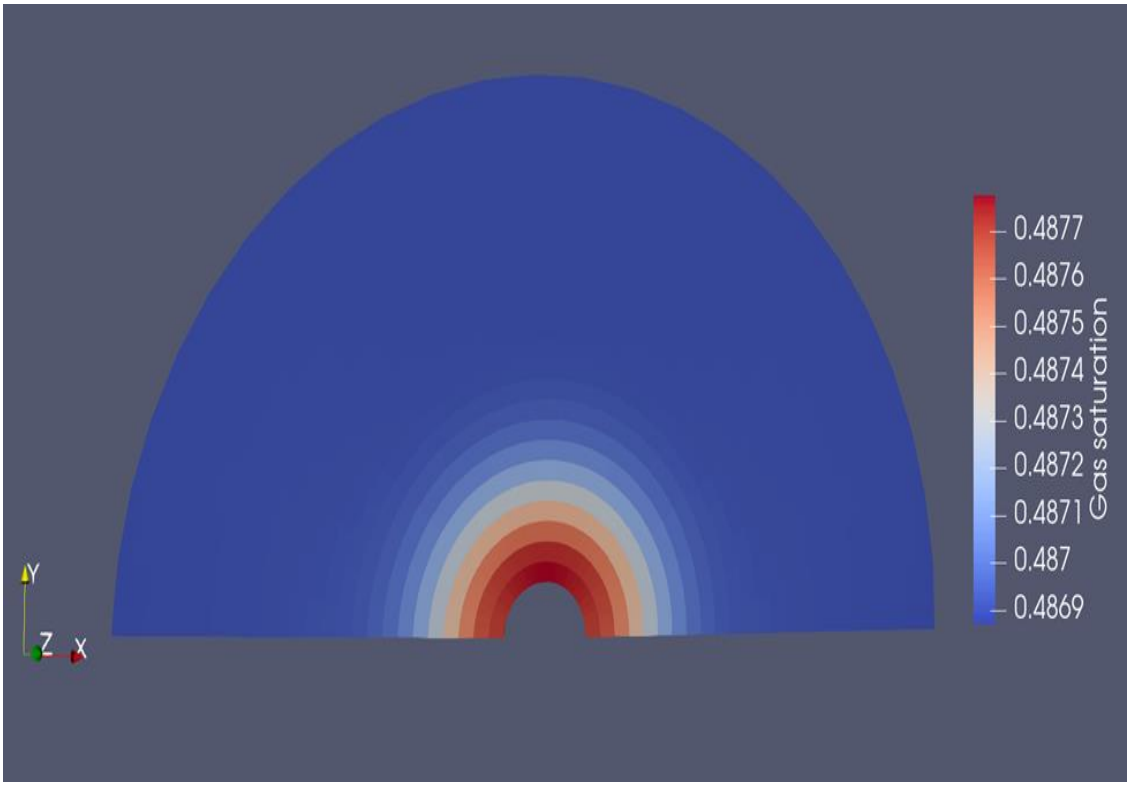

Figure 61: Gas saturation for production test

After producing gas for a six-day period, the pressure near the wellbore boundary becomes less in value for both the water and gas as can be seen in Figure 62 and Figure 63, respectively. Figure 62 and Figure 63 also show that the pressure near a vug is a bit less in value than the matrix. This is expected as it is easy to produce the gas from those regions due to the wettability of the matrix system. The matrix system is water-wet; thus, the water tends to stick to the matrix rocks whereas the gas stays in the vugs and becomes easier to flow.

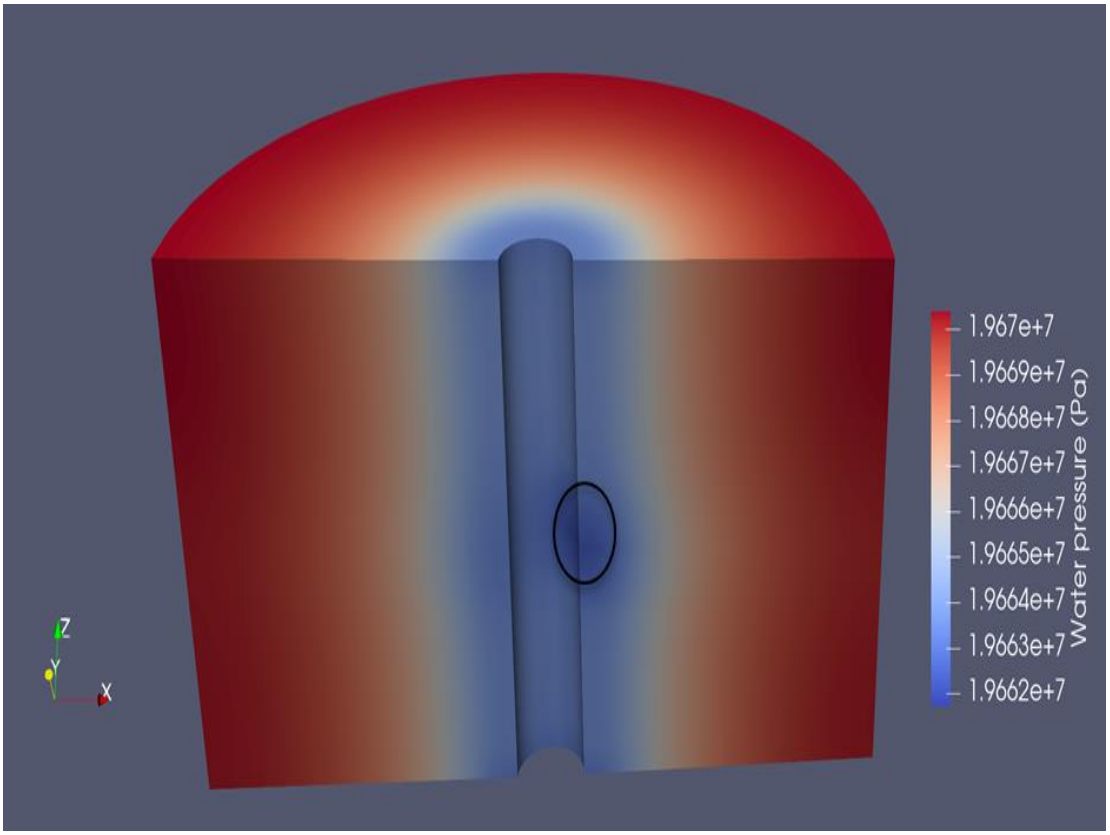

Figure 62: Water pressure after six days of production

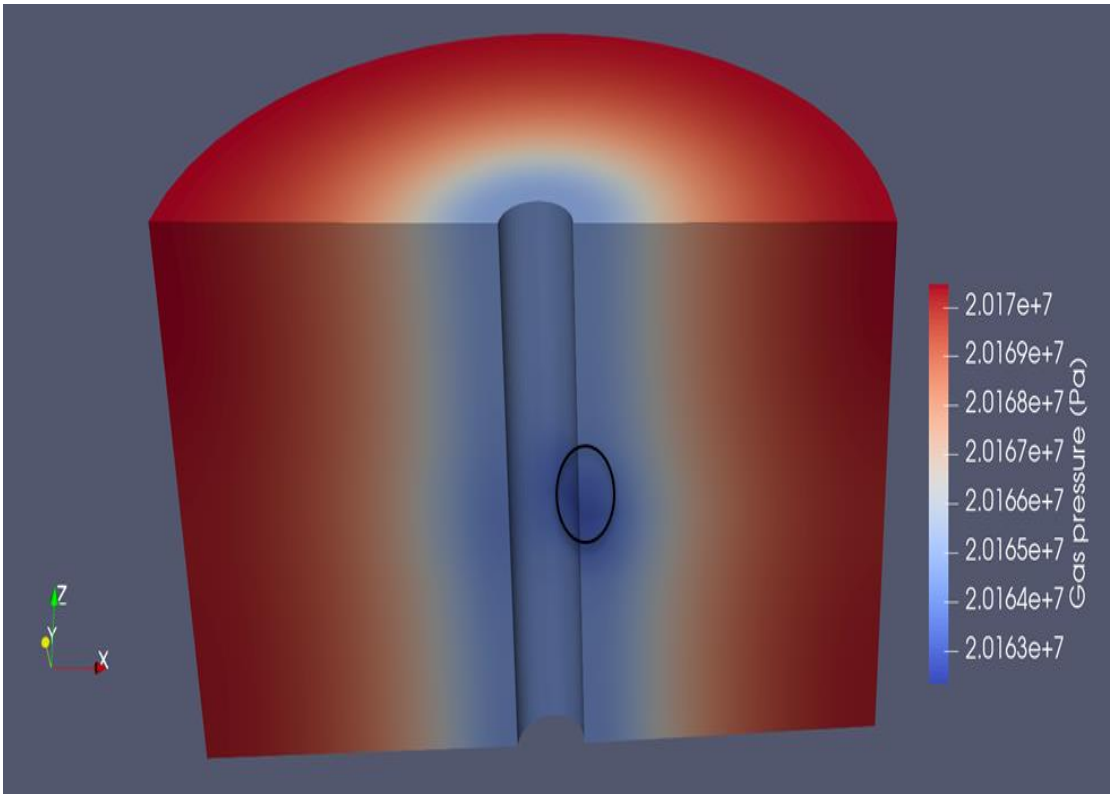

Figure 63: Gas pressure after six days of production

4.2.3 Effect of Capillary Pressure on Injectivity

This test is conducted to examine the effect of the capillary pressure by mimicking the flow injection in different pore sizes by using a relatively low and high values for the capillary pressure where the reservoir permeability is 1 (mD). The relative permeability curves are shown in Figure 64. The data for the capillary pressure test is provided in Table 9 where the capillary pressure input data is taken from a carbonate formation published by (Egermann, Lombard, & Bretonnier, 2006; Hosseinzadeh Hejazi, Shah, & Pini, 2019).

Table 9: Two-phase model data for the capillary pressure test

Parameter	Value
Reservoir outer radius (m)	10

Reservoir height (m)	12
Fracture and vugs porosity	1
Matrix porosity	0.1
Matrix permeability (mD)	1
Initial pressure (psi)	2900
Injection rate (bbl/min)	1.5
Young's modulus (GPa)	66
Poisson's ratio	0.18
Biot poroelastic coefficient	1
lambda parameter for relative permeability	2
m parameter for capillary pressure	0.6
Residual saturation of liquid phase	0.15
Residual saturation of gas phase	0.1

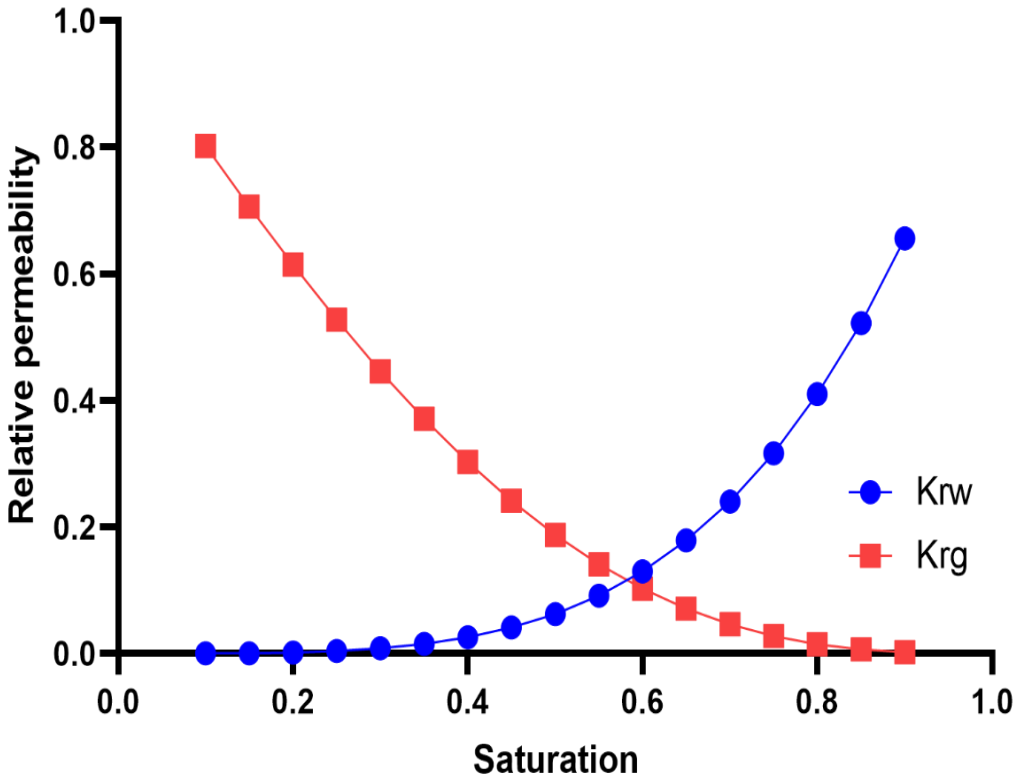

Figure 64: Relative permeability

The capillary pressure curves for the low and high values are shown in Figure 65 and Figure 66, respectively.

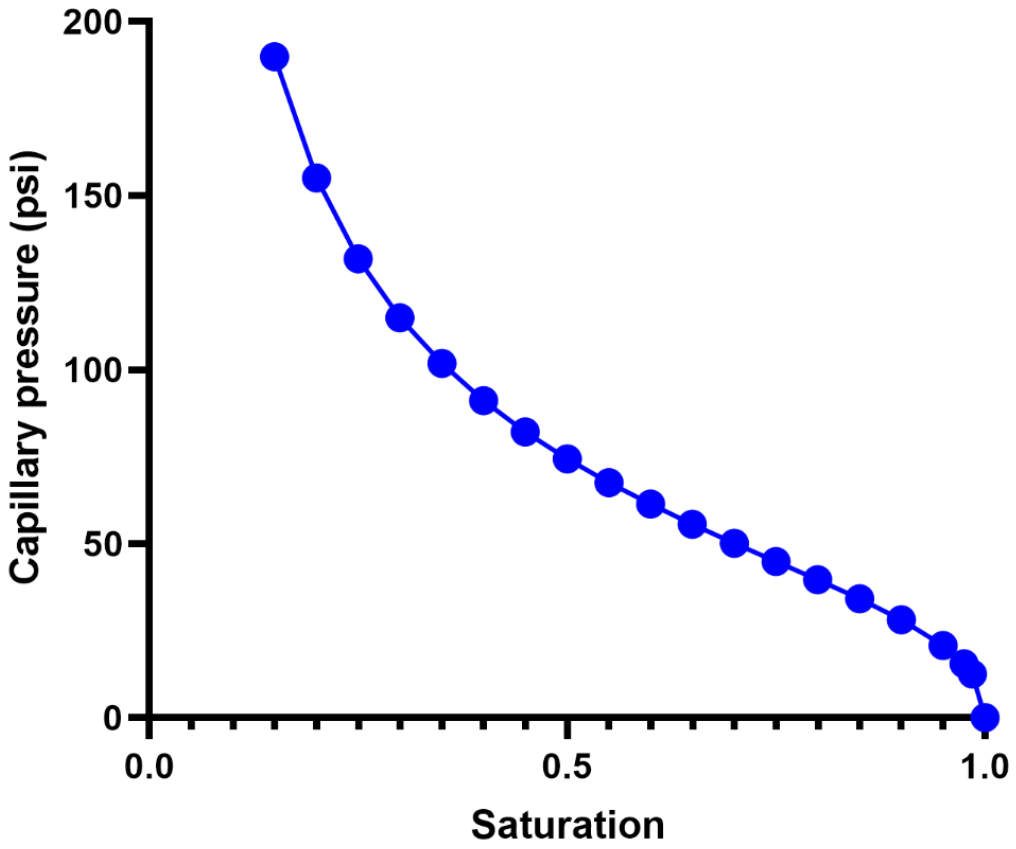

Figure 65: Relatively low capillary pressure test

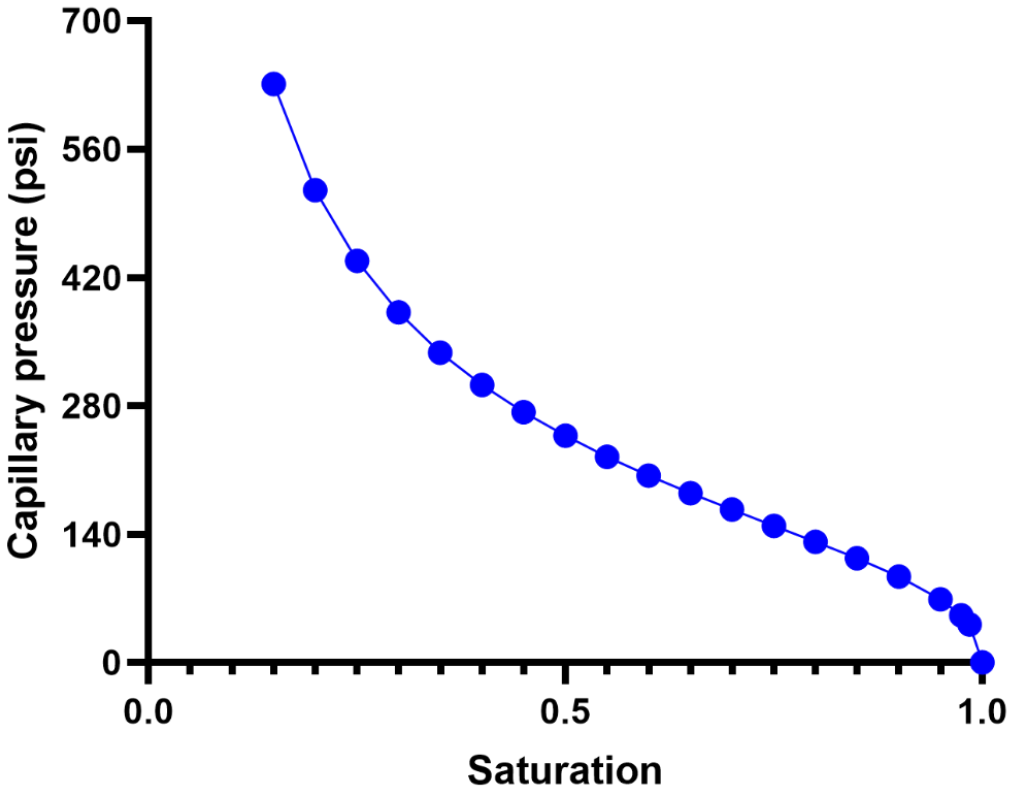

Figure 66: High capillary pressure test

The gas saturation, gas pressure and water pressure results of the two capillary pressure values are presented in Figure 67, Figure 68 and Figure 69, respectively. The results show that the saturation of the gas is higher when the capillary pressure is lower compared with the cases with higher capillary pressure, and the gas and water pressures are lower when the capillary pressure is low. This is due to the wettability of the matrix system. The matrix system is water-wet; thus, the water tends to stick to the matrix rocks whereas the gas stays in the vugs.

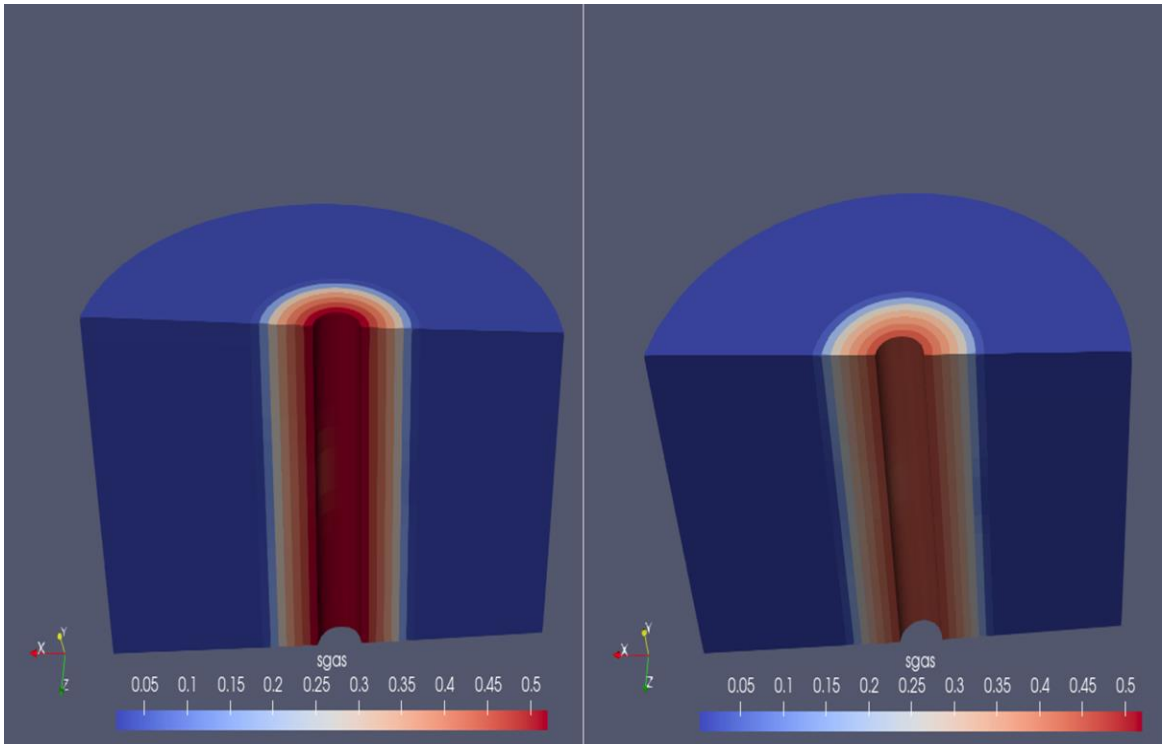

Figure 67: Gas saturation after 3 days of injection at low Pc (left) and high Pc (right)

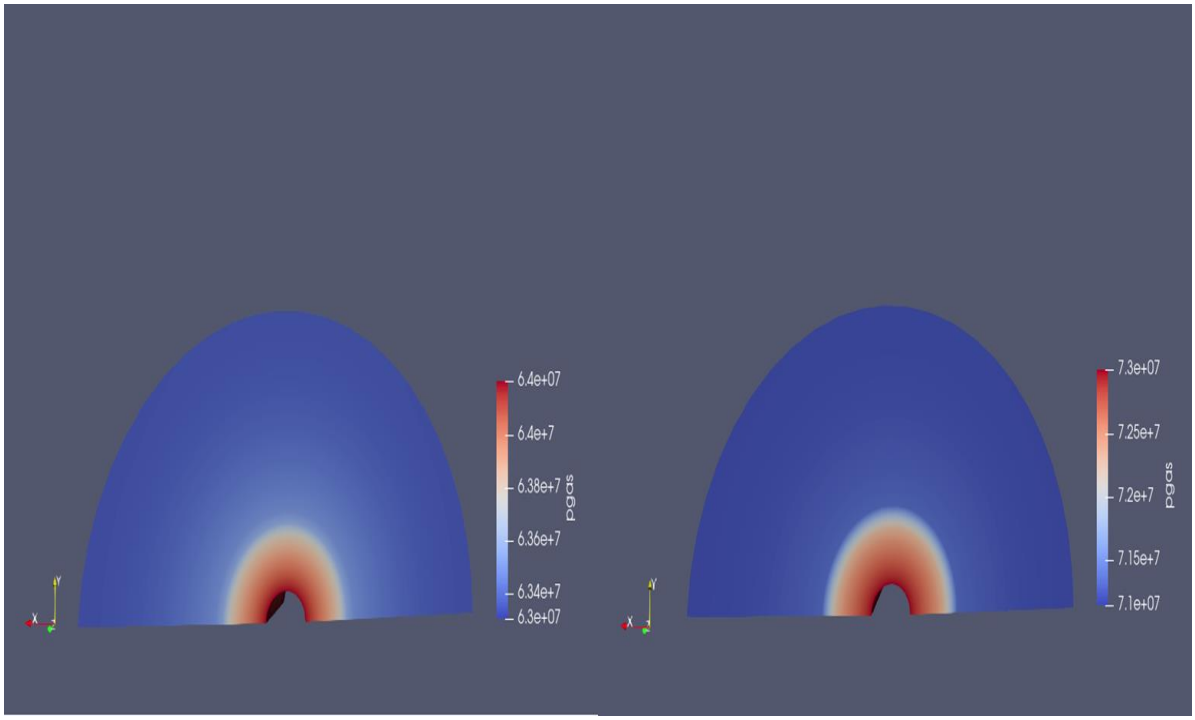

Figure 68: Gas pressure after 3 days of injection at low Pc (left) and high Pc (right)

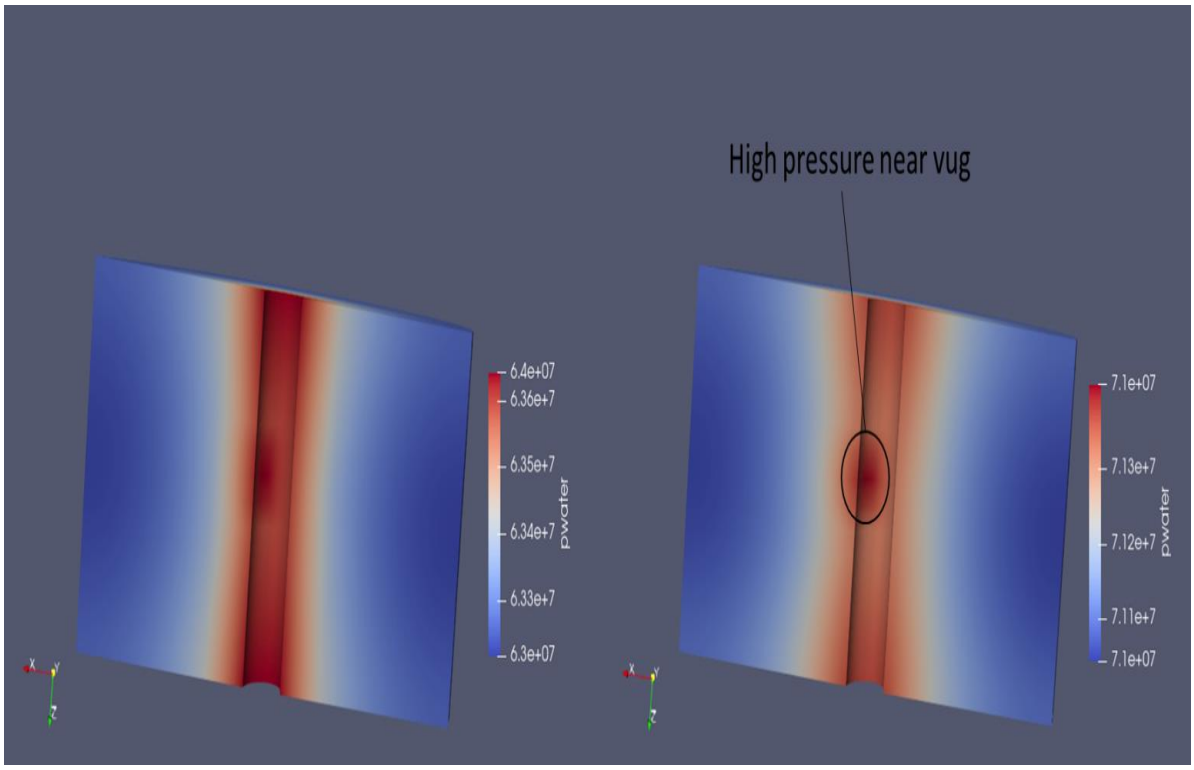

Figure 69: Water pressure after 3 days of injection at low Pc (left) and high Pc (right)

It is obvious that higher pressure is required to inject the gas when the capillary pressure is high as can be seen in the right-hand side of Figure 68 and Figure 69. This test shows the importance of the capillary pressure in the two-phase model. Consequently, lower values for the capillary pressure (e.g., Figure 70) would change the water and gas pressure significantly and as can be seen in Figure 71.

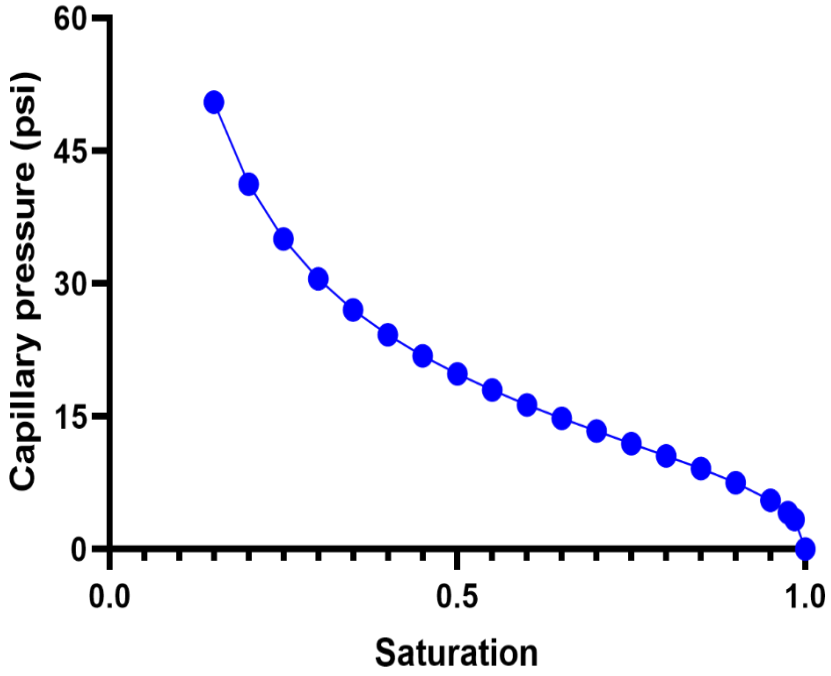

Figure 70: Low capillary pressure

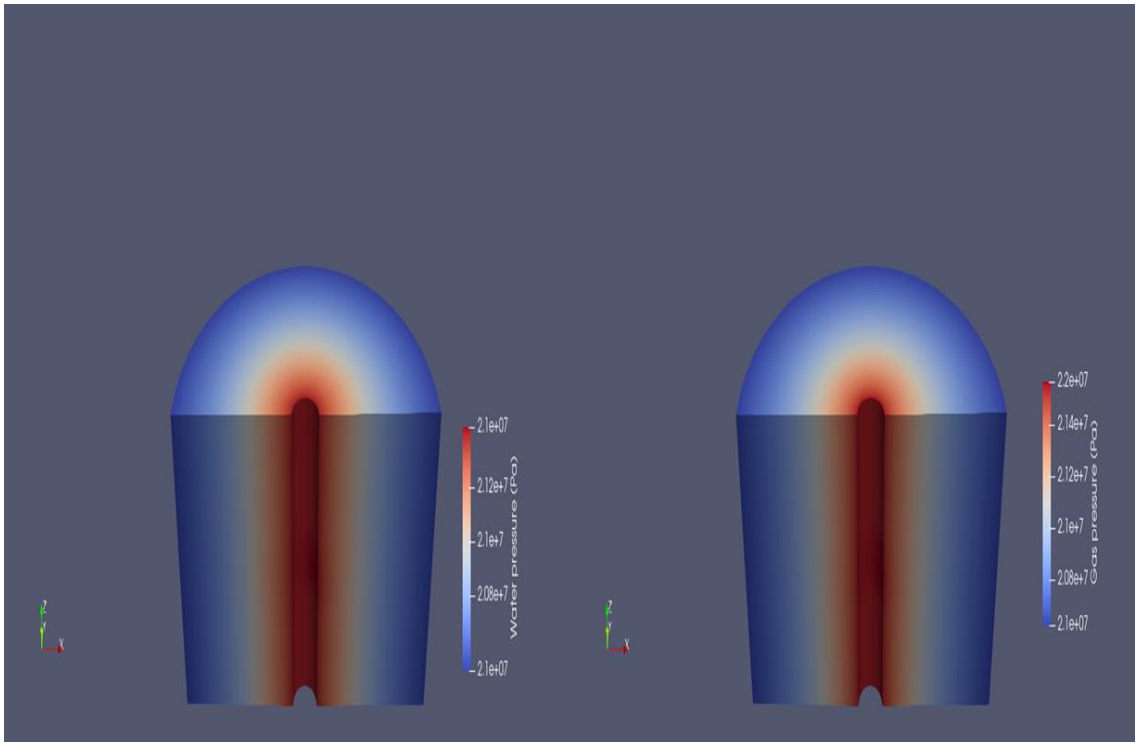

Figure 71: Water and gas pressure at low Pc

The capillary pressure and wettability of the matrix system play major roles in the two-phase models. In general, if the matrix system is water-wet, then the water tends to stick to the matrix rocks whereas the oil tends to fill the vugs. Consequently, the saturation of the oil becomes higher in the open regions as more volume of oil stays there. However, if the matrix system is oil-wet, the oil would stick to the matrix rocks and the water would fill the vugs. In oil-wet vuggy carbonate rocks, large amount of water might be produced from those formation as the vugs would be filled with water, and also it is easier for the water to flow than the oil due to the capillary pressure and wettability effects. These effects were experienced in the conducted tests above as was shown in the pressure and saturation profiles.

Finally, there are two main challenges or limitations in the developed model. First, to accurately capture the fine-scale heterogeneities in the model, the mesh of the created geometry must be refined. The mesh refinement results in a high number of elements and nodes, and ultimately, a significantly high number of degrees of freedom (DOFs), and that leads to the second challenge. The second challenge is the demand of the computational power. A high number of DOFs means the system requires substantial processing and memory capabilities in order to be solved; thus, the computational time and computational requirements become intensive.

5 Chapter V: Conclusions

A fully coupled-multiscale 3D model that simulates the fluid flow in heterogeneous fractured-vuggy carbonate rocks has been developed. The model considers the co-existing flow in the porous matrix and in the free-flow regions and accounts for the geomechanical effects and the evolution of porosity and permeability. The developed model is novel as it: 1) utilizes the advanced numerical finite element method with mixed elements to solve the sophisticated governing equations, 2) employs the Brinkman's equation and ensures flow continuity in the matrix and free-flow regions without the need of complex boundary conditions, 3) considers the second-order stress-strain gradient in the rock mechanical equation, which makes the model more responsive to the geomechanical effects by accounting for nonlocality, 4) accounts for the porosity evaluation, and 5) the model is capable of handling two-phase flow. It was shown that the developed model gives more realistic results compared to the classical models; thus, the model facilitates the characterization of the fractured-vuggy carbonate rocks. Consequently, more informed decisions can be made to improve the field development plans and ultimately improving the recovery factor.

The developed model was utilized to examine several aspects of the heterogeneous fractured-vuggy carbonate and here are the main findings from the conducted tests:

1) The developed model accurately captures the fluid flow behavior in the matrix and in the free-flow regions (i.e., vugs and fractures.)
2) The second-order stress-strain gradient in the rock mechanical equation significantly improves the converges of the model.
3) Assigning an average permeability value for the open regions and using Darcy's law to capture the fluid flow in the free-flow regions, which is practiced by the existing models, is not an ideal practice as the cumulative production can be underestimated or

overestimated if the assigned average permeability value does not properly capture the overall heterogeneities of the reservoir system. Overall, Darcy's law fails to capture the flow behavior within the vugs as Darcy's law is only applicable in porous media and not the free-flow regions.

4) Assigning the same value of stiffness modulus for the matrix and the open regions (i.e., vugs and fractures) influences the outcome of the simulator. Hence, to accurately account for the geomechanical effects (e.g., vug deformation), different stiffness modulus values should be assigned for the open regions which depends on the open regions being sediment-filled or fluid-filled.
5) The vugs' deformation becomes more difficult as the stiffness modulus near the vugs' region increases. The vugs deform due to compaction, and more deformation occurs near the production boundary as the effective stress on the vugs is higher there. However, when the production is halted, the vugs would return to their original shape after some time if the injection is continued and if they do not experience fracturing stress. This is due to elasticity as the model is developed for elastic material.
6) When no mesh refinement is applied, there might be a shift or a discontinuity in the stress profile at the boundary of the vug entrance. The discontinuity occurs due to the different fluid flow behavior before the vug (i.e., Darcy's flow) and in the vug (i.e., free-flow region). However, the convergence and continuity can be improved by refining the mesh.
7) The model is also tested for two-phase flow, and it was found that when the water is considered to be the wetting-phase and the gas is the non-wetting phase, the pressure near the vugs' region is a bit higher during the injection of gas and lower during the production

of gas. This is due to the wettability effects as the water tends to stick at the matrix rocks as the system is water-wet whereas the gas tends to stay in the vugs.

8) The effects of the capillary pressure were also examined, and it was found that the capillary pressure plays a significant role in the water and gas pressures during injection and production as the wettability affects the capillary pressure as was discussed above.

6 References

Aarnes, J. E., Kippe, V., & Lie, K. A. (2005). Mixed multiscale finite elements and streamline methods for reservoir simulation of large geomodels. *Advances in Water Resources*, *28*(3), 257–271. https://doi.org/10.1016/j.advwatres.2004.10.007

Abdassah, D., & Ershaghi, I. (1986). *Triple-Porosity Systems for Representing Naturally Fractured Reservoirs*. SPE Formation Evaluation. https://doi.org/10.2118/13409-PA

Akbar, M., Vissapragada, B., Alghamdi, A., Allen, D., Herron, M., & Carnegie A. Saxena, K. (2000). *A Snapshot of Carbonate Reservoir Evaluation. Oilfield Review.* Schlumberger.

Alhubail, M.M., Misra, A., & Barati, R. (2017). A novel acid transport model with robust finite element discretization. In *Society of Petroleum Engineers - SPE Kingdom of Saudi Arabia Annual Technical Symposium and Exhibition 2017*. https://doi.org/10.2118/188030-MS

Alhubail, Mustafa M., Misra, A., Maulianda, B., & Barati, R. (2020). Application of finite element discretization with weak formulation for simulation of acid fracturing in tight carbonate reservoirs. *Journal of Petroleum Science and Engineering*. https://doi.org/10.1016/j.petrol.2020.107047

Alotaibi, M., Azmy, R., & Nasr-El-Din, H. (2010). *Wettability Challenges in Carbonate Reservoirs*. SPE Improved Oil Recovery Symposium. Tulsa: Society of Petroleum Engineers. https://doi.org/10.2118/129972-MS

Angot, P. (1999). *Analysis of singular perturbations on the Brinkman problem for fictitious domain models of viscous flows*. Mathematical Methods in the Applied Sciences.

Arbogast, T. (1997). *Computational Aspects of Dual-Porosity Models*. In U. Hornung Homogenization and Porous Media: Springer.

Arbogast, T., & Brunson, D. (2007). *A computational method for approximating a Darcy Stokes system governing a vuggy porous medium*. Computational Geosciences. https://doi.org/10.1007/s10596-007-9043-0

Arbogast, T., & Lehr, H. (2006). *Homogenization of a Darcy Stokes system modeling vuggy porous media*. Computational Geosciences. https://doi.org/10.1007/s10596-006-9024-8

Bacci, G., Korre, A., & Durucan, S. (2011). *An experimental and numerical investigation into the impact of dissolution/precipitation mechanisms on CO2 injectivity in the wellbore and far field regions*. International Journal of Greenhouse Gas Control. https://doi.org/10.1016/j.ijggc.2010.05.007

Bai, M., Elsworth, D., & Roegiers, J.-C. (1993). *Multiporosity/multipermeability approach to the simulation of naturally fractured reservoirs*. Water Resources Research. https://doi.org/10.1029/92WR02746

Barenblatt, G., Zheltov, I., & Kochina, I. (1960). *Basic concepts in the theory of seepage of homogeneous liquids in fissured rocks [strata]*. Journal of Applied Mathematics and Mechanics. https://doi.org/10.1016/0021-8928(60)90107-6

Bažant, Z. P., & Pijaudier-Cabot, G. (1988). Nonlocal continuum damage, localization instability and convergence. *Journal of Applied Mechanics, Transactions ASME*. https://doi.org/10.1115/1.3173674

Beavers, G., & Joseph, D. (1967). *Boundary conditions at a naturally permeable wall*. Journal of Fluid Mechanics. https://doi.org/10.1017/S0022112067001375

Benner, P., Dolgov, S., Onwunta, A., & Stoll, M. (2016). Low-rank solvers for unsteady Stokes-Brinkman optimal control problem with random data. *Computer Methods in Applied Mechanics and Engineering*. https://doi.org/10.1016/j.cma.2016.02.004

Biot, M. (1941). *General Theory of Three-Dimensional Consolidation*. Journal of Applied Physics.

Biot, M. (1955). Theory of Elasticity and Consolidation for a Porous Anisotropic Solid. *Journal of Applied Physics*, *26*(2), 182–185. https://doi.org/10.1063/1.1721956

Biot, M. (1956). General solutions of the equations of elasticity and consolidation for a porous material. *Jounral of Applied Mechanics*, *23*(1), 91–96.

Biot, M. (1962). Mechanics of deformation and acoustic propagation in porous media. *Journal of Applied Physics*, *33*, 4. https://doi.org/https://doi.org/10.1063/1.1728759

Biot, M., & Willis, D. (1957). *The Elastic Coefficients of the Theory of Consolidation*. Journal of Applied Mechanics.

Brinkman, C. (1947). *A Calculation of the Viscous Force Exerted by a Flowing Fluid on a Dense Swarm of Particles*. Journal of Applied Sciences Research.

Brooks, R., & Corey, A. (1966). Properties of Porous Media Affecting Fluid Flow. *Journal of the Irrigation and Drainage Division*.

Burchette, T. (2012). *Carbonate rocks and petroleum reservoirs: a geological perspective from the industry*. Geological Society. https://doi.org/10.1144/SP370.14

Cao, Y., Gunzburger, M., Hua, F., & Wang, X. (2008). *Coupled Stokes-Darcy model with*

Beavers-Joseph interface boundary condition. Communications in Mathematical Sciences. https://doi.org/10.4310/CMS.2010.v8.n1.a2

Carman. (1938). Determination of the specific surface of powders I. Transactions. *J. Soc. Chemical Industries.*, *57*, 225–234. Retrieved from http://ci.nii.ac.jp/naid/10029440079/en/

Carrillo, F. J., & Bourg, I. C. (2019). A Darcy-Brinkman-Biot Approach to Modeling the Hydrology and Mechanics of Porous Media Containing Macropores and Deformable Microporous Regions. *Water Resources Research*. https://doi.org/10.1029/2019WR024712

Chen, H., Teufel, L., & Lee, R. (1995). *Coupled Fluid Flow and Geomechanics in Reservoir Study - I. Theory and Governing Equations. SPE Annual Technical Conference and Exhibition*. Dallas: Society of Petroleum Engineers. https://doi.org/10.2118/30752-MS

Chen, W., Gunzburger, M., Hua, F., & Wang, X. (2011). *A Parallel Robin Robin Domain Decomposition Method for the Stokes Darcy System*. SIAM Journal on Numerical Analysis. https://doi.org/10.1137/080740556

Chen, Z., Huan, G., & Ma, Y. (2006). *Computational Methods for Multiphase Flows in Porous Media*. Philadelphia: Society for Industrial and Applied Mathematics. https://doi.org/ISBN: 0-89871-606-3

Chilingar, G., Bissell, H., & Wolf, K. (1967). *Diagenesis of Carbonate Rocks*. In G. Larsen, & G. Chilingar, Diagenesis in sediments. NEW YORK: ELSEVIER PUBLISHING COMPANY.

Chilingarian, G., Mazzullo, S., & Rieke, H. (1992). *Chapter 1: Introdution*. In G. Chilingarian, S. Mazzullo, & H. Rieke, Carbonate reservoir characterization a geologic- engineering analysis, part I: Elsevier Science. https://doi.org/ISBN 0-444-88849-7

Chilingarian, G., Mazzullo, S., & Rieke, H. (1996). *carbonate reservoir characterization: a geologic - engineering analysis, part II*. Elsevier Science. https://doi.org/ISBN: 0-444-82103-1

Darcy, H. (1856). *Darcy's law*. Paris: Les fo ntain es Publiques de lu Ville de Dijon.

David, C. W. (2003). Goodbye, Hazen; Hello, Kozeny-Carman. *Journal of Geotechnical and Geoenvironmental Engineering*, *129*(11), 1054–1056. https://doi.org/10.1061/(ASCE)1090-0241(2003)129:11(1054)

Dehghani, K., Edwards, K., & Harris, P. (1997). *Modeling of Waterflood in a Vuggy Carbonate Reservoir*. San Antonio: Society of Petroleum Engineers. https://doi.org/10.2118/38910-MS

Dell'Isola, F., Sciarra, G., & Vidoli, S. (2009). Generalized hooke's law for isotropic second gradient materials. *Proceedings of the Royal Society A: Mathematical, Physical and Engineering Sciences*. https://doi.org/10.1098/rspa.2008.0530

Detournay, E., & Cheng, A. (1993). *Fundamentals of Poroelasticity. Analysis and Design Methods*. https://doi.org/10.1016/B978-0-08-040615-2.50011-3

Dominguez, G., Fernando, S., & Chilingarian, G. (1992). *Simulation of Carbonate Reservoirs*. In G. Chilingarian, S. Mazzullo, & H. Rieke, Carbonate Reservoir Characterization A Geologic-engineering Analysis, Part I: Elsevier. https://doi.org/10.1016/S0376-7361(09)70135-9

Ebenbeck, M., & Garcke, H. (2019). Analysis of a Cahn–Hilliard–Brinkman model for tumour growth with chemotaxis. *Journal of Differential Equations*. https://doi.org/10.1016/j.jde.2018.10.045

Egermann, P., Lombard, J. M., & Bretonnier, P. (2006). A fast and accurate method to measure threshold capillary pressure of caprocks under representative conditions. *Sca*.

Farquhar, R. A., Somerville, J. M., & Smart, B. G. D. (1994). Porosity as a Geomechanical Indicator: An Application of Core and Log Data and Rock Mechanics. *European Petroleum Conference*. London, United Kingdom: Society of Petroleum Engineers. https://doi.org/10.2118/28853-MS

Gartling, D., Hickox, C., & Givler, R. (1996). *Simulation of Coupled Viscous and Porous Flow Problems*. International Journal of Computational Fluid Dynamics. https://doi.org/10.1080/10618569608940751

Gaus, I. (2010). *Role and impact of CO2 rock interactions during CO2 storage in sedimentary rocks*. International Journal of Greenhouse Gas Control. https://doi.org/10.1016/j.ijggc.2009.09.015

Geertsma, J. (1966). *Problems of Rock Mechanics In Petroleum Production Engineering. 1st ISRM Congress*. Lisbon: International Society for Rock Mechanics and Rock Engineering.

Ghabezloo, S., Sulem, J., & Saint-Marc, J. (2009). *Evaluation of a permeability porosity relationship in a low-permeability creeping material using a single transient test*. International Journal of Rock Mechanics and Mining Sciences. https://doi.org/10.1016/j.ijrmms.2008.10.003

Goldscheider, N., Mádl-Szőnyi, J., Erőss, A., & Schill, E. (2010). Review: Thermal water

resources in carbonate rock aquifers. *Hydrogeology Journal*, *18*(6), 1303–1318. https://doi.org/10.1007/s10040-010-0611-3

Gomes, J., Narayanan, R., Parra, H., Saputelli, L., & Bansal, Y. (2018). *Benchmarking Recovery Factors for Carbonate Reservoirs: Key Challenges and Main Findings from Middle Eastern Fields*. Abu Dhabi International Petroleum Exhibition & Conference. Abu Dhabi: Society of Petroleum Engineers. https://doi.org/10.2118/193094-MS

Gozalpour, F., Ren, S., & Tohidi, B. (2005). *CO2 EOR and Storage in Oil Reservoirs*. Oil & Gas Science and Technology IFP. https://doi.org/10.2516/ogst:2005036

Gulbransen, A., Hauge, V., & Lie, K.-A. (2010). *A Multiscale Mixed Finite Element Method for Vuggy and Naturally Fractured Reservoirs*. SPE Journal. https://doi.org/10.2118/119104-PA

Guo, J., Nie, R., & Jia, Y. (2012). *Dual permeability flow behavior for modeling horizontal well production in fractured-vuggy carbonate reservoirs*. Journal of Hydrology. https://doi.org/10.1016/j.jhydrol.2012.07.021

Hallack, D. M. C., de Araujo Cavalcante Filho, J. S., & Couto, P. (2020). Implementation of a two-phase simulator based on the Brinkman's equation for vuggy-karstified reservoirs. In *Offshore Technology Conference Brasil 2019, OTCB 2019*. https://doi.org/10.4043/29776-ms

He, J., Killough, J., Fadlelmula, M., & Fraim, M. (2015). *A Unified Finite Difference Model for The Simulation of Transient Flow in Naturally Fractured Carbonate Karst Reservoirs*. SPE Reservoir Simulation Symposium. Society of Petroleum Engineers. https://doi.org/10.2118/173262-MS

Hidajat, I., Mohanty, K., Flaum, M., & Hirasaki, G. (2004). *Study of Vuggy Carbonates Using NMR and X-Ray CT Scanning*. SPE Reservoir Evaluation & Engineering. https://doi.org/10.2118/88995-PA

Holloway, S. (1997). *An overview of the underground disposal of carbon dioxide*. Energy Conversion and Management. https://doi.org/10.1016/S0196-8904(96)00268-3

Hosseinzadeh Hejazi, S. A., Shah, S., & Pini, R. (2019). Dynamic measurements of drainage capillary pressure curves in carbonate rocks. *Chemical Engineering Science*. https://doi.org/10.1016/j.ces.2019.02.002

Hubbert, M. (1957). *Darcys law and the field equations of the flow of underground fluids*.

International Association of Scientific Hydrology. https://doi.org/10.1080/02626665709493062

Jager, W., & Mikelic, A. (2000). *On the Interface Boundary Condition of Beavers, Joseph, and Saffman*. SIAM Journal on Applied Mathematics.

Kazemi, H., & Merrill, L. (1979). *Numerical Simulation of Water Imbibition in Fractured Cores*. Society of Petroleum Engineers Journal. https://doi.org/10.2118/6895-PA

Ketzer, J., Iglesias, R., & Einloft, S. (2012). *Reducing Greenhouse Gas Emissions with CO2 Capture and Geological Storage*. J. Seiner, T. Suzuki, & M. Lackner, Handbook of Climate Change Mitigation. Springer: In W. Chen. https://doi.org/10.1007/978-1-4419-7991-9_37

Khvatova, I., Renaud, A., Malyutina, G.-B., Sansiev, G., Kuzilov, I., & Minnibaeva, T. (2012). *Simulation of Complex Carbonate Field: Double Medium vs*. Single Medium - Kharyaga Field Case. SPE Russian Oil and Gas Exploration and Production Technical Conference and Exhibition. Moscow: Society of Petroleum Engineers. https://doi.org/10.2118/160585-MS

Kilisek, R. (2015). Why We Need to Get from Carbon Capture & Storage (CCS) to Carbon Capture & Utilization (CCU). Retrieved from https://breakingenergy.com/2015/06/03/why-we-need-to-get-from-carbon-capture-storage-ccs-to-carbon-capture-utilization-ccu/

Kossack, C., & Gurpinar, O. (2001). *A Methodology for Simulation of Vuggy and Fractured Reservoirs. SPE Reservoir Simulation Symposium*. Houston: Society of Petroleum Engineers. https://doi.org/10.2118/66366-MS

Kovacs, T., Poulussen, D., & de Dios, C. (2015). *Stratedies for Injection of CO2 into Carbonate Rocks at Hontomin*. Global Carbon Capture and Storage Institute.

Kozeny, J. (1927). Uber kapillare Leitung des Wassers im Boden. *Akad. Wiss.Wien*.

Layton, W., Schieweck, F., & Yotov, I. (2002). *Coupling Fluid Flow with Porous Media Flow*. SIAM Journal on Numerical Analysis. https://doi.org/10.1137/S0036142901392766

Li, L., Khorsandi, S., Johns, R., & Dilmore, R. (2015). *CO2 enhanced oil recovery and storage using a gravity-enhanced process*. International Journal of Greenhouse Gas Control. https://doi.org/10.1016/j.ijggc.2015.09.006

Lian, P., Ma, C., Ji, B., Duan, T., & Tan, X. (2017). *Numerical Simulation Modeling of Carbonate Reservoir Based on Rock Type*. Journal of Engineering. https://doi.org/10.1155/2017/6987265

Lie, K. A., Aarnes, J. E., Kippe, V., & Rustad, A. B. (2007). Modelling of multiscale structures

in flow simulations for petroleum reservoirs. In *Geometric Modelling, Numerical Simulation, and Optimization: Applied Mathematics at SINTEF*. https://doi.org/10.1007/978-3-540-68783-2_10

Lucia, F. (1983). *Petrophysical Parameters Estimated From Visual Descriptions of Carbonate Rocks: A Field Classification of Carbonate Pore Space*. Journal of Petroleum Technology. https://doi.org/10.2118/10073-PA

Luquot, L., & Gouze, P. (2009). *Experimental determination of porosity and permeability changes induced by injection of CO2 into carbonate rocks*. Chemical Geology. https://doi.org/10.1016/j.chemgeo.2009.03.028

Martínez-Martínez, J., Benavente, D., & García-del-Cura, M. A. (2012). Comparison of the static and dynamic elastic modulus in carbonate rocks. *Bulletin of Engineering Geology and the Environment*. https://doi.org/10.1007/s10064-011-0399-y

Martys, N., Bentz, D., & Garboczi, E. (1994). *Computer simulation study of the effective viscosity in Brinkmans equation*. Physics of Fluids. https://doi.org/10.1063/1.868258

Menke, H., Gao, Y., Linden, S., & Andrew, M. (2019). Using nano-XRM and high-contrast imaging to inform micro-porosity permeability during Stokes-Brinkman single and two-phase flow simulations on micro-CT images. *EarthArXiv*. https://doi.org/https://doi.org/10.31223/osf.io/ubg6p

Menke, H. P., Gao, Y., & Andrew, M. (2018). Using nano-CT and high-contrast imaging to inform microporosity permeability during Stokes-Brinkman flow simulations on μCT images. In *American Geophysical Union, Fall Meeting 2018*.

Metz, B., Davidson, O., de Coninck, H., Loos, M., & Meyer, L. (2005). *Carbon Dioxide Capture and Storage.* IPCC Special Report: IPCC.

Mikelic, A. (1997). *On the Transmission Conditions at the Contact Interface between a Porous Medium and a Free Fluid*. Homogenization and Porous Media. Springer: In U. Hornung. https://doi.org/ISBN 978-1-4612-7339-4

Misra, A., & Poorsolhjouy, P. (2016). Granular micromechanics based micromorphic model predicts frequency band gaps. *Continuum Mechanics and Thermodynamics*. https://doi.org/10.1007/s00161-015-0420-y

Morales, F. (2013). *The formal asymptotic expansion of a Darcy Stokes coupled system*. Revista de la Facultad de Ciencias.

Morales, F., & Showalter, R. (2017). *A Darcy Brinkman model of fractures in porous media*. Journal of Mathematical Analysis and Applications. https://doi.org/10.1016/j.jmaa.2017.03.063

Morris, B. L., Lawrence, A. R. L., Chilton, P. J. C., Adams, B., Calow, R. C., & Klinck, B. A. (2003). *Groundwater and its susceptibility to degradation : a global assessment of the problem and options for management* (Vol. 03–3). United Nations Environment Programme. Retrieved from http://nora.nerc.ac.uk/id/eprint/19395/

Nemes, J. A., & Spéciel, E. (1996). Use of a rate-dependent continuum damage model to describe strain-softening in laminated composites. *Computers and Structures*. https://doi.org/10.1016/0045-7949(95)00229-4

Nermoen, A. (2018). *Porosity Evolution during Chemo-Mechanical Compaction*. Porosity. IntechOpen: In T. Ghrib. https://doi.org/10.5772/intechopen.72795

Nuckols, E. (1992). *A Review of Shallow-Shelf Carbonate Reservoirs in the United States*. New Orleans: Department of Energy.

Oda, M. (1986). *An equivalent continuum model for coupled stress and fluid flow analysis in jointed rock masses*. Water Resources Research. https://doi.org/10.1029/WR022i013p01845

Olson, J., Laubach, S., & Lander, R. (2004). Improving Fracture Permeability Prediction By Combining Geomechanics And Diagenesis. *Gulf Rocks, 2004*.

Ornés, A. I., Deisman, N. L., & Chalaturnyk, R. J. (2013). Discontinuum modelling of vuggy carbonate specimens: Impact of vugs on strength and stiffness. In *47th US Rock Mechanics / Geomechanics Symposium 2013*.

Peng, X., Du, Z., Liang, B., & Qi, Z. (2009). *Darcy-Stokes Streamline Simulation for the Tahe-Fractured Reservoir With Cavities*. SPE Journal. https://doi.org/10.2118/107314-PA

Philip, Z., Jennings, J., Olson, J., Laubach, S., & Holder, J. (2005). *Modeling Coupled Fracture-Matrix Fluid Flow in Geomechanically Simulated Fracture Networks*. SPE Reservoir Evaluation & Engineering. https://doi.org/10.2118/77340-PA

Placidi, L., Misra, A., & Barchiesi, E. (2018). Two-dimensional strain gradient damage modeling: a variational approach. *Zeitschrift Fur Angewandte Mathematik Und Physik*. https://doi.org/10.1007/s00033-018-0947-4

Popov, P., Qin, G., Bi, L., Efendiev, Y., Ewing, R., Kang, Z., & Li, J. (2007). *Multiscale Methods for Modeling Fluid Flow Through Naturally Fractured Carbonate Karst*

Reservoirs. SPE Annual Technical Conference and Exhibition. Anaheim: Society of Petroleum Engineers. https://doi.org/10.2118/110778-MS

Popov, P., Qin, G., Bi, L., Efendiev, Y., Ewing, R., & Li, J. (2009). *Multiphysics and Multiscale Methods for Modeling Fluid Flow Through Naturally Fractured Carbonate Karst Reservoirs*. SPE Reservoir Evaluation & Engineering. https://doi.org/10.2118/105378-PA

Pruess, K. (1985). *A Practical Method for Modeling Fluid and Heat Flow in Fractured Porous Media*. Society of Petroleum Engineers Journal. https://doi.org/10.2118/10509-PA

Rasoulzadeh, M., & Panfilov, M. (2018). *Asymptotic solution to the viscous/inertial flow in wavy channels with permeable walls*. Physics of Fluids. https://doi.org/10.1063/1.5041748

Rathish Kumar, B. ~V., & Chowdhury, M. (2019). Subgrid multiscale stabilized finite element analysis of fully-coupled unified Stokes-Darcy-Brinkman/Transport model. *ArXiv E-Prints*, arXiv:1911.11392.

Reddy, J. N. (2004). *An Introduction to Nonlinear Finite Element Analysis*. OUP Oxford. Retrieved from https://books.google.com/books?id=gV2EN71IjwgC

Reddy, J. N. (2014). *An Introduction to Nonlinear Finite Element Analysis: with applications to heat transfer, fluid mechanics, and solid mechanics*. OUP Oxford. Retrieved from https://books.google.com/books?id=K0xVBQAAQBAJ

Rice, J., & Cleary, M. (1976). *Some Basic Stress Diffusion Solutions for Fluid-Saturated Elastic Porous Media With Compressible Constituents*. Reviews of Geophysics and Space Physics.

Rieke, H., Chilingarian, G., & Mazzullo, S. (1996). *Performance and Classification of Carbonate Reservoirs*. In G. Chilingarian, S. Mazzullo, & H. Rieke, carbonate reservoir characterization a geologic, engineering analysis, part II.: Elsevier. https://doi.org/ISBN: 0-444-82103-1

Rieke, H., Mannon, R., & Chilingar, G. (1972). *Oil and Gas Production from Carbonate Rocks*. New York: Elsevier.

Saidi, S. (1983). *Simulation of Naturally Fractured Reservoirs. SPE Reservoir Simulation Symposium*. San Francisco: Society of Petroleum Engineers. https://doi.org/10.2118/12270-MS

Salinger, A., Aris, R., & Derby, J. (1994). *Finite element formulations for large-scale, coupled flows in adjacent porous and open fluid domains*. International Journal for Numerical Methods in Fluids. https://doi.org/10.1002/fld.1650181205

Sarkar, S., Toksoz, N., & Burns, D. (2002). *Fluid Flow Simulation in Fractured Reservoirs*. Massachusetts Institute of Technology. Earth Resources Laboratory. https://doi.org/http://hdl.handle.net/1721.1/67856

Schlumberger. (2007). *Carbonate Reservoirs: Meeting unique challenges to maximize recovery*. Schlumberger.

Sheng, J. (2013). *Surfactant Enhanced Oil Recovery in Carbonate Reservoirs*. In J. Sheng, Enhanced Oil Recovery Field Case Studies. Waltham: Gulf Professional Publishing. https://doi.org/ISBN: 978-0-12-386545-8

Silbernagel, M. (2007). *Modeling coupled fluid flow and geomechanical and geophysical phenomena within a finite element framework*. Colorado School of Mines.

Siqueira, T., Iglesias, R., & Ketzer, J. (2017). *Carbon dioxide injection in carbonate reservoirs a review of CO2-water-rock interaction studies*. Greenhouse Gases: Science and Technology. https://doi.org/10.1002/ghg.1693

Sitharam, T., Sridevi, J., & Shimizu, N. (2001). *Practical equivalent continuum characterization of jointed rock masses*. International Journal of Rock Mechanics and Mining Sciences. https://doi.org/10.1016/S1365-1609(01)00010-7

SPE. (2019). *Upscaling of grid properties in reservoir simulatio*. Retrieved from https://petrowiki.org/Upscaling_of_grid_properties_in_reservoir_simulation

Stokes, G. (1851). *On the Effect of the Internal Friction of Fluids on the Motion of Pendulums*. Cambridge: Transactions of the Philosophical Society.

Surana, K. S., & Reddy, J. N. (2016). *The Finite Element Method for Boundary Value Problems: Mathematics and Computations*. CRC Press. Retrieved from https://books.google.com/books?id=xJe_DQAAQBAJ

Tambach, T., Koenen, M., Wasch, L., & van Bergen, B. (2015). *Geochemical evaluation of CO2 injection and containment in a depleted gas field*. International Journal of Greenhouse Gas Control. https://doi.org/10.1016/j.ijggc.2014.10.005

Terzaghi, K. (1943). *Theoretical Soil Mechanics*. John and Sons Inc: Wiley.

Thiele, M., Batycky, R., & Fenwick, D. (2010). *Streamline Simulation for Modern Reservoir-Engineering Workflows*. Journal of Petroleum Technology. https://doi.org/10.2118/118608-JPT

Thordsen, J., Gans, K., Thomas, R., Kharaka, Y., & Cole, D. (2013). *Geochemical Monitoring*

for Potential Environmental Impacts of Geologic Sequestration of CO2. Reviews in Mineralogy and Geochemistry. https://doi.org/10.2138/rmg.2013.77.11

Total. (2017). *Carbonate Geology Know-How*. Paris: Total: Exploration & Production.

U.S. DOE. (2016). *Carbon Capture, Utilization, and Storage: Climate Change, Economic Competitiveness and Energy Security*.

van Genuchten, M. T. (1980). A Closed-form Equation for Predicting the Hydraulic Conductivity of Unsaturated Soils. *Soil Science Society of America Journal*. https://doi.org/10.2136/sssaj1980.03615995004400050002x

Vasquez-Cruz, R., & Castrejon-Aivar, M. (2005). *Pressure Transient and Decline Curve Behaviors in Naturally Fractured Vuggy Carbonate Reservoirs*. SPE Reservoir Evaluation & Engineering. https://doi.org/10.2118/77689-PA

Vassilevski, P. S., & Villa, U. (2014). A mixed formulation for the Brinkman problem. *SIAM Journal on Numerical Analysis*. https://doi.org/10.1137/120884109

Vik, B., Sylta, K., & Skauge, A. (2012). *Connectivity in Vuggy Carbonates, New Experimental Methods and Applications*. Transport in Porous Media. https://doi.org/10.1007/s11242-012-9969-0

Walsh, J. B. (1965a). The effect of cracks in rocks on Poisson's ratio. *Journal of Geophysical Research*. https://doi.org/10.1029/jz070i020p05249

Walsh, J. B. (1965b). The effect of cracks on the uniaxial elastic compression of rocks. *Journal of Geophysical Research*. https://doi.org/10.1029/jz070i002p00399

Wang, H. (2000). *Theory of Linear Poroelasticity with Applications to Geomechanics and Hydrogeology*. Princeton University Press. https://doi.org/ISBN 0-691-03746-9

Wardlaw, N. (1996). *Factors Affecting Oil Recovery From Carbonate Reservoirs*. In G. Chilingarian, S. Mazzullo, & H. Rieke, characterization: a geologic, engineering analysis, part II.: Amsterdam: Elsevier. https://doi.org/ISBN: 0-444-82103-1

Warren, J., & Root, P. (1963). *The Behavior of Naturally Fractured Reservoirs*. Society of Petroleum Engineers Journal. https://doi.org/10.2118/426-PA

Wildgust, N., Gilboy, C., & Tontiwachwuthikul, P. (2013). *Introduction to a decade of research by the IEAGHG Weyburn Midale CO2 Monitoring and Storage Project*. International Journal of Greenhouse Gas Control. https://doi.org/10.1016/j.ijggc.2013.03.014

Williamson, K., Burda, P., & Sousedík, B. (2019). A posteriori error estimates and adaptive

mesh refinement for the Stokes–Brinkman problem. *Mathematics and Computers in Simulation*, *166*, 266–282. https://doi.org/https://doi.org/10.1016/j.matcom.2019.05.015

Wu, Y.-S. (2000). *On the Effective Continuum Method for Modeling Multiphase Flow, Multicomponent Transport, and Heat Transfer in Fractured Rock*. P. Witherspoon, & S. Benson, Dynamics of Fluids in Fractured Rock. American Geophysical Union: In B. Faybishenko. https://doi.org/ISBN 0-87590-980-9

Wu, Y., Qin, G., Ewing, R., Efendiev, Y., Kang, Z., & Ren, Y. (2006). *A Multiple-Continuum Approach For Modeling Multiphase Flow in Naturally Fractured Vuggy Petroleum Reservoirs*. International Oil & Gas Conference and Exhibition in China. Beijing: Society of Petroleum Engineers. https://doi.org/10.2118/104173-MS

Yan, B., Alfi, M., Wang, Y., & Killough, J. (2013). *A New Approach for the Simulation of Fluid Flow In Unconventional Reservoirs Through Multiple Permeability Modeling. SPE Annual Technical Conference and Exhibition*. New Orleans: Society of Petroleum Engineers. https://doi.org/10.2118/166173-MS

Yan, B., Wang, Y., & Killough, J. (2016). *Beyond dual-porosity modeling for the simulation of complex flow mechanisms in shale reservoirs*. Computational Geosciences. https://doi.org/10.1007/s10596-015-9548-x

Yang, Y., Ching, W. Y., & Misra, A. (2011). Higher-order continuum theory applied to fracture simulation of nanoscale intergranular glassy film. *Journal of Nanomechanics and Micromechanics*. https://doi.org/10.1061/(ASCE)NM.2153-5477.0000030

Yang, Y., & Misra, A. (2012). Micromechanics based second gradient continuum theory for shear band modeling in cohesive granular materials following damage elasticity. *International Journal of Solids and Structures*. https://doi.org/10.1016/j.ijsolstr.2012.05.024

Yao, J., Huang, Z., Li, Y., Wang, C., & Lv, X. (2010). *Discrete Fracture-Vug Network Model for Modeling Fluid Flow in Fractured Vuggy Porous Media*. International Oil and Gas Conference and Exhibition in China. Society of Petroleum Engineers. https://doi.org/10.2118/130287-MS

Youssef, A. A. A., & Awotunde, A. A. (2019). Modelling fluid flow in karst reservoirs using Darcy Model with estimated permeability distribution. *Computers and Geosciences*. https://doi.org/10.1016/j.cageo.2019.104311

Yuan, T., & Qin, G. (2020). Numerical Investigation of Wormhole Formation During Matrix

Acidizing of Carbonate Rocks by Coupling Stokes-Brinkman Equation with Reactive Transport Model Under Radial Flow Conditions. *SPE International Conference and Exhibition on Formation Damage Control*. Lafayette, Louisiana, USA: Society of Petroleum Engineers. https://doi.org/10.2118/199262-MS

Zhang, F., An, M., Yan, B., & Wang, Y. (2017). *Modeling the Depletion of Fractured Vuggy Carbonate Reservoir by Coupling Geomechanics with Reservoir Flow. SPE Reservoir Characterisation and Simulation Conference and Exhibition*. Abu Dhabi: Society of Petroleum Engineers. https://doi.org/10.2118/186050-MS

Zhang, L., Bryant, S., Jennings, J., Arbogast, T., & Paruchuri, R. (2004). *Multiscale Flow and Transport in Highly Heterogeneous Carbonates. SPE Annual Technical Conference and Exhibition*. Houston: Society of Petroleum Engineers. https://doi.org/10.2118/90336-MS

Zhao, L., Chung, E., & Lam, M. F. (2020). A new staggered DG method for the Brinkman problem robust in the Darcy and Stokes limits. *Computer Methods in Applied Mechanics and Engineering*. https://doi.org/10.1016/j.cma.2020.112986

Zimmerman, R. (1984). *The effect of pore structure on the pore bulk compressibilities of consolidated sandstones*. Berkeley: University of California.

7 Appendix A

The constitutive equations for stress, strain and fluid content increment (Biot & Willis, 1957; Wang, 2000).

$$\varepsilon = a_{11}\sigma + a_{12}\,p \qquad \textit{Eq. 76}$$

$$\xi = a_{21}\,\sigma + a_{22}\,p \qquad \textit{Eq. 77}$$

$$a_{11} = \frac{1}{K} \qquad \textit{Eq. 78}$$

$$a_{12} = a_{21} = \frac{1}{H} \qquad \textit{Eq. 79}$$

$$a_{22} = \frac{1}{R} \qquad \textit{Eq. 80}$$

where K is the bulk modulus, H is the reciprocal of poroelastic expansion coefficient and R is the Biot modulus

Strain, pore pressure and fluid content increment relationship for pure compliance:

$$\varepsilon = \frac{1}{K}\,\sigma + \frac{\alpha}{K}p \qquad \textit{Eq. 81}$$

$$\xi = \frac{\alpha}{K}\sigma + \frac{\alpha}{KB}\,p \qquad \textit{Eq. 82}$$

$$\sigma = K\varepsilon - \alpha p \qquad \textit{Eq. 83}$$

Thus:

$$\xi = \alpha\varepsilon + \frac{\alpha}{K_u B}p \qquad \textit{Eq. 84}$$

where Ku is undrained bulk modulus and B is Skempton's coefficient

$$K_u = K + \alpha^2 \Gamma \qquad \textit{Eq. 85}$$

$$B = \frac{K_u - K}{\alpha K_u} \qquad \textit{Eq. 86}$$

$$\nu = \frac{3K - 2G}{6K + 2G} \qquad \textit{Eq. 87}$$

The strain and shear stress components are related by the following constitutive equations (Wang, 2000):

$$\varepsilon_1 = \frac{\sigma_1}{E} - \frac{\nu}{E}\sigma_2 - \frac{\nu}{E}\sigma_3 + \frac{p}{3H} \qquad \textit{Eq. 88}$$

$$\varepsilon_2 = -\frac{\nu}{E}\sigma_1 + \frac{\sigma_2}{E} - \frac{\nu}{E}\sigma_3 + \frac{p}{3H} \qquad \textit{Eq. 89}$$

$$\varepsilon_3 = -\frac{\nu}{E}\sigma_1 - \frac{\nu}{E}\sigma_2 + \frac{\sigma_3}{E} + \frac{p}{3H} \qquad \textit{Eq. 90}$$

$$\xi = \frac{1}{3H}(\sigma_1 + \sigma_2 + \sigma_3) + \frac{p}{R} \qquad \textit{Eq. 91}$$

Now, replace the principle stress with normal stress and use the shear modulus expression:

$$\varepsilon_{xx} = \frac{1}{2G}\left[\sigma_{xx} - \frac{\nu}{1+\nu}\sigma_{kk}\right] + \frac{\alpha}{3K}p \qquad \textit{Eq. 92}$$

$$\varepsilon_{yy} = \frac{1}{2G}\left[\sigma_{yy} - \frac{\nu}{1+\nu}\sigma_{kk}\right] + \frac{\alpha}{3K}p \qquad \textit{Eq. 93}$$

$$\varepsilon_{zz} = \frac{1}{2G}\left[\sigma_{zz} - \frac{\nu}{1+\nu}\sigma_{kk}\right] + \frac{\alpha}{3K}p \qquad \textit{Eq. 94}$$

$$\varepsilon_{xy} = \frac{1}{2G}\sigma_{xy} \qquad \textit{Eq. 95}$$

$$\varepsilon_{yz} = \frac{1}{2G}\sigma_{yz} \qquad \textit{Eq. 96}$$

$$\varepsilon_{xz} = \frac{1}{2G}\sigma_{xz} \qquad \textit{Eq. 97}$$

In notation form:

$$\varepsilon_{ij} = \frac{1}{2G}\left[\sigma_{ij} - \frac{\nu}{1+\nu}\sigma_{kk}\delta_{ij}\right] + \frac{\alpha}{3K}\, p\, \delta_{ij} \qquad \textit{Eq. 98}$$

Solving Eq. 98 for the stress components yields:

$$\sigma_{ij} = 2G\, \varepsilon_{ij} + 2G\, \frac{\upsilon}{1-2\upsilon}\varepsilon_{kk}\, \delta_{ij} - \alpha p \delta_{ij} \qquad \textit{Eq. 99}$$

In tensor components, the effective stress is defined by Eq. 100.

$$\sigma'_{ij} = \sigma_{ij} - \alpha\, P_p\, \delta_{ij} \qquad \textit{Eq. 100}$$

where α is the poroelastic constant and δ_{ij} is the Kronecker delta

$$\alpha = \frac{\Delta V_p}{\Delta V} \qquad \textit{Eq. 101}$$

where, ΔV_p is the change of pore volume and ΔV is the change of bulk volume

$$\delta_{ij} = \begin{cases} 1 & if\ i = j \\ 0 & if\ i \neq j \end{cases} \qquad \textit{Eq. 102}$$

8 Appendix B

Table 10-Table 15 show the results of the test of the vug deformation due to compaction.

Table 10: vug deformation test with 10 GPa stiffness modulus

Data	Vug 1		Vug 2		Vug 3	
Stimulation period	5 days	30 days	5 days	30 days	5 days	30 days
Stiffness modulus (GPa)	10	10	10	10	10	10
Vug initial Volume (cc)	125	125	27	27	3	3
Change of vug volume	0.02413%	0.03953%	0.00919%	0.08550%	0.06358%	0.18701%

Table 11: vug deformation test with 20 GPa stiffness modulus

Data	Vug 1		Vug 2		Vug 3	
Stimulation period	5 days	30 days	5 days	30 days	5 days	30 days
Stiffness modulus (GPa)	20	20	20	20	20	20
Vug initial Volume (cc)	125	125	27	27	3	3
Change of vug volume	0.01839%	0.02849%	0.00707%	0.05107%	0.04458%	0.12412%

Table 12: vug deformation test with 40 GPa stiffness modulus

Data	Vug 1		Vug 2		Vug 3	
Stimulation period	5 days	30 days	5 days	30 days	5 days	30 days
Stiffness modulus (GPa)	40	40	40	40	40	40
Vug initial Volume (cc)	125	125	27	27	3	3
Change of vug volume	0.01120%	0.01449%	0.00420%	0.00870%	0.02237%	0.05025%

Table 13: vug deformation test with 66 GPa stiffness modulus

Data	Vug 1		Vug 2		Vug 3	
Stimulation period	5 days	30 days	5 days	30 days	5 days	30 days
Stiffness modulus (GPa)	66	66	66	66	66	66

Vug initial Volume (cc)	125	125	27	27	3	3
Change of vug volume	0.00800%	0.01254%	0.00333%	0.00422%	0.00510%	0.00870%

Table 14: vug deformation test with 75 GPa stiffness modulus

Data	Vug 1		Vug 2		Vug 3	
Stimulation period	5 days	30 days	5 days	30 days	5 days	30 days
Stiffness modulus (GPa)	75	75	75	75	75	75
Vug initial Volume (cc)	125	125	27	27	3	3
Change of vug volume	0.00736%	0.00816%	0.00318%	0.00349%	0.00481%	0.00497%

Table 15: vug deformation test with 100 GPa stiffness modulus

Data	Vug 1		Vug 2		Vug 3	
Stimulation period	5 days	30 days	5 days	30 days	5 days	30 days
Stiffness modulus (GPa)	100	100	100	100	100	100
Vug initial Volume (cc)	125	125	27	27	3	3
Change of vug volume	0.00539%	0.00676%	0.00314%	0.00340%	0.00476%	0.00352%

9 Appendix C

Figure 72, Figure 73, Figure 74 and Figure 75 show the saturation profiles for the injection test of the two-phase flow model. It is clear from the figures that the gas saturation increases, and the water pressure decreases. It is important to note that during the injection treatment, the system is pressurized, and consequently, the stress field in the system would be altered. Thus, the vugs' shape and volume would be affected accordingly.

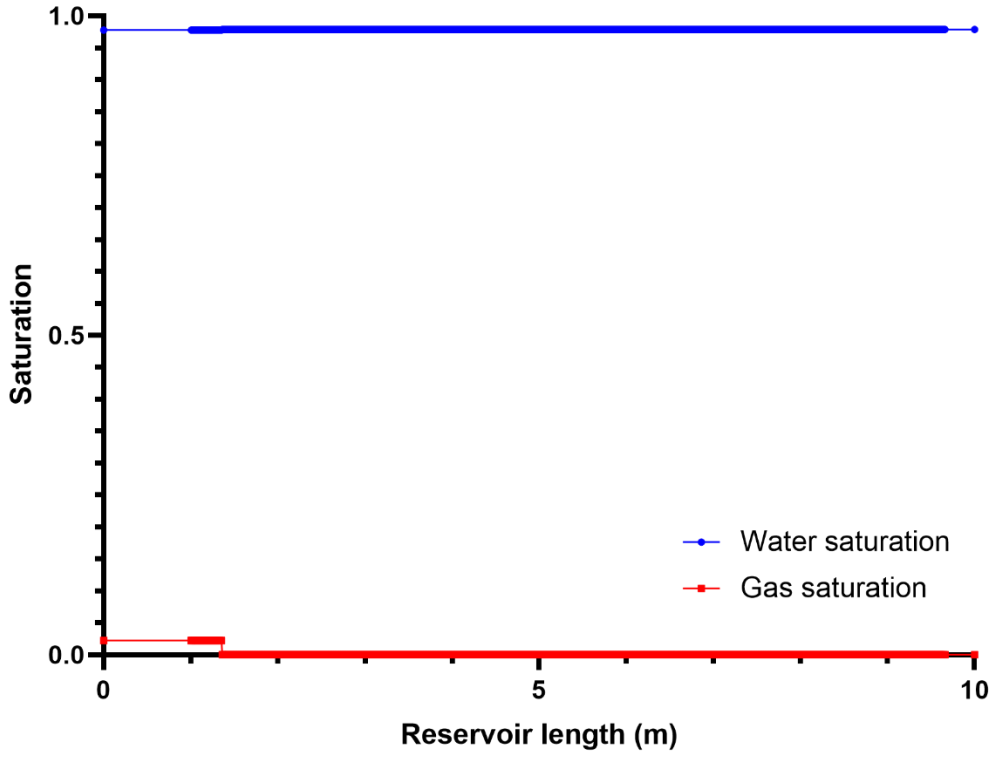

Figure 72: Saturation profile for injection test of two-phase flow model after 10 minutes

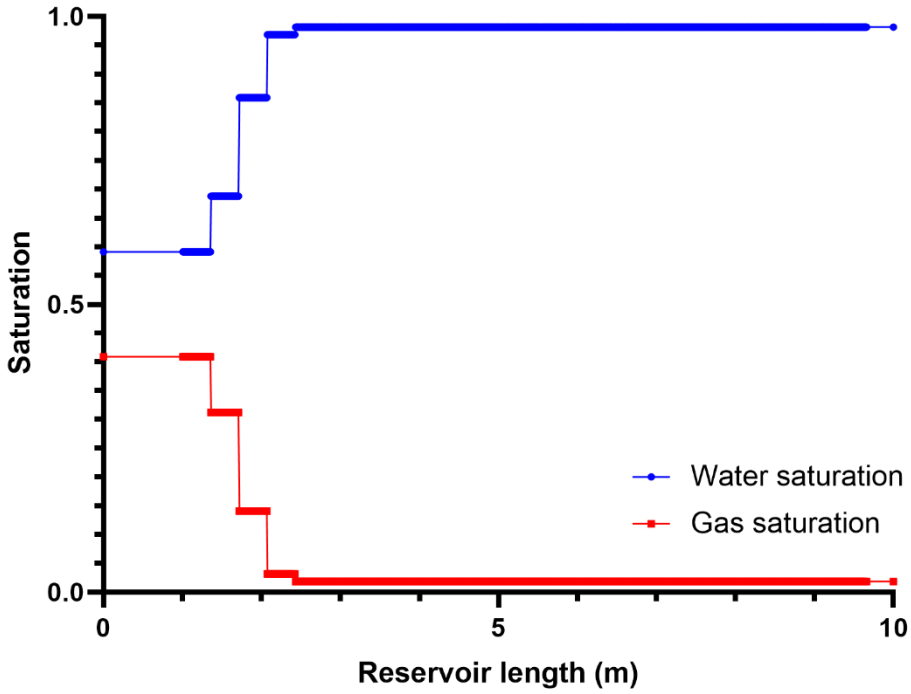

Figure 73: Saturation profile for injection test of two-phase flow model after 1 day

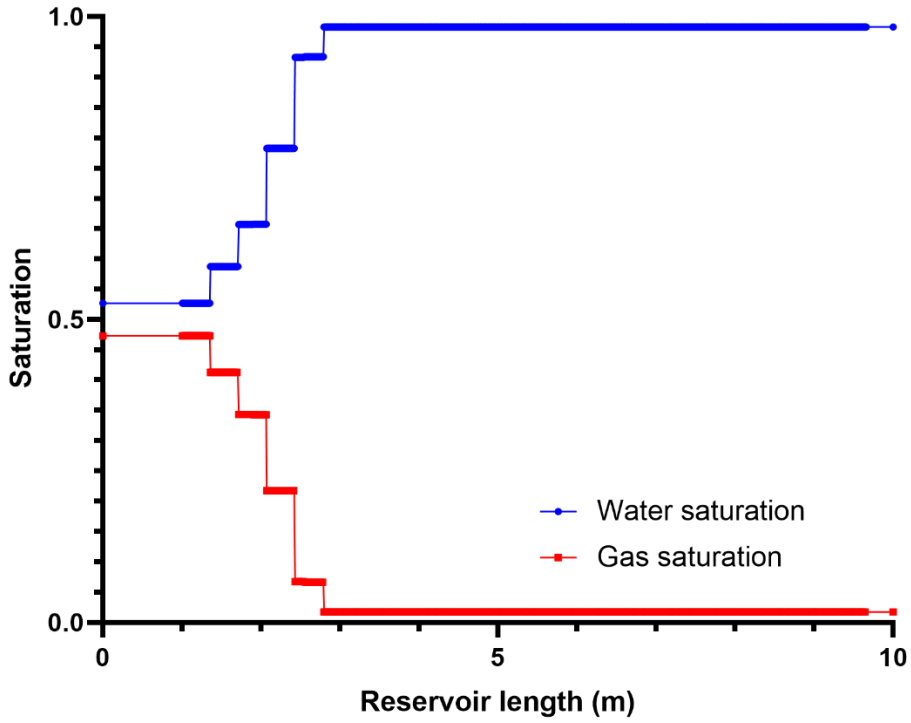

Figure 74: Saturation profile for injection test of two-phase flow model after 2 days

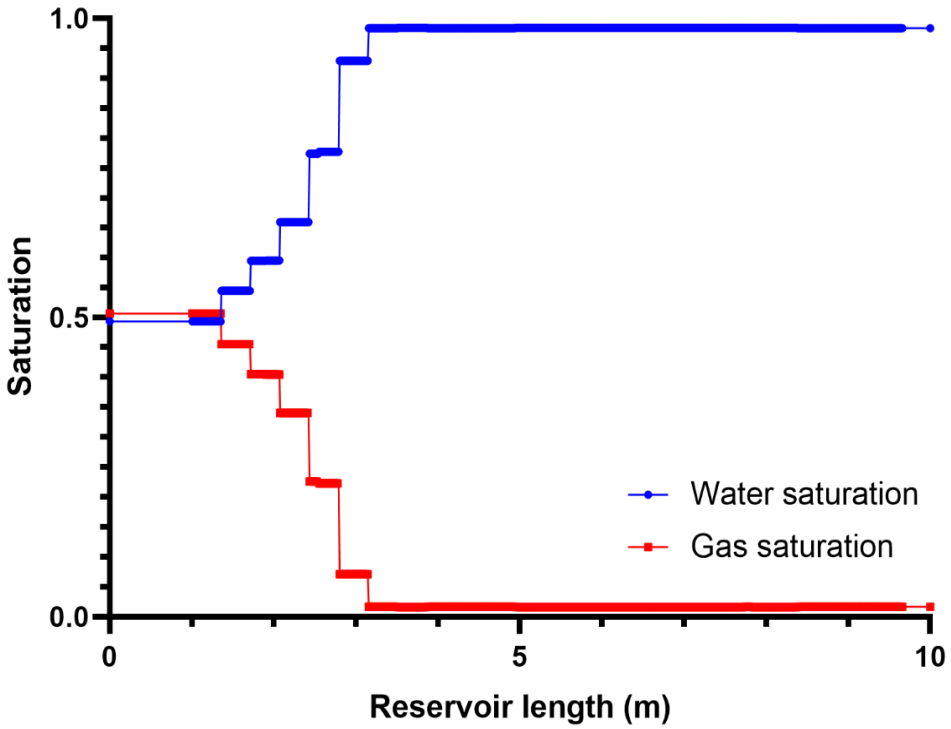

Figure 75: Saturation profile for injection test of two-phase flow model after 3 days